Fatigue Behaviour of Steel Fibre Reinforced Concrete

by

Humaira Fataar

Dissertation presented for the degree of

Doctor of Philosophy in Engineering

in the Faculty of Engineering

at Stellenbosch University

Supervisor: Prof Riaan Combrinck

Co-supervisor: Prof William Peter Boshoff

April 2022

Declaration

By submitting this dissertation electronically, I declare that the entirety of the work contained therein is my own, original work, that I am the sole author thereof (save to the extent explicitly otherwise stated), that reproduction and publication thereof by Stellenbosch University will not infringe any third party rights and that I have not previously in its entirety or in part submitted it for obtaining any qualification.

April 2022

Abstract

Concrete is a heterogeneous material that is known to have a weak tensile capacity. The construction industry has successfully utilised steel reinforcement in concrete to overcome its brittle tensile behaviour, however, steel reinforcement is generally not sufficient to resist the formation and propagation of tensile cracks. As a result, discrete fibres are added to the concrete mixing stage to produce fibre reinforced concrete (FRC). The use of steel fibres has been known to improve the post-cracking behaviour of steel fibre reinforced concrete (SFRC), and is one of the most readily available fibres in industry.

Due to concrete's popularity as a construction material, many of its applications may experience flexural fatigue loading at some point during its lifespan. A significant amount of research has been conducted on the fatigue behaviour of plain concrete and FRC in the past century. However, the research focused primarily on the uncracked behaviour, with few researchers considering the cracked behaviour. In FRC, the fibres are activated only at crack initiation and therefore, this work aimed to investigate the fatigue life and failure mechanisms of pre-cracked SFRC subjected to fatigue loading. Experiments were conducted at a single fibre and macroscopic level, using hooked-end steel fibres. The pre-cracks ranged from 0.6 mm to 2.5 mm, at fatigue load levels of 50%, 70% and 85% of the maximum static load. Various methods were used to attempt to predict the fatigue life and failure mechanisms.

A single fibre pull-out model was developed to categorise the various fibre pull-out phases and the level of deformation associated with each phase. When subjected to a static pre-slip of the fibre, followed by fatigue loading, the failure mechanisms were both fibre pull-out and fibre rupture. The fatigue capacity and failure mechanisms of the single fibre specimens vary depending on the combination of pre-slip and load level. The pull-out failures are generally unable to resist many load cycles due to a diminished fibre anchorage. The rupture failures tend to occur after a significant number of cycles have already passed, since the fibres rupture due to fatigue failure.

The macroscopic behaviour subjected to fatigue loading shows fibre rupture to be the dominant failure mechanism, which differs from the static behaviour, where fibre pull-out occurs. The fatigue resistance decreases with an increase in pre-crack and load level. The single fibre pull-out model is used to classify the fibres into the different phases along the height of the crack for the various pre-cracks.

A fatigue life prediction approach developed from the macroscopic fatigue results in the form of a modified S-N curve, was used to predict the fatigue behaviour. Experimental results from similar work performed was compared with the modified S-N curve and the results show that for deflection softening behaviour of SFRC, the model overestimates the fatigue capacity. Therefore, post-cracking behaviour influences the fatigue capacity of SFRC. The framework for an analytical model was developed to predict the fatigue failure mechanisms of pre-cracked SFRC. Fibre pull-out is likely to occur when large pre-cracks are present, whereas fibre rupture is more likely at low pre-cracks.

Opsomming

Beton is ‘n heterogene materiaal met ‘n swak trek kapasiteit. Die konstruksiebedryf het staalbewapening suksesvol gebruik om die bros trekgedrag van beton te oorkom. Die staalbewapening is egter nie genoeg om die vorming en verspreiding van trekkrake te voorkom nie. Gevolglik, word diskrete vesels in die mengfase by die beton gevoeg om vesel versterkte beton (VVB) te produseer. Dit is bekend dat die gebruik van staalvesels die gekraakte staal vesel versterkte beton (SVVB) verbeter, en dit is een van die mees vrylik beskikbare vesels in die industrie.

As gevolg van die gewildheid van beton as ‘n konstruksiemateriaal, is daar verskeie toepassings waar beton sikliese belading in buiging ondervind. Baie navorsing is gedoen oor die sikliese gedrag van gewone beton en VVB in die afgelope eeu. Die navorsing fokus egter hoofsaaklik op die ongekraakte gedrag, met min navorsers wat onlangs die gekraakte gedrag oorweeg het. In VVB, word die vesels slegs geaktiveer by die aanvang van die kraak. Daarom is hierdie werk daarop gemik om die sikliese lewensduur en falingsmeganismes van gekraakte SVVB te ondersoek wat aan sikliese belading blootgestel word. Eksperimente word uitgevoer op ‘n enkele vesel en makroskopiese vlak, met behulp van gehakte staalvesels. Die vooraf-krake wissel van 0.6 mm tot 2.5 mm, met belading van 50%, 70% en 85% van die maksimum statiese las. Daarna is verskillende metodes geïmplementeer om die sikliese gedrag en falingsmeganismes te voorspel.

‘n Enkeleveseluittrekmodel is ontwikkel om die verskillende fases van vesel uittrek te kategoriseer, tesame met die vlak van vervorming wat met elke fase geassosieer word. Met ‘n statiese voorafglip van die vesel gevolg deur sikliese belading, is die falingsmeganismes beide veseluitrekking en veselbreek. Die sikliese kapasiteit en falingsmeganismes van die enkelveselmonsters wissel afhangende van die kombinasie van voorafglip en beladingsvlak. As gevolg van die verminderde veselverankering, kan die uittrekfalings oor die algemeen nie baie belading siklusse weerstaan nie. Die breekfalings kom gewoonlik voor nadat ‘n beduidende aantal siklusse reeds verby is, aangesien die vesel faal as gevolg van siklieseefaling.

Die makroskopiese gedrag onder siklieseebelading het getoon dat veselbreek die dominante falingsmeganisme is, en verskil van die statiese gedrag, waar veseluittrek plaasgevind het. Die sikliese weerstand neem af met ‘n toename in voorafkraak en beladingsvlak. Die

enkelvesel uittrekmodel word gebruik om die vesels in verskillende fases oor die hoogte van die kraak te plaas.

‘n Sikliese lewensduur voorspellingsbenadering wat ontwikkel is uit die makroskopiese sikliese resultate in die vorm van ‘n aangepaste S-N kurwe word gebruik om die sikliese gedrag te voorspel. Eksperimentele resultate van soortgelyke werk wat voorheen uitgevoer was, is vergelyk met die aangepaste S-N kurwe en die resultate toon aan dat die model die sikliese kapasiteit oorskat vir defleksie versagtende-gedrag van SVVB. Daarom, beïnvloed die nakraak gedrag die sikliese kapasiteit van SVVB. Verder is die raamwerk vir ‘n analitiese model ontwikkel om die sikliese falingsmeganismes van vooraf-gekraakte SVVB te voorspel. Uittrekking van vesels sal waarskynlik voorkom as daar groot voorafkrake is, terwyl veselbreek meer waarskynlik is by lae voorafkrake.

Acknowledgements

I would like to appreciate and thank the following people for their assistance and support during this study.

- My supervisor Prof Riaan Combrinck and co-supervisor Prof Billy Boshoff for your encouragement, guidance, patience, and continued support throughout this study.
- The laboratory manager, technical staff, and workshop staff at the Civil Engineering Department of Stellenbosch University, for your time and assistance in performing experiments.
- My colleagues, for your continued support and guidance.
- To my siblings, nephew, and niece, for always showing an interest in my work, motivating me, and giving me laughs when I needed it.
- To my parents, for your unconditional love and endless support throughout my studies. Without your encouragement, none of this would have been possible.
- To my husband and biggest supporter, Muaz Ahmad Jan. Words cannot describe your contribution to this study. Thank you for being my support, my lifeline, my shoulder to lean on, my biggest cheerleader, and my best friend!

Notations and symbols

Acronyms

FRC	Fibre reinforced concrete
SFRC	Steel fibre reinforced concrete
ACI	American Concrete Institute
SNFRC	Synthetic fibre reinforced concrete
GFRC	Glass fibre reinforced concrete
MRI	Magnetic resonance imaging
NFRC	Natural fibre reinforced concrete
RC	Reinforced concrete
ITZ	Interfacial transition zone
CH	Calcium-hydroxide
HPPE	High performance polyethylene
PE	Polyethylene
PP	Polypropylene
PVA	Polyvinyl acetate
UHPC	Ultra-high performance concrete
MOR	Modulus of rupture
DFRCC	Ductile fibre reinforced cement composites
HPFRCC	High performance fibre reinforced cement composites
S-N	Stress versus number of cycles
HGV	Heavy goods vehicles
N	Number of cycles
CMOD	Crack mouth opening displacement

FEM	Finite Element Modelling
GGCS	Ground Granulated Corex® Slag
PPC	Pretoria Portland Cement
FM	Fineness modulus
LVDT	Linear Variable Differential Transducer
PID	Proportional-Integral-Derivative
X-ray	X-radiation
CT	Computed Tomography

Symbols

V_f	Fibre volume dosage	[%]
S	Stress	$[Pa]$
N	Number of cycles	$[-]$
σ_m	Mean stress	$[Pa]$
σ_a	Amplitude stress	$[Pa]$
σ_{max}	Maximum stress	$[Pa]$
R	Stress ratio	$[-]$
τ_{max}	Maximum bond shear stress	$[Pa]$
τ_f	Interfacial shear stress	$[Pa]$
P	Applied force	$[N]$
d	Fibre pull-out	$[mm]$
$\Delta CMOD$	Crack opening range	$[mm]$
$dCMOD/dn$	Crack opening increment per cycle	$[-]$
f_{ct}	Tensile stress	$[Pa]$
w	Crack width	$[mm]$
f_s	Static flexural strength	$[Pa]$
β	Material parameter = 0.0685	$[-]$
T	Time period of repeated loads	$[s]$
a, b, c	Experimental material parameters	$[-]$
f	Loading frequency	$[Hz]$
R'	Reversed stress ratio	$[-]$
c_1, c_2	Experimental coefficients	$[-]$
l	Length	$[mm]$
d	Diameter	$[mm]$
l/d	Aspect ratio	$[-]$
A_{max}	Maximum load	$[N\ or\ kN]$
A_{min}	Minimum load	$[N\ or\ kN]$
F_{min}	Minimum force experienced in fibre	$[N\ or\ kN]$
F_{med}	Medium force experienced in fibre	$[N\ or\ kN]$
F_{max}	Maximum force experienced in fibre	$[N\ or\ kN]$
N_{min}	Number of cycles sustained from maximum force	$[-]$

N_{med}	Number of cycles sustained from medium force	$[-]$
N_{max}	Number of cycles sustained from minimum force	$[-]$
h	Crack height	$[mm]$
$F_{fPO_{max}}$	Average maximum fibre pull-out force	$[N]$
F_{fPO}	Average fibre pull-out force	$[N]$
δ_f	Fibre end displacement	$[mm]$
F_f	Force in an individual fibre	$[N\ or\ kN]$

Table of Contents

List of Figures

List of Tables

1. Introduction

1.1. Background

Concrete is one of the most important building materials globally, with its demand and consumption increasing in all countries and regions. Concrete has a high compressive strength and durability when compared to other construction materials (Domone & Illston, 2010). It comprises of materials that are generally easily obtainable and inexpensive. The production of concrete is relatively simple, and the applications are endless in the building and civil infrastructure works. Over the past few decades, research has focussed on improving concrete behaviour (Brandt, 2008). Through advances in concrete technology, compressive strengths are constantly improved, resulting in a more brittle concrete, which is prone to sudden failure (Boulekbache, Hamrat, Chemrouk, *et al.*, 2016). One major disadvantage of concrete is its brittleness, i.e., poor tensile capacity and resistance to crack opening and propagation. To overcome this problem, steel reinforcement is generally used in the tensile zone. The successful use of steel reinforcement in concrete means that it is still the foremost reinforcement used in the construction industry (Yakut, 2004). Steel reinforcement is however not effective in suppressing the formation and propagation of tensile cracks in concrete. To overcome this problem, discrete fibres are added to concrete, enhancing its toughness, tensile capacity, crack resistance, fatigue life, etc., and is called fibre reinforced concrete (FRC) (Daniel, Ahmad, Arockiasamy, *et al.*, 2002).

The use of fibres to reinforce brittle materials date back to ancient times, where straw, horse hair, and vegetables were used for strengthening building materials (Daniel *et al.*, 2002). More recently, materials used as fibres include steel, glass, and an array of synthetic fibres (Buratti, Mazzotti & Savoia, 2011; Daniel *et al.*, 2002). Fibres play an important role in concrete since it suppresses the formation of cracks and slow down the crack propagation (Banthia & Trottier, 1991; Buratti *et al.*, 2011; Namur, Alwan & Najm, 1991; di Prisco, Plizzari & Vandewalle, 2009). Fibres bridging the cracked surface provides a significant residual tensile strength to the composite. Fibres are not only used to resist crack growth, but also to improve toughness, impact and wear resistance, and ductility. The two main fibre types used in industry are steel and synthetic fibres. For structural applications such as highways, industrial pavements, tunnel linings, etc., steel fibres are

more applicable, while synthetic fibres have effectively been used to reduce shrinkage induced cracks, since they are smaller than steel fibres (Buratti *et al.*, 2011).

Most of the abovementioned FRC applications are subjected to fatigue loading throughout their service life. As a result, the fatigue characteristics of the material become important performance and design parameters (Lee & Barr, 2004). Fatigue is described as the process of continuous, permanent internal structural changes to a material that is subjected to cyclic loading (Farzam, Hogan, Holub, *et al.*, 2000). In concrete, the internal structural changes refer to the progressive growth of internal microcracks (Keerthana & Chandra Kishen, 2018; Lee & Barr, 2004; Parvez & Foster, 2017). The bridging activity of fibres in concrete is only activated at crack initiation, and it is then that the fibres contribute to the load-carrying capacity. Most of the research done by scholars on the fatigue behaviour of FRC does not consider the effects of crack initiation on the fatigue life of FRC. More research is required in order to develop design codes and expand the understanding and confidence in FRC as a commercial construction material.

1.2. Research problem statement

Since concrete is a heterogeneous and brittle material, small flaws or discontinuities may develop internally or superficially. These flaws could lead to microcracks prior to any externally applied loading, and this could be exacerbated to form macrocracks once an external load is applied. For structures such as concrete pavements which are subjected to fatigue loading, a sudden overload of a heavy goods vehicle (HGV) can cause these microcracks to quickly result in crack propagation, which leads to degradation of the material, and ultimately fatigue failure (Banjara & Ramanjaneyulu, 2018).

As a result of the fibre bridging mechanisms across cracked surfaces, FRC provides significant post-cracking tensile residual strength (Buratti *et al.*, 2011; di Prisco *et al.*, 2009). FRC subjected to fatigue loading has garnered a significant amount of research over the past few decades, with investigations focusing on compressive fatigue behaviour (Cachim, Figueiras & Pereira, 2002; Medeiros, Zhang, Ruiz, *et al.*, 2015; Otter & Naaman, 1988; Yin & Hsu, 1995), tensile fatigue behaviour (Plizzari, Cere & Cangiano, 2000; Zhang, Stang & Li, 2000), and flexural fatigue behaviour (Boulekbache *et al.*, 2016; Jun & Stang, 1998; Ramakrishnan, Tatnal & Oberling, 1987). However, for FRC structures subjected to fatigue in flexure, the current literature focuses mainly on the uncracked

behaviour, and few researchers have investigated the cracked behaviour of concrete under fatigue loading (Carlesso, de la Fuente & Cavalaro, 2019; Germano, Tiberti & Plizzari, 2016; Gettu & Stephen, 2020; Mailhot, Bissonnette, Saucier, *et al.*, 2001). This is significant since the fibres are activated once there is crack initiation. Prior to crack initiation, the FRC composite deforms elastically, and the longitudinal displacement of the fibre and matrix is proportional (Bentur & Mindess, 2006). However, at crack initiation, the stress is transferred from the matrix to the fibre through shear deformation at the fibre-matrix interface (Beaudoin, 1990; Bentur & Mindess, 2006; Ghoddousi, Ahmadi & Sharifi, 2010; Namur *et al.*, 1991).

In order to fully understand and develop a framework to ultimately model the post-cracking behaviour of FRC subjected to fatigue loading, more research on this topic is required. This research aimed to characterise the fatigue behaviour and identify the failure mechanisms of pre-cracked FRC at a single fibre and macroscopic level.

1.3. Motivation for the research

In reinforced concrete subjected to flexural fatigue, the compressive stress is carried by the concrete and the tensile stress by the steel reinforcement. This results in fatigue failure occurring either in the tension steel or compression of concrete (Hsu, 1981; Jun & Stang, 1998). As a result, the initial research on the fatigue of concrete focused on the compressive behaviour under fatigue loading (Gao & Hsu, 1999; Holmen, 1982; Park, 1990). Since the addition of steel fibres significantly improved the post-cracking tensile behaviour, the focus has shifted to tensile and flexural fatigue behaviour (Buratti *et al.*, 2011).

Work done by Jun & Stang (1998) on the flexural fatigue of steel fibre reinforced concrete (SFRC) showed that the steel fibres significantly improved the fatigue performance as compared to polypropylene fibres for fibre volume dosages between 1.0% and 2.0%. Johnston & Zemp (1991) investigated the influence of fibre dosage, aspect ratio, and fibre type on the flexural fatigue behaviour of SFRC. The results showed that the fibre dosage was the governing factor for the fatigue life, followed by the aspect ratio and fibre type, respectively. The optimum fibre dosage was between 1.0% and 1.5%. Mailhot et al. (2001) investigated the flexural fatigue behaviour of SFRC before and after cracking in order to quantify the fatigue capacity after crack initiation. Various stress levels and fibre

geometries were investigated at a fibre dosage of 0.5%. The fatigue capacity after cracking exceeded 80% of the overall life span for some specimens. However, at high stress levels, the fatigue capacity was low. The results showed large variability, which was mainly attributed to the low fibre dosage. Germano et al. (2016) investigated the flexural fatigue behaviour of cracked SFRC at two different fibre dosages. It was found that the optimum fibre dosage was 0.5%, since the addition of more fibres introduced additional flaws in the concrete and did not improve the fatigue behaviour, especially under high-cycle fatigue.

The effects of fibres in concrete have been investigated over the years, and steel fibres were found to be most suitable for structural applications, especially when subjected to fatigue loading (Daniel *et al.*, 2002; Jun & Stang, 1998). Although SFRC provided improved residual strength when compared to plain concrete, the results were generally more scattered, especially under fatigue loading, which then required more research (Buratti *et al.*, 2011; Naaman & Hammoud, 1998; Nanni, 1991; Singh & Kaushik, 2003). Few researchers have considered the effects of pre-cracked flexural fatigue behaviour of SFRC. Investigating the fatigue behaviour of uncracked FRC may provide information on the overall behaviour of the concrete in tension and compression, but it does not provide much information on the damage in real structures, which already have pre-existing cracks (Germano *et al.*, 2016).

1.4. Research objectives

From the research problem and motivation in the previous sections, the research aimed to investigate the fatigue behaviour of pre-cracked SFRC. The objectives are outlined as follows:

- Investigate the fatigue behaviour at a single fibre level on pre-slipped SFRC.
- Investigate the fatigue behaviour at a macroscopic level on pre-cracked SFRC.
- Characterise the fatigue behaviour and develop a framework to predict the fatigue life and failure mechanisms.

1.5. Outline of content

In Chapter 2, a comprehensive literature study is presented, which focuses on FRC at the single fibre level as well as the macroscopic level, the fatigue behaviour of concrete and FRC, with an emphasis on crack initiation and propagation.

Chapter 3 provides a detailed description of the experimental framework conducted in this research study. Experimental tests are performed on two levels, namely, the single fibre level and the macroscopic level. The specimen casting, test preparations, fatigue loading conditions and data acquisition are outlined in detail.

The experimental results of the single fibre pull-out tests in fatigue are presented and characterised in Chapter 4.

Chapter 5 discusses the experimental results of the flexural fatigue tests performed at the macroscopic level. Various behavioural aspects are reported and used as a basis for Chapter 6.

In Chapter 6, empirical models are developed based on the fatigue behaviour observed in Chapters 4 and 5. Steps towards developing an analytical model based on the fatigue behaviour are also presented.

Chapter 7 presents the significant findings of the research study, as well as the aspects identified for further investigation.

2. Literature review

2.1. Fibre reinforced concrete

Concrete is a composite construction material composed of cement, fine and coarse aggregates, water, and chemical admixtures. Additional binder materials such as fly ash and slag may also be used to replace a certain percentage of the cement depending on the application of the concrete (Wu, Tan, Liu, *et al.*, 2016). Concrete is the most commonly used building material and most modern infrastructure has been built using concrete in some or other form (Owens, 2013). Its constituents are easily available and generally inexpensive (Brandt, 2008). Concrete has a variety of uses ranging from pipes and architectural structures to bridges and floor foundations (Wu *et al.*, 2016). Since concrete is a heterogeneous material, it is inherently full of flaws, which could include air voids, shrinkage cracks, and water pockets trapped beneath the surface of coarse aggregates (Lee & Barr, 2004). The low tensile strength and brittle nature of unreinforced concrete matrices are particularly vulnerable to crack opening and propagation since it deforms elastically under tensile loads, which leads to micro-cracking, followed by macro-cracking and ultimately, failure (Brandt, 2008; Zandi Hanjari, 2006). To overcome this problem, the use of steel reinforcement in the tensile zone of concrete has been successfully implemented in the construction industry (Yakut, 2004). Discrete fibres are also added to concrete during the mixing stage to improve the brittle behaviour and crack propagation.

According to the American Concrete Institute (ACI), fibre reinforced concrete (FRC) is defined as concrete that contains dispersed, randomly orientated fibres (Farzam *et al.*, 2000). The use of fibres to reinforce brittle materials dates back to ancient times when straw was used to reinforce sun-baked clay bricks, and horsehair was used to reinforce masonry mortar. At the start of the 1900s, the concept of fibre reinforced concrete was adapted, and asbestos was used in the Hatschek process to reinforce cement-paste matrices. However, due to the health hazards associated with asbestos fibres, alternate fibres were introduced from the 1950s (Bentur & Mindess, 1990; Brandt, 2008; Daniel *et al.*, 2002; Hoff, 1984). The incorporation of fibres into the concrete matrix enhanced its composite properties such as the tensile strength, elastic modulus, compressive strength, ductility, crack formation and propagation, fatigue life, shrinkage, impact resistance, thermal properties, and fire resistance (Daniel *et al.*, 2002; Fantilli, Mihashi & Vallini, 2009).

2.1.1. Background for types of fibre reinforced concrete

There are four main types of fibre reinforced concrete based on the fibre material type, which include steel fibres, synthetic fibres, glass fibres and natural fibres (Brandt, 2008; Daniel *et al.*, 2002). The fibre type, geometry and volume percentage added are dependent on the mechanical response required from the concrete (Buratti *et al.*, 2011; Fantilli *et al.*, 2009). The two types of fibres most commonly used and investigated are steel fibres and synthetic fibres (Buratti *et al.*, 2011).

2.1.1.1. Steel fibre reinforced concrete (SFRC)

Steel reinforcing elements dates back to 1910, where various steel objects such as wires, nails and metal segments were used to enhance the properties of concrete (Naaman, 1985). In the early 1960s, a study in the United States was conducted to determine the viability of steel fibres as a reinforcement in concrete (Romualdi & Batson, 1963), and as a result, experimentation for the applications of steel fibre reinforced concrete have been conducted since. Steel fibres typically have a high modulus of elasticity and relatively high strength. Due to the alkaline environment of the cementitious matrix, the fibres are generally protected from corrosion. Based on the environmental exposure of the SFRC, different grades of stainless-steel fibres may be used. However, there are minimum strength requirements which the fibres must adhere to (Daniel *et al.*, 2002).

2.1.1.2. Synthetic fibre reinforced concrete (SNFRC)

Synthetic fibres as a construction material were first reported in 1965, providing an effective and relatively inexpensive method of reinforcement for concrete. It is also a replacement for materials such as asbestos and steel fibres. Synthetic fibres were the result of research into the petrochemical and textile industries. They are man-made fibres that are derived from organic polymers. Types of synthetic fibres that have been tested in cement composites include acrylic, nylon, carbon, aramid, polyester, polyethylene and polypropylene (Bentur & Mindess, 1990; Brandt, 2008; Daniel *et al.*, 2002). Synthetic fibres are typically used to improve the strength and toughness in concrete when used in high volumes (0.5-2.0%), but can also be used to control plastic shrinkage cracking of concrete when used in small doses (up to 1.0 kg/m^3) (Brandt, 2008; Buratti *et al.*, 2011; di Prisco *et al.*, 2009).

2.1.1.3. Glass fibre reinforced concrete (GFRC)

The use of glass fibres was introduced in the late 1950s, but it was soon discovered that the ordinary glass fibres used, such as borosilicate E-glass fibres, were attacked and destroyed by the high alkalinity in the cement matrix (Daniel *et al.*, 2002). Although glass fibres possess a high tensile strength and elastic modulus, there was still a serious concern with regards to its durability in alkaline environments. Researchers then found a way to develop alkali-resistant zirconia glass, which provided a measure of resistance to alkali attacks in cement composites (Beaudoin, 1990; Brandt, 2008). The alkali-resistant glass fibres became very popular and a widely used material for glass fibre reinforced concrete (Daniel *et al.*, 2002). GFRC is useful for structures in aggressive environments due to its corrosion resistance. It is also preferred for buildings that house magnetic resonance imaging (MRI) equipment which is sensitive to electromagnetic fields (De Luca, Matta & Nanni, 2010).

2.1.1.4. Natural fibre reinforced concrete (NFRC)

Natural fibres have been utilised for making low-cost construction materials. Materials such as coconut husk, bamboo, sisal, cellulose fibres, and many more are used as natural fibres. Even though natural fibres are cheap, it requires greater skill in procuring, mixing and placing than conventional FRC (Aziz, Paramasivam & Lee, 1981). Natural fibres are also used in cement-based matrices, although they are not as common as steel and synthetic fibres. These fibres are generally used for residential housing, limited to external applications such as roofing and low-cost housing in developing countries. Natural fibres can be divided into two categories: unprocessed and processed natural fibres. Unprocessed fibres are a continuously renewable resource, readily available in many countries. They are obtained using local labour and technology, and at low cost and energy consumption. In contrast, processed fibres require sophisticated manufacturing procedures to extract the fibres. One main disadvantage of natural fibres is the large variation of its properties, which leads to unpredictable concrete properties (Abiola, 2017).

2.1.2. Behaviour of fibres in FRC

2.1.2.1. Fibre bridging behaviour

Since concrete is a brittle material, it exhibits poor tensile strength and resistance to crack propagation (Bentur & Mindess, 1990). As a result, concrete in service is more prone to cracks, which creates easy access routes for deleterious agents, thus resulting in freeze-thaw damage, early saturation, discolouration, and steel corrosion. Due to concrete

being a heterogeneous material, there are also flaws and micro cracks in the material at the interfaces before the application of any external loads. The micro cracks may arise from plastic settlement, shrinkage and thermal strains, bleeding, and from stress concentrations of external restraints (Löfgren, 2005).

Although fibres do not replace the reinforcement in reinforced concrete (RC) – which is used to increase the load-carrying capacity – the fibres provide tensile capacity to allow resistance to cracking, deflection and other serviceability conditions (Bentur & Mindess, 1990; Van Chanh, 2004; Marković, 2006; di Prisco *et al.*, 2009). di Prisco et al. (2009) stated that conventional reinforcement may also be completely substituted with fibres usually for structural elements with a high degree of redundancies, and where the fibres provide a more effective reinforcement system (di Prisco *et al.*, 2009).

Fibres are generally randomly aligned with respect to the cracked surface, but since they are closely spaced, they are better at controlling the cracks (Bentur & Mindess, 1990; Marković, 2006). An effective manner of replicating the fibre bridging behaviour in cracks is by performing single fibre pull-out tests. This is one of the most commonly used test methods to determine the bond strength between the fibre and the surrounding matrix (Ghoddousi *et al.*, 2010; Marković, 2006). Poor bond between the fibre and the surrounding matrix may lead to poor efficiency of the fibres. The better the bond, the more efficient the fibre will be (Karadelis & Lin, 2015; Marković, 2006). Fibres are most efficient during crack bridging when its tensile capacity is used optimally (Marković, 2006).

Bentur & Mindness (2006) suggested that the best way to maximise the fibres' efficiency, without compromising the fresh or hardened properties of FRC was to: (1) use fibres with different geometry to increase the bond, (2) improve the fibre dispersion in the matrix by prior chemical treatment of the fibres, (3) use admixtures to improve the rheology of the mix, and (4) use special mixing and placing techniques to allow for the dispersion of large volumes of fibres.

2.1.2.2. Fibre-matrix interface

The addition of steel fibres to concrete results in a fibre reinforced cementitious composite, where the fibres are bonded to the surrounding matrix by the interfacial transition zone (ITZ). The strength of the ITZ depends on the quality of the materials comprising of the

matrix, which includes the water/cement ratio, properties of the binder, and the inclusion of additives (Cunha, Barros & Sena-Cruz, 2007; Marković, 2006).

The ITZ was found to have significantly lower strength and stiffness in comparison to the bulk cement matrix (Diamond & Huang, 2001). This is attributed to the higher porosity matrix around the fibre, as well as an increase in calcium-hydroxide (CH) crystals, seen in Figure 2.1. During the fresh state, local bleeding around the fibre causes the particles of the cement matrix to be packed inefficiently. This results in an increase in voids, which gets only partially filled with hydration products (Abdallah, Fan & Rees, 2018; Cunha *et al.*, 2007; Marković, 2006).

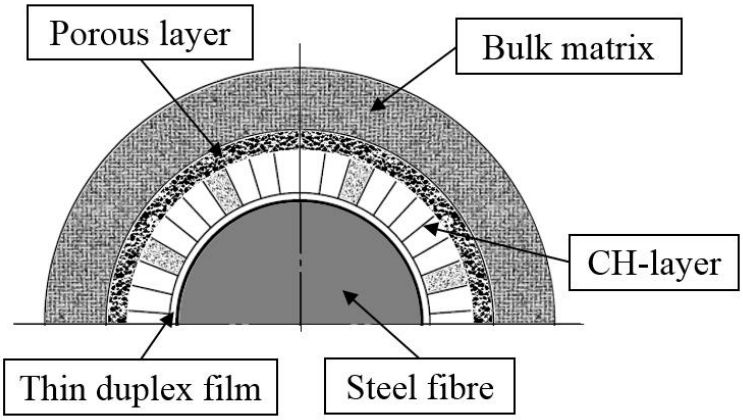

Figure 2.1: Schematic representation of Interfacial Transition Zone (ITZ) (based on Löfgren, 2005)

Various techniques are used to improve the ITZ, which includes improving the size and particle packing of the matrix material, reducing the water/cement ratio, and/or using micro fillers in the matrix (Cunha *et al.*, 2007; Nieuwoudt, 2016). Although the densification of the ITZ is effective, it is not fully effective in increasing the interfacial bond strength between the fibre and the matrix (Abdallah *et al.*, 2018). However, the bond strength can be enhanced by improving the mechanical anchorage of the fibre (Bentur & Mindess, 1990).

2.1.2.3. Fibre bond

The ability of fibres to bond to the cementitious matrix is important since it has a significant influence on the mechanical behaviour of the cement composite (Beaudoin, 1990; Daniel *et al.*, 2002). The characteristics of the fibre-matrix interface are the most

important factors which affect the bond strength (Beaudoin, 1990; Beglarigale & Yazici, 2015; Cunha *et al.*, 2007). The fibre bond is dependent on the aspect ratio of the fibre, which typically ranges from 20 to 100. Fibres come in various shapes and sizes, and the bond to the cementitious matrix can also be improved by mechanical anchorage and increasing the surface roughness of the fibre (Daniel *et al.*, 2002).

Since FRC is a composite material, it resists tensile forces through a composite action. Some of the tensile force is resisted by the matrix, while the rest of the tensile force is resisted by the fibres. The tensile forces are transmitted between the fibres and the matrix through a bond defined as shearing stress at the interface between the fibre and the surrounding matrix (Gopalaratnam & Shah, 1987; Namur *et al.*, 1991). The primary bond mechanisms involved with the fibre pull-out, which also contributes to the ductility of the composite material, are predominantly adhesion, friction, and mechanical interlock (Naaman & Najm, 1991).

The adhesion can be related to the characteristics of the ITZ. It is described as the bond between the fibre and the surrounding matrix and is the first mechanism to be activated during pull-out (Cunha *et al.*, 2007). The interface is only able to sustain small displacements before overcoming the adhesion component and breaking the bond (Naaman, Namur, Alwan, *et al.*, 1991). Once the fibre has fully debonded, frictional stresses are induced due to the abrasion and compaction on the ITZ throughout the fibre slippage cavity (Cunha *et al.*, 2007). The ITZ can be improved and strengthened by mechanical anchorage of the fibre. For steel fibres, it is easily achieved by modifying the shape of the fibre, such as hooked-end fibres, crimped steel fibres, indented fibres, etc.

One of the most commonly used test methods to determine the bond strength is the single fibre pull-out test. Low levels of interfacial shear strength may result in fibre debonding from the matrix and fibre pull-out. Conversely, high interfacial shear stress levels may prevent the complete debonding of fibres from the matrix and cause fibre rupture (Abdallah *et al.*, 2018; Ghoddousi *et al.*, 2010). These are two of the most common fibre failure mechanisms (Beaudoin, 1990).

2.1.3. Influence on the single fibre pull-out behaviour

2.1.3.1. Fibre type

The material which the fibre is made of influences its pull-out behaviour. The material can be natural, such as sisal or bamboo, or it can be man-made, such as glass or steel fibres. Each material type bonds differently to the matrix, thereby influencing the pull-out behaviour. The mechanical properties of the material, which includes the elastic modulus, tensile strength, elongation, etc., may also significantly affect the pull-out behaviour. Based on the type of fibre chosen, its pull-out response can have an infinite number of outcomes, since its physical properties such as its geometry, length, and diameter among others, can be altered accordingly (Cunha *et al.*, 2007). Table 2.1 displays the properties of various fibre materials.

Table 2.1: Various fibre types and their properties (Beaudoin, 1990; Bentur & Mindess, 2006; Daniel *et al.*, 2002; Löfgren, 2005)

Type of fibre	**Diameter [µm]**	**Specific gravity [g/cm^3]**	**Tensile strength [MPa]**	**Elastic modulus [GPa]**	**Ultimate elongation [%]**
Metallic					
Steel	5 - 1 000	7.85	200 - 2 600	195 - 210	0.5 - 5
Glass					
E glass	8 - 15	2.54	2 000 - 4 000	72	3.0 - 4.8
AR glass	8 - 20	2.70	1 500 - 3 700	80	2.5 - 3.6
Synthetic					
Acrylic (PAN)	5 - 17	1.18	200 - 1 000	14.6 - 19.6	7.5 - 50
Aramid (e.g. Kevlar)	10 - 12	1.4 - 1.5	2 000 - 3 500	62 - 130	2 - 4.6
Carbon (low modulus)	7 - 18	1.6 - 1.7	800 - 1 100	38 - 43	2.1 - 2.5
Carbon (high modulus)	7 - 18	1.7 - 1.9	1 500 - 4 000	200 - 800	1.3 - 1.8
Nylon (polyamide)	20 - 25	1.16	965	5.17	20
Polyester (e.g. PET)	8 - 10	1.34 - 1.39	280 - 1 200	10 - 18	10 - 50
Polyethylene (PE)	25 - 1 000	0.96	80 - 600	5	12 - 100
Polyethylene (HPPE)	-	0.97	3 000 - 4 100	80 - 150	2.9 - 4.1
Polypropylene (PP)	10 - 200	0.90 - 0.91	310 - 760	3.5 - 4.9	6 - 15

Polyvinyl acetate (PVA)	3 - 8	1.2 - 2.5	800 - 3 600	20 - 80	4 - 12
Natural – Organic					
Cellulose (wood)	15 - 125	1.5	300 - 2 000	10 - 50	20
Coconut	100 - 400	1.12 - 1.15	120 - 200	19 - 25	10 - 25
Bamboo	50 - 400	1.50	50 - 350	33 - 40	-
Jute	100 - 200	1.02 - 1.04	250 - 350	25 - 32	1.5 - 1.9
Natural – Inorganic					
Asbestos	0.02 - 25	2.55	200 - 1 800	164	2 - 3
Wollastonite	25 - 40	2.87 - 3.09	2 700 - 4 100	303 - 530	-

Gokoz & Naaman (1981) tested the effect of the strain rate on the pull-out behaviour of glass, steel, and polypropylene fibres. The results showed that while straight steel fibres pulled out at all the testing rates, the glass fibres almost always ruptured. The polypropylene fibre results varied depending on the loading rate. Babafemi & Boshoff (2017) reported only pull-out failures for macro-synthetic polypropylene fibres, but attributed the failure mode to the type and properties of the synthetic fibre.

2.1.3.2. Fibre geometry

Depending on the material, the fibre can be manufactured to have various geometries. Fibres may be straight, hooked, crimped, indented, twisted, and more, all of which affects the pull-out behaviour.

Pull-out tests performed on polypropylene fibres were conducted by Singh, Shukla & Brown (2004). The tests were done using straight polypropylene fibres, but due to its poor bond with the matrix, the fibres were indented mechanically to provide better anchorage. The results showed that the increase in surface friction improved the pull-out strength of the fibres to as much as three times that of the straight fibre pull-out strength. However, the mechanically applied indentations resulted in the fibre strength decreasing as the indentations increased.

Banthia, Trottier & Pigeon (1989) performed single fibre pull-out tests on a range of steel fibres from straight to highly deformed geometries. The results showed that straight steel fibres demonstrated a weak resistance to pull-out, since it only required a low applied force to overcome the adhesion or bond between the fibre and the surrounding matrix. Once the

bond was broken, the fibre was pulled out. In contrast, the excessively deformed fibres resulted in fibre rupture or matrix failure instead of fibre pull-out. Hooked-end steel fibres were found to contribute at least 50% more to the total pull-out energy than straight fibres (Qi, Wu, Ma, *et al.*, 2018).

There is a general consensus in the literature that the geometry of fibres may improve the pull out strength compared to straight fibres (Abu-Lebdeh, Hamoush, Heard, *et al.*, 2011; Banthia *et al.*, 1989; Isla, Ruano & Luccioni, 2015; Qi *et al.*, 2018; Singh *et al.*, 2004; Yoo, Park & Kim, 2017; Zīle & Zīle, 2013).

2.1.3.3. Fibre embedment length and diameter

An increase in embedment length and/or diameter is expected to increase pull-out loads. This is, however, predominantly valid for straight fibres. The increased embedment length means a larger portion of the fibre surface area is in contact with the matrix, thereby increasing the bond and pull-out strength (Isla *et al.*, 2015; Yoo *et al.*, 2017). However, for hooked fibres, the hook determines the pull-out strength, and the effect of the embedment length is secondary (Isla *et al.*, 2015). Abdallah, Fan & Zhou (2017) showed similar results, where an increase in embedment length had no significant effect on the maximum pull-out load. Only the pull-out work showed a slight improvement due to the greater fibre surface area in contact with the matrix.

Robins, Austin & Jones (2002) reported that the maximisation of hooked-end steel fibre pull-out loads could only be attained if the fibre embedment length exceeded the length of the fibre hook. If not, the hook would not be fully utilised and only partial straightening of the hook would occur, which results in decreased fibre pull-out load.

The effects of the embedment length, fibre diameter and orientation angle were tested on hooked-end steel fibres with high tensile strength in ultra-high performance concrete (UHPC). The results showed that the fibres with smaller diameters and shorter embedment lengths failed predominantly in fibre rupture under the tested orientation angles. An increase in embedment length and diameter showed complete fibre pull-out and a more ductile response to the different tested angles. A small embedment length coupled with a large diameter resulted in matrix failure (Cao & Yu, 2018).

2.1.3.4. Fibre orientation

The orientation angle of the fibre varies for different fibre geometries. Qi et al. (2018) investigated the effect of changing the fibre orientation angle for straight and hooked-end steel fibres. The results indicated that an orientation angle of 30° and 45° increased the bond strength of straight fibres by 19.2% and 52.9%, and hooked-end fibres by 13.6% and 26.2% respectively. Depending on the orientation angle, the main failure mechanisms were fibre pull-out or rupture failure (Isla *et al.*, 2015; Qi *et al.*, 2018). A further increase in the orientation angle to 60° resulted in a decrease in the maximum pull-out load. However, as the orientation angle increased, the maximum pull-out load occurred at much higher fibre slips (Isla *et al.*, 2015).

Cao & Yu (2018) tested high tensile strength hooked-end steel fibres at varying inclination angles in UHPC. Fibres with small diameters showed similar maximum pull-out loads under the tested orientation angles. When the diameter increased, the pull-out behaviour increased as well. For larger diameter fibres, the optimum orientation angle for the maximum pull-out capacity was 20°.

2.1.3.5. Matrix properties

Since the fibre-matrix bond is influenced by the properties of the ITZ, the matrix properties play a significant role in the pull-out behaviour of fibres. The mechanical properties of the matrix can be determined by its compressive strength, which depends upon various factors, including water/cement ratio, type and quality of cement, fine filler materials, type and dimension of aggregates, etc. (Cunha *et al.*, 2007).

Single fibre pull-out tests were performed using four different steel fibres – two with hooked ends, one flat end and one twisted. The fibres were embedded in ultra-high strength concrete. The results indicated that an increase in matrix strength resulted in increased total pull-out energy and maximum pull-out strength. Increased concrete compressive strength also resulted in fibre rupture failure for some of the specimens, especially the flat end and twisted fibres (Abu-Lebdeh *et al.*, 2011)

Yoo et al. (2017) found that the increased matrix strength improved the bond strength and fibre pull-out work of straight steel fibres more effectively than that of hooked-end fibres. The short straight fibres showed an improvement in the average bond strength, whereas the longer straight fibres improved the pull-out work.

2.1.4. Behaviour under static loading

2.1.4.1. Compressive behaviour

FRC generally displays little to no change in compressive behaviour when compared to plain concrete. For concretes with a normal range of fibre content (< 2.0%), the increase in compressive strength generally ranges from 0% to approximately 25% (Adepegba & Regan, 1981; Arunakanthi & Kumar, 2016). The inclusion of fibres in concrete was however found to improve the concrete toughness. Concrete under compression experiences lateral expansion and the addition of fibres allows for a more ductile concrete, as it bridges the longitudinal cracks shown in Figure 2.2. This confines the lateral expansion, thereby increasing the concrete toughness (Ou, Tsai, Liu, *et al.*, 2012).

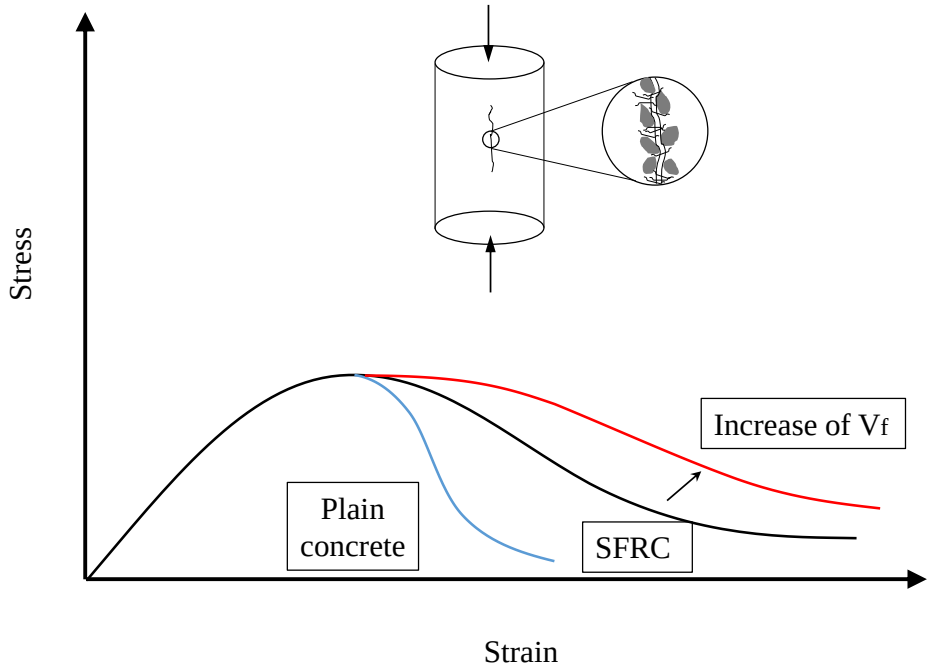

Figure 2.2: Illustration of plain concrete and SFRC behaviour in compression (based on (Löfgren, 2005))

From Figure 2.2, it can be seen how the lateral expansion is bridged by the fibres. An increase in the fibre volume dosage also increases the peak stress. However, the mechanical properties of FRC are dependent on the type of fibres used, the fibre dosage, as well as the properties of the matrix (Bentur & Mindess, 2006; Löfgren, 2005; Ou *et al.*, 2012).

2.1.4.2. Tensile behaviour

Concrete is known to be weak in tension (Akita, Koide, Tomon, *et al.*, 2003; Barr, Asghari & Hughes, 1988; Brandt, 2008). The tensile response of concrete can be obtained with direct tensile tests or by indirect means of tensile splitting tests, both of which come with various limitations (Denneman, Kearsley & Visser, 2011). The tensile behaviour can be classified as either strain hardening or strain softening (Löfgren, 2005).

The post-cracking tensile response may be characterised by non-linear behaviour. During the non-linear phase, the mechanical behaviour of the material may depend on various factors, which includes the shape and size of fibres, fibre characteristics, fibre volume dosage and fibre orientation. External conditions such as the loading application rate, ambient temperature and curing procedures can also affect the mechanical behaviour (Chanvillard, Banthia & Aïtcin, 1990).

As the material reaches its maximum post-cracking strength, failure of the material occurs. due to fibre pull-out, or fibre rupture as a result of stress concentrations. Fibre pull-out is associated with a ductile failure response, whereas fibre rupture failure is generally associated with a brittle failure. Fibre rupture generally occurs when the fibre-matrix bond strength is larger than the strength of the fibre. It is often associated with synthetic fibres, even though it can occur with steel fibres (Bentur & Mindess, 2006; Fantilli *et al.*, 2009).

2.1.4.3. Flexural behaviour

The addition of fibres to concrete provides a significant post-cracking tensile strength, due to the fibres bridging the cracked surfaces (Buratti *et al.*, 2011). The increase in flexural strength depends mainly on the fibre volume, the aspect ratio of the fibres, and the fibre distribution and orientation (Bentur & Mindess, 2006; Stähli, Custer & van Mier, 2008). A larger aspect ratio generally yields better flexural strength results (Bentur & Mindess, 2006). Improved flexural strength has been obtained when using steel fibres, even though fewer fibres are bridging the crack, than when compared to using macro-synthetic fibres (Buratti *et al.*, 2011).

SNFRC can generally be categorised into three groups based on the fibre volume content. Low fibre volume content (< 1.0%) is used mainly to control plastic shrinkage cracking and does not provide any strength improvement. Medium fibre volume content (1.0–2.0%) is generally used for precast elements and does not require special processing methods.

High fibre volume content (>2.0%) may provide improved fracture toughness, enhanced ductility and strain hardening (Soufeiani, Raman, Jumaat, *et al.*, 2016). The fibre volume fraction is generally restricted to 3.0% for normal FRC since higher dosages require special techniques for mixing, placing, etc. Fine fibres are densely dispersed throughout the concrete matrix to reduce shrinkage by controlling the propagation of micro cracks. Larger fibres ranging from 50 to 80 mm in length control the larger cracks and ultimately contribute to the increase in the overall final strength of FRC (Brandt, 2008; di Prisco *et al.*, 2009). This is illustrated in Figure 2.3, where the fine fibres, also referred to as micro fibres, bridge the micro cracks under a tensile load P. Similarly, the larger fibres are responsible for bridging the larger cracks.

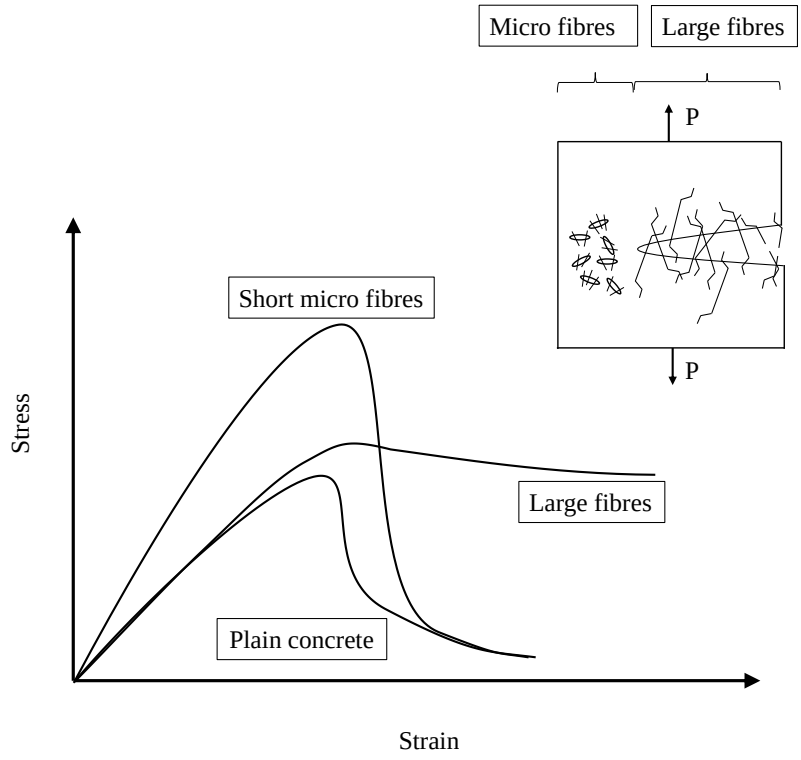

Figure 2.3: Various fibres bridging cracks (adapted from (Betterman, Ouyang & Shah, 1995))

The real contribution of fibres to concrete is to increase the toughness of the concrete under any given load (Van Chanh, 2004). High-modulus fibres can be used to increase the concrete toughness for structural applications and can be used to substitute conventional reinforcement partially or completely (Brandt, 2008; di Prisco *et al.*, 2009).

2.1.4.4. Post-cracking behaviour

In general, all FRC composites can be classified according to their post-cracking behaviour. Figure 2.4 illustrates the array of post-cracking classifications based on the tensile response of the composite. The first key classification is whether the composite displays tensile strain hardening or strain softening. The second classification can be further subdivided into deflection hardening and deflection softening (Naaman & Reinhardt, 2006).

Strain hardening composites generally perform better mechanically, displaying a significant improvement in the behaviour of seismic resistance of structures subjected to reversed loading. Furthermore, its impact and blast resistance are also improved. The deflection hardening composites under the strain softening classification, are better suited to structural applications where bending dominates. The deflection softening composites can be used for a wide range of applications, including the control of plastic shrinkage cracks, concrete pavements and slabs on grade (Naaman & Reinhardt, 2006).

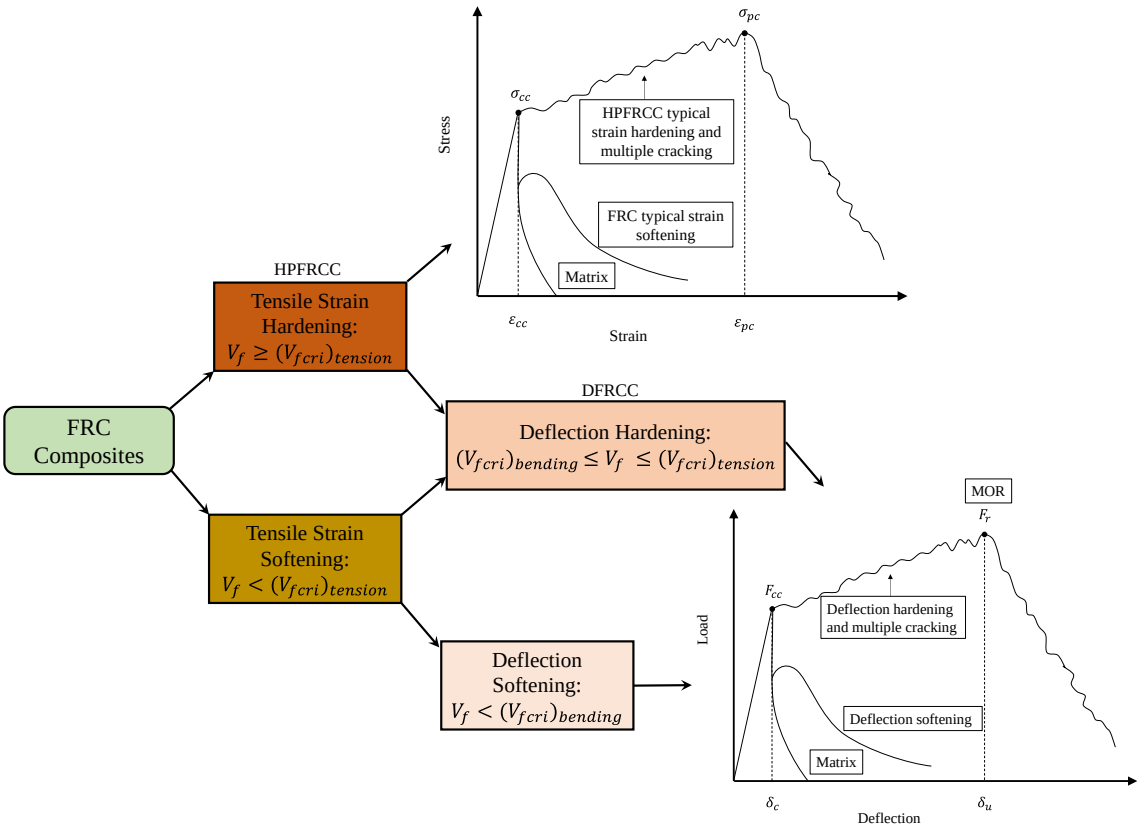

Figure 2.4: FRC composite classification based on tensile stress-strain response (from (Naaman & Reinhardt, 2006))

The fib Model Code (2010) further characterises the post-cracking residual tensile strength of FRC materials in three-point bending by their load-CMOD relationship as shown in Figure 2.5. The post-cracking residual strengths that are significant for service (f_{R1k}) and ultimate (f_{R3k}) conditions are considered, and determined as follows:

$$f_{R,j} = \frac{3F_j l}{2bh_{sp}^2} \tag{2.1}$$

Where:

f_{Rj} – is the residual flexural tensile strength corresponding with CMOD = $CMOD_j$

F_j – is the load corresponding with CMOD = $CMOD_j$

l – is the span length (mm)

b – is the width of the specimens (mm)

h_{sp} – is the distance between the notch tip and the top of the specimen (mm), 125 mm

The strength interval (f_{R1k}) of the post-cracking strength is classified using two subsequent numbers in the following series:

1.0, 1.5, 2.0, 2.5, 3.0, 4.0, 5.0, 6.0, 7.0, 8.0 [MPa]

While the letters *a*, *b*, *c*, *d* correspond to the residual strength (f_{R3k}/f_{R1k}) ratios:

a if $0.5 \leq (f_{R3k}/f_{R1k}) \leq 0.7$

b if $0.7 \leq (f_{R3k}/f_{R1k}) \leq 0.9$

c if $0.9 \leq (f_{R3k}/f_{R1k}) \leq 1.1$

d if $1.1 \leq (f_{R3k}/f_{R1k}) \leq 1.3$

e if $1.3 \leq (f_{R3k}/f_{R1k})$

The designer should specify the class, residual strength ratio and the material of the fibre when classifying the post-cracking residual strength.

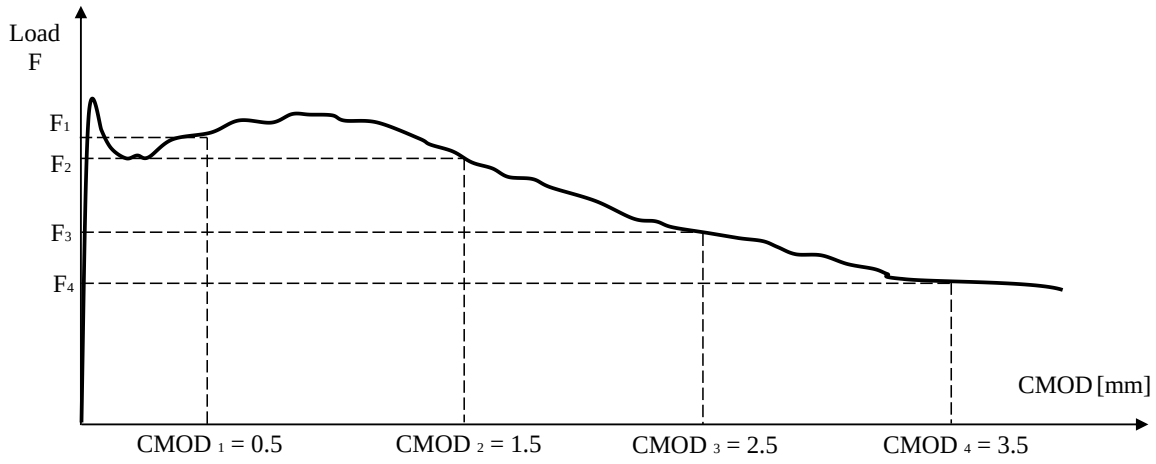

Figure 2.5: Typical load-CMOD diagram (j = 1,2,3,4) (adapted from fib Model Code (2010))

2.2. Fatigue of materials

2.2.1. Introduction to fatigue

According to the ACI 116R (Farzam *et al.*, 2000), fatigue refers to the permanent alteration and weakening of a materials' properties due to the application of repetitive stress cycles. The internal structural changes in concrete are associated with the progressive growth of internal micro cracks (Bathias & Pineau, 2010; Keerthana & Chandra Kishen, 2018; Lee & Barr, 2004; Parvez & Foster, 2017). The continuous exposure to cyclic loading results in a decrease in stiffness, which may lead to fatigue failure (Lee & Barr, 2004).

Fatigue failure is responsible for a large portion of all mechanical failures (Stephens, Fatemi, Stephens, *et al.*, 2000). Fatigue failures are almost always unexpected and can be catastrophic. The damage from fatigue costs the engineering industry several percent of the gross domestic product (Anderson, 2017; Bathias & Pineau, 2010; Stephens *et al.*, 2000). It involves a complex interaction between time, load, and environment. The loading may be cyclic, steady, variable, uniaxial or multiaxial. The duration of the loading could range from seconds, as in firing a handgun, or it could span over many years, such as in steel bridges (Stephens *et al.*, 2000).

The first major cases involving fatigue failure occurred during the 1840s, when the railway industry experienced failures due to repeated stresses (Stephens *et al.*, 2000). This type of failure was of great importance during the development of rail transportation (Bathias & Pineau, 2010). Fatigue failure also affected many other mechanical structures such as

aircrafts, vehicles, ships and many more. During the 1850s, laboratory fatigue tests under repeated stresses were conducted by August Wöhler in Germany. The tests focused on the railway axle failures, and was considered to be the first systematic investigation of fatigue. Wöhler discovered that the fatigue life decreased with an increase in the stress amplitude, and that below a certain amplitude, test specimens did not fail (Stephens *et al.*, 2000). The fatigue life is generally illustrated on a stress-versus-number of cycles (S-N) diagram as shown in Figure 2.6. The S-N curve illustrates the relationship between the maximum applied stress (S), and the number of load cycles (N), which causes failure (Oh, 1986).

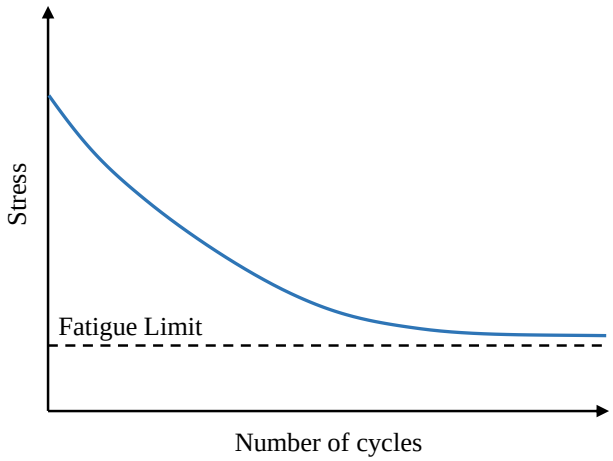

Figure 2.6: General S-N curve

2.2.2. Fatigue loading

Fatigue loading can generally be divided into two categories: low-cycle loading and high-cycle loading, which directly refers to the range of loading. The low-cycle loading comprises of a few load cycles applied at high stress levels, and the high-cycle loading has a large number of cycles at lower stress levels (Lee & Barr, 2004). Table 2.2 indicates the various fatigue loadings, along with its common applications. Structures which are subjected to earthquakes may undergo several hundred or thousand load cycles, according to Lee & Barr (2004) and Hsu (1981), and are classified as low-cycle fatigue. Airport pavements are generally designed for a moderate number of load cycles, whereas concrete pavements are subjected to millions of cycles throughout its lifespan due to the repeated axle loadings of automobiles and larger heavy goods vehicles (HGV). Both applications are classified as high-cycle fatigue loadings (Hsu, 1981; Lee & Barr, 2004; Zhang *et al.*,

2000). Super high-cycle fatigue loading is attributed to mass rapid transit systems and sea structures, which are continually subjected to loading (Hsu, 1981; Lee & Barr, 2004).

Table 2.2: Types of fatigue loadings (Hsu, 1981; Lee & Barr, 2004)

Low-cycle fatigue	**High-cycle fatigue**		**Super high-cycle fatigue**	
$1 – 10^3$	$10^3 – 10^5$	$10^5 – 10^7$	$10^7 – 10^8$	10^9
Structures subjected to earthquakes	Airport pavements and bridges	Highway and railway bridges, highway pavements	Mass rapid transit structure	Sea structures

2.2.2.1. Loading rates

Concrete behaviour can vary when tested under static loads as compared to dynamic loads. Dynamic tests performed by Fu, Erki & Seckin (1991) on concrete in compression found that the compressive strength, as well as the concrete stiffness, increased as the strain rate increased. Furthermore, concrete tested at high strain rates resulted in explosive failures (Fu *et al.*, 1991). Compressive fatigue tests conducted by Graf & Brenner (1934) showed that the fatigue behaviour had no change in behaviour within a frequency range of 4.5 Hz to 7.5 Hz. There was, however, a decrease in the fatigue life as the frequency decreased below 0.16 Hz as it resulted in fatigue creep.

Compressive fatigue tests were conducted on plain and fibre reinforced concrete (Medeiros *et al.*, 2015). Two types of fibres were used, including 40 mm polypropylene fibres and 35 mm hooked end steel fibres with loading frequencies ranging from 1/16 Hz, 1/4 Hz, 1.0 Hz to 4.0 Hz. The results showed that the fatigue compressive behaviour was highly influenced by the loading frequency. This was more significant for the plain concrete than the FRC. As the loading frequency decreased, the number of cycles to failure decreased as well. The addition of fibres provided an improvement in the fatigue life, especially at the lower frequencies (< 4.0 Hz), since the fibres inhibited the crack growth during the fatigue loading (Medeiros *et al.*, 2015).

2.2.2.2. Stress application range

Fatigue loading can also be conducted under various stresses, as displayed in Figure 2.7, and it is dependent on the values of the mean stress σ_m or the alternating amplitude stress σ_a. The amplitude of the maximum stress (σ_{max}) during a single cycle can be termed as

uniaxial loading. The stress ratio (R) is the ratio of the minimum stress to the maximum stress. The following criteria can then be used to differentiate between the fatigue stresses (Bathias & Pineau, 2010).

- fully reversed: $\sigma_m = 0$, $R = -1$;
- asymmetrically reversed: $0 < \sigma_m < \sigma_a$, $-1 < R < 0$;
- repeated tension: $R = 0$;
- alternating tension: $\sigma_m > \sigma_a$, $0 < R < 1$.

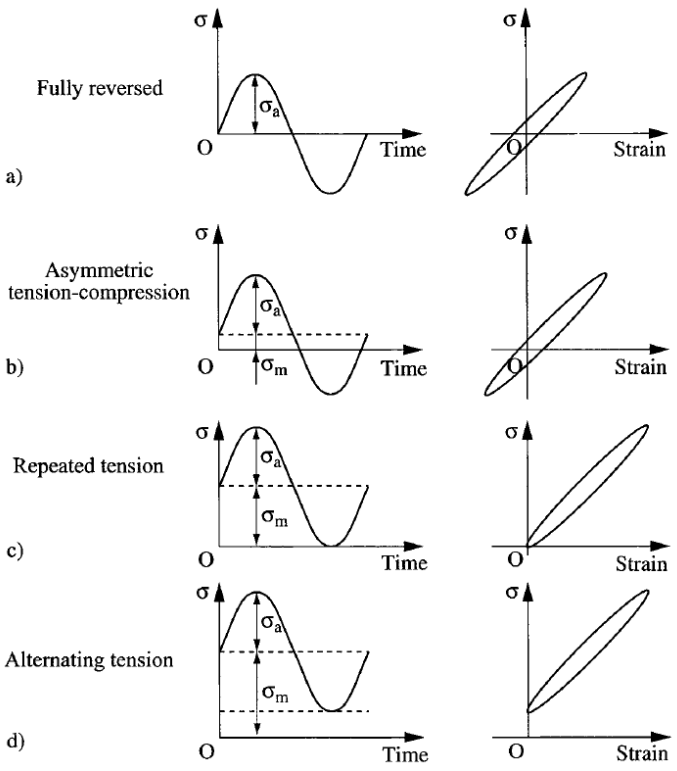

Figure 2.7: Various types of fatigue stresses under constant amplitude loading (Bathias & Pineau, 2010)

The fully reversed fatigue stress in Figure 2.7 (a) is loaded in both tension and compression, with the mean stress equal to zero. The asymmetric tension-compression in Figure 2.7 (b) is loaded partly in compression, with a majority tensile loading. The repeated tension loading in Figure 2.7 (c) is loaded in complete tension, with a minimum stress of zero. The alternating tension loading in Figure 2.7 (d) is in complete tension and has a non-zero value for the minimum stress (Bathias & Pineau, 2010).

The fatigue behaviour under constant amplitude and variable amplitude can vary significantly. In the case of constant amplitude loading, the crack propagation depends mainly on the applied loading and the crack size, whereas for variable amplitude loading, the crack propagation depends on the loading history. Sudden load increases in variable amplitude loading may increase the size and density of microcracks or drastically accelerate the crack size of the concrete, especially plain concrete (Keerthana & Chandra Kishen, 2018).

There are also other forms of damage due to indirect fatigue stresses, some of which include corrosion fatigue and thermal fatigue. Corrosion fatigue occurs when the material is subjected to a corrosive environment, in addition to an applied fatigue loading and could result in a shorter lifespan of the material. The environment to which the material is exposed to plays a vital role in the acceleration of the fatigue failure. Thermal fatigue occurs as a result of a material exposed to a constant variation in temperature gradient, which results in induced cyclic stresses. With the continuous expansions and contractions, the fatigue process could be accelerated (Bathias & Pineau, 2010).

2.2.3. Fatigue of plain concrete

Concrete is a widely used material and it is typically subjected to repeated loadings over its lifespan. As a result, the occurrence of fatigue is very common in many concrete structures, including concrete highway pavements, airport runways, railway bridges, etc. (Bhowmik & Ray, 2018; Chen, Bu, Fan, *et al.*, 2017). The continuous loading results in a steady decrease in the stiffness of the structure, which could lead to fatigue failure (Kolluru, O'Neil, Popovics, *et al.*, 2000; Lee & Barr, 2004).

The fatigue strength of concrete is defined as the percentage of static strength which the concrete is able to sustain repeatedly for a predetermined number of cycles. The fatigue strength depends on the rate of loading, material properties, range of stresses, loading history, loading eccentricity and environmental conditions. For unreinforced concrete, it was found that the fatigue life under tension, compression or flexure, at 10 million cycles is approximately 55% of the static strength (Hanson, Ballinger & Linger, 1974).

The results obtained from fatigue tests generally exhibit a significant scatter when compared to static tests (Hanson *et al.*, 1974; Naaman & Hammoud, 1998; Nanni, 1991; Singh & Kaushik, 2003). As a result, probabilistic procedures are implemented to account

for the inherently varying nature of fatigue test results. Given the loading conditions and number of cycles, the probability of failure may be predicted, and S-N curves for varying various probabilities of failure may be plotted (Hanson *et al.*, 1974).

Banjara & Ramanjaneyulu (2018) performed flexural fatigue tests on plain and fibre reinforced concrete at various load levels, which included 65%, 75% and 85% of the ultimate static loading, at a frequency of 5 Hz. The results in Figure 2.8 (a) showed that at the 65% load level, the specimens were able to withstand a large number of load cycles before failure. The load cycles decreased as the load level increased to 75% in Figure 2.9 (a). At the 85% load level in Figure 2.10 (a), the fatigue capacity decreased drastically. Furthermore, the stiffness degradation in Figure 2.8 (b), Figure 2.9 (b) and Figure 2.10 (b) show that the stiffness degradation occurs at a slower rate at the lower load level. At the 85% load level, the stiffness decreased very rapidly until failure.

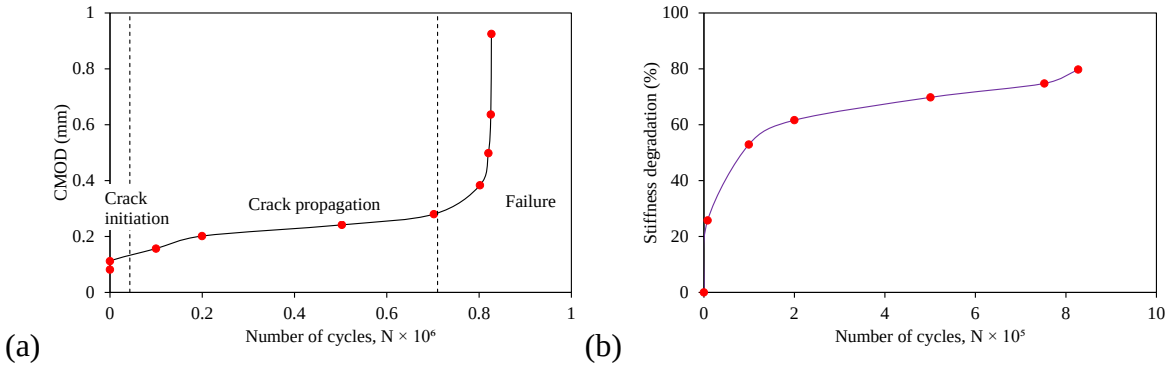

Figure 2.8: Fatigue behaviour of plain concrete under 65% load level (a) CMOD versus number of cycles (b) Stiffness degradation (from (Banjara & Ramanjaneyulu, 2018))

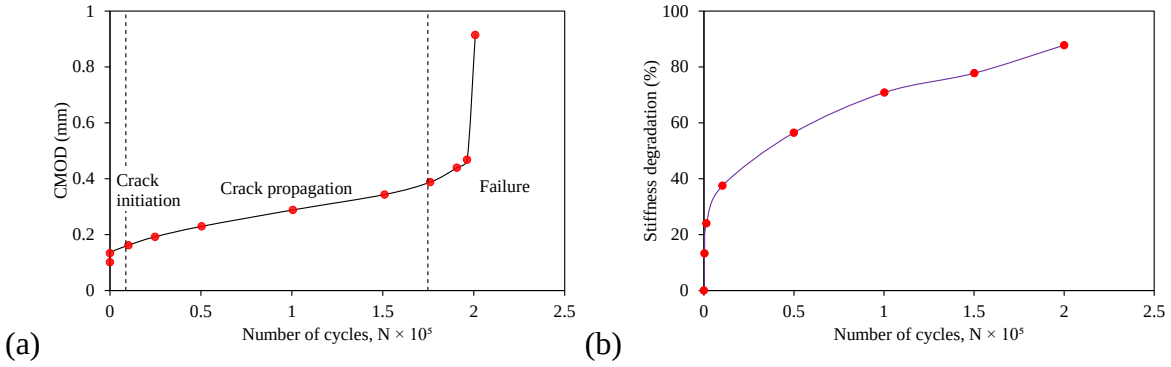

Figure 2.9: Fatigue behaviour of plain concrete under 75% load level (a) CMOD versus number of cycles (b) Stiffness degradation (from (Banjara & Ramanjaneyulu, 2018))

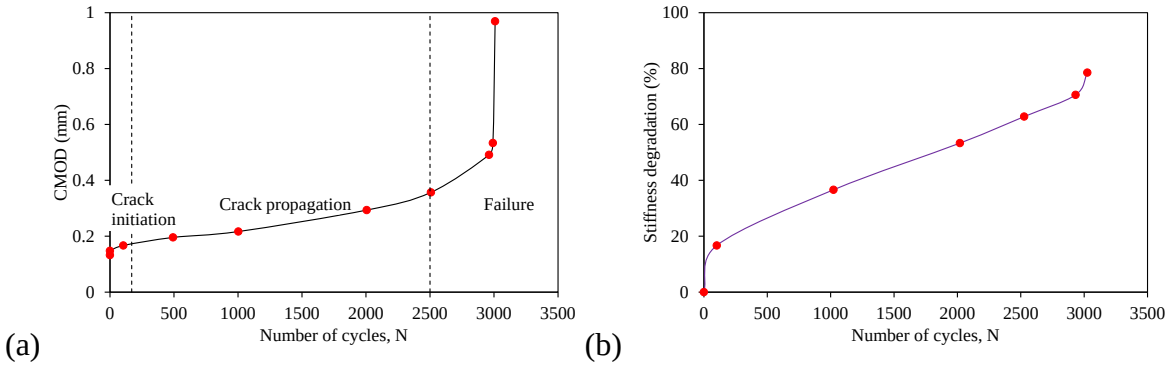

Figure 2.10: Fatigue behaviour of plain concrete under 85% load level (a) CMOD versus number of cycles (b) Stiffness degradation (from (Banjara & Ramanjaneyulu, 2018))

Chen et al. (2017) performed tensile fatigue tests on plain concrete and reported a decrease in the stiffness degradation under fatigue loading at higher load levels. The loading frequency however had no influence on the stiffness loss during the fatigue loading. Do, Chaallal & Aïtcin (1993) reported a smaller stiffness degradation for high strength concrete than for normal concrete.

2.2.4. Flexural fatigue of FRC

In conventional concrete subjected to bending, the fatigue failure may occur either in tension of the reinforcing steel, or in compression of the concrete. However, the general applications of concrete subjected to fatigue loading, such as highway and airport pavements, are usually unreinforced, and the concrete is required to resist the tension in bending (Singh & Kaushik, 2000). To overcome this, fibres may be added to the concrete mix to aid in the tensile resistance and retard crack growth (Mailhot *et al.*, 2001). The addition of fibres to concrete may significantly improve the flexural fatigue strength and endurance limit. However, the extent of improvement depends on the fibre dosage, fibre type, and fibre geometry, among others. Based on the combination of the abovementioned parameters, the fatigue behaviour may vary (Nanni, 1991).

Mailhot et al. (2001) performed research on the flexural fatigue behaviour of SFRC at varying load levels. Various types of steel fibres were tested, which included hooked-end, nail-anchored, and crimped fibres. The results showed a large degree of variability. The fatigue life of specimens tested at high load levels was very poor, whereas at the lower load levels, the fatigue life was able to exceed 80% of the overall life-cycle. The recommendation was to increase the fibre volume dosage to more than 40 kg/m^3 to decrease the variability of the fatigue life.

The influence of the fibre dosage, aspect ratio and fibre type was investigated by Johnston & Zemp (1991). The fibre dosage ranged from 0.5% to 1.5%, with aspect ratios between 47 and 100, and four different types of fibres. S-N relationships were plotted based on the percentage of the first crack strength under static loading, as well as the ultimate strength under static loading. Due to the small difference between the first crack strength and the ultimate strength, the difference in the S-N relationships were very small. The fibre dosage was the governing factor which affected the S-N relationships, followed by the aspect ratio and fibre type, respectively. The 1.0% fibre dosage with aspect ratio greater than 70 performed best in terms of stress as a percentage of the first crack strength. When considering the actual applied flexural stress, the 1.5% dosage coupled with a fibre aspect ratio of 75 performed best. An aspect ratio of greater than 75 did not further improve the fatigue behaviour.

Germano, Tiberti & Plizzari (2016) performed flexural fatigue tests on pre-cracked specimens with 0.5% and 1.0% fibre dosage, containing one type of hooked-end steel fibre. The maximum load levels applied varied between 65% and 85% of the mean maximum static load. As a constant load amplitude of 50% was maintained throughout all the fatigue tests, this meant that the lower load limit varied accordingly. At higher load levels, the effects of the fibres were more pronounced when compared to plain concrete. At lower load levels the benefits provided by the fibres were significantly diminished. In Figure 2.11 (a), crack opening range (ΔCMOD) over the fatigue life is compared with the CMOD vs load in Figure 2.11 (b). The crack opening increment per cycle (dCMOD/dn) is initially constant and the CMOD grows gradually until the envelope curve is reached at point $CMOD_e$. Once it passes this point, dCMOD/dn increases rapidly until failure. The combination of the ΔCMOD and the dCMOD/dn is said to govern the fatigue life, with the dCMOD/dn being the dominating factor.

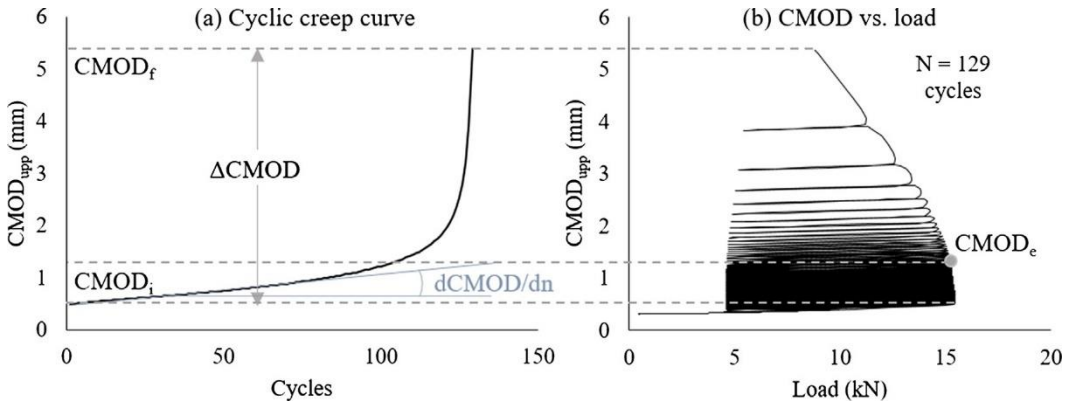

Figure 2.11: Flexural fatigue CMOD behaviour (a) cyclic creep, (b) CMOD vs load (Carlesso *et al.*, 2019)

Various researchers (Germano *et al.*, 2016; Johnston & Zemp, 1991; Jun & Stang, 1998; Singh & Kaushik, 2000) agree that the optimum fibre dosage for improved flexural fatigue behaviour of FRC is in the order of 1.0%. Increasing the fibre dosage past this optimum dosage proved to have no significant improvement on the fatigue behaviour. According to Germano et al. (2016), a fibre dosage of 0.5% may be sufficient to enhance the fatigue life of FRC in certain cases. Further research on the flexural fatigue of FRC can be found by (Banjara, Ramanjaneyulu, Sasmal, *et al.*, 2016; Carlesso *et al.*, 2019; Gettu & Stephen, 2020; Goel, Singh & Singh, 2012; Lee & Barr, 2004; Nanni, 1991).

2.2.5. Crack initiation and propagation

The failure of concrete is a complex phenomenon, due to its multiphase and multiscale nature (Shah, Swartz & Ouyang, 1995; Simon & Kishen, 2016). The mechanisms of fatigue failure of concrete or mortar can be divided into three levels, namely the micro, meso and macro (Wittmann, 1989).

Level one – the micro level comprises the initial defects within the concrete or mortar, and is termed flaw initiation, see Figure 2.12. The micro level consists of the hardened cement matrix. At this level, the main inhomogeneity considered are pores with a maximum size of 10^{-1} mm. These pores may have a variety of different sizes and shapes. As a result of the geometry, cracks may arise due to stress concentrations. Cracks may also occur as a result of shrinkage stress in the unloaded specimen (Zaitsev & Wittmann, 1981).

The second level – meso level – is termed micro cracking, which involves the slow and progressive growth of the defects to a crucial size. At this level, the concrete consists of the matrix, aggregate and the matrix-aggregate interface. The microcracks form at the

matrix-aggregate interface due to bond failure between the coarse aggregate and the matrix as shown in Figure 2.12. This results in the deterioration of the concrete (Zanuy, Albajar & de la Fuente, 2011). At this level, there are already a large number of pre-existing cracks prior to any external load application (Wittmann, 1989).

At the last level – macro level – the concrete material behaviour may be influenced by spatial distribution, geometry, and individual material properties of the mix constituents (Simon & Kishen, 2016). At this level, the microcracks converge to form macrocracks, which ultimately cause specimen failure. Substantial material deterioration occurs at this level (Batson, Ball, Bailey, *et al.*, 1972; Gao & Hsu, 1999; Zanuy *et al.*, 2011).

The rate of fatigue crack growth can be divided into three stages – deceleration stage, followed by a steady state stage, and finally the accelerated stage, see Figure 2.13. During the first stage, the rate of crack growth decreases as the crack length increases and is followed by the steady state stage where the crack length increases gradually. At the acceleration stage, the crack growth rate increases up to failure (Bhowmik & Ray, 2018; Zandi Hanjari, 2006).

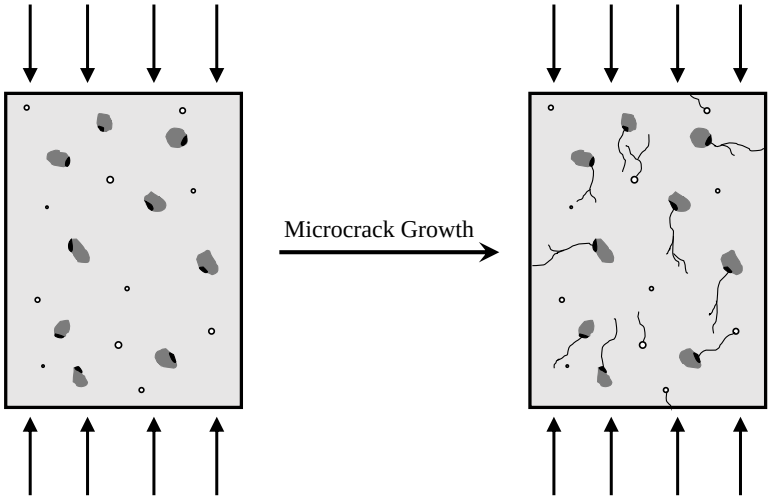

Figure 2.12: Microcrack propagation at the matrix-aggregate interface (adapted from (Zanuy *et al.*, 2011))

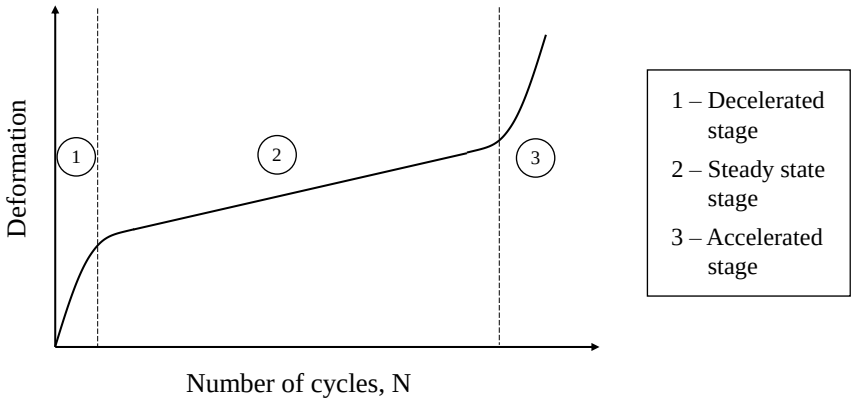

Figure 2.13: Fatigue crack growth schematic (from (Zandi Hanjari, 2006) based on (Lee & Barr, 2004))

2.2.5.1. Aggregate bridging

The tensile cracking zone in concrete is dominated by complicated mechanisms due to concrete being a heterogeneous material. The crack formation in concrete when subjected to tensile stresses arises from the development of microcracks as alluded to in the previous section. Various mechanisms are involved in the plain concrete fracture process, which includes (see Figure 2.14): (a) crack shielding, (b) crack deflection, (c) aggregate bridging, (d) crack surface roughness-induced closure, (e) crack tip blunted by void, and (f) crack branching. These mechanisms are referred to as toughening mechanisms (Shah *et al.*, 1995).

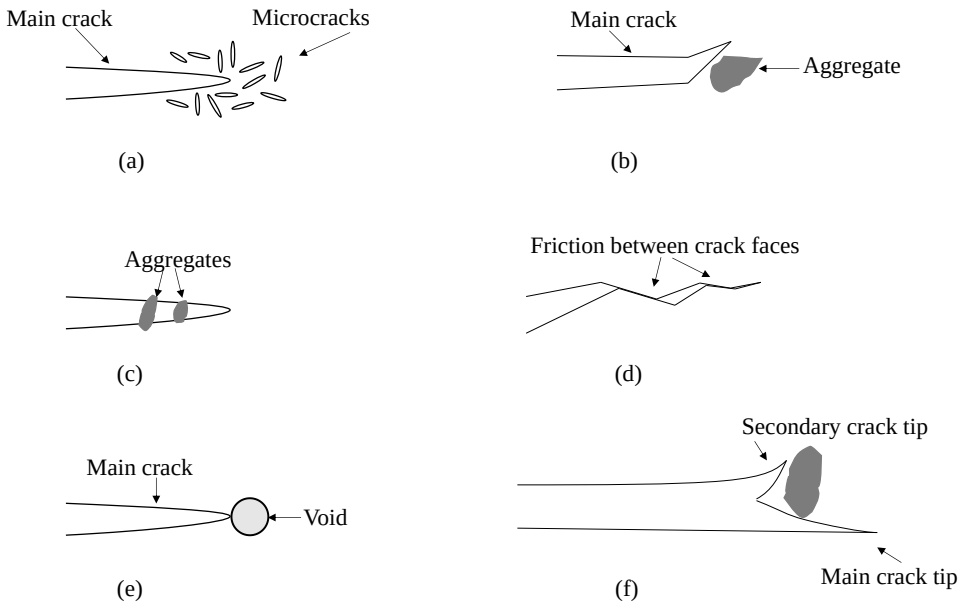

Figure 2.14: Toughening mechanisms in plain concrete fracture zone (Shah *et al.*, 1995)

For plain concrete, aggregate bridging is a major toughening mechanism and therefore, the characteristics of the aggregates are important, especially for the stress-crack opening relationship. Some of the important aggregate characteristics include the stiffness and strength, surface texture, grading, shape, and content. The characteristics of the cement and supplementary materials also influence the aggregate bridging behaviour (Löfgren, 2005). Numerous researchers have investigated the effects of aggregates in concrete (Buyukozturk & Hearing, 1998; Van Mier, 1991; Tasdemir & Karihaloo, 2001; Wu, Chen, Yao, *et al.*, 2001).

2.2.5.2. Fibre bridging

In FRC, the bridging ability of fibres is activated at crack initiation when the fibres start contributing to the load-carrying capacity. The load is then transferred from the concrete matrix to the fibres at the fibre-matrix interface (Beaudoin, 1990; Ghoddousi *et al.*, 2010; Namur *et al.*, 1991).

When fibres are properly bonded, they interact with the hardened matrix at the micro crack level to effectively bridge cracks. This provides a medium for the transfer of stress, which delays the merging and growth of cracks. An increase in the tensile strength of the matrix may be experienced if the fibre volume fraction is sufficiently high (Van Chanh, 2004; Ghoddousi *et al.*, 2010).

FRC's mechanical behaviour is not only dependent on the fibre orientation and volume dosage, but also to a large extent, on the pull-out behaviour of the embedded fibres. When a crack forms in concrete, and advances towards an individual fibre, various mechanisms may come into play and contribute to the energy dissipation. These include: (1) matrix fracture, (2) fibre-matrix interface debonding, (3) fibre pull-out, (4) fibre rupture, and (5) fibre abrasion and plastic deformation of the fibre (Löfgren, 2005). The individual fibre pull-out behaviour has been extensively investigated by various researchers (Banthia *et al.*, 1989; Ghoddousi *et al.*, 2010; Naaman *et al.*, 1991; Namur *et al.*, 1991; Sujivorakul, Waas & Naaman, 2000).

For straight, single fibre pull-out behaviour, there is usually gradual debonding at the fibre-matrix interface, followed by frictional slip, and eventually fibre pull-out (Löfgren, 2005). However, for hooked-end fibres, the behaviour is more complex due to the mechanical anchorage of the fibre hooks. As the fibre pulls out from the surrounding

matrix, the bond between the fibre and the matrix gradually breaks. The illustration in Figure 2.15 depicts the partial debonding stress distribution of a fibre. Once the bond shear stress reaches its maximum value (τ_{max}), it implies that the adjacent matrix has already debonded from the fibre. The interfacial shear stress at this debonded region remains constant and equal to τ_f (Ghoddousi *et al.*, 2010).

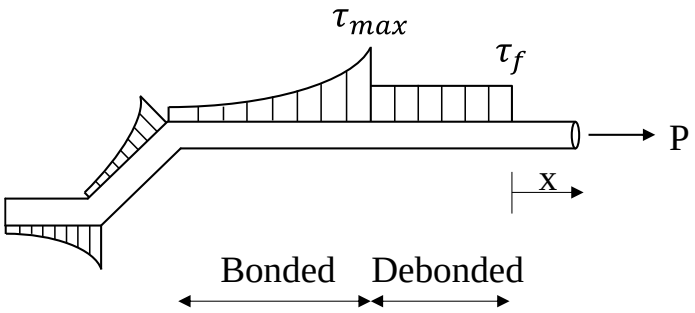

Figure 2.15: Stress distribution for partial debonding of hooked-end fibre (from (Ghoddousi *et al.*, 2010))

The single fibre pull-out behaviour of a hooked-end steel fibre is illustrated in Figure 2.16. Five regions categorise the pull-out behaviour as the fibre moves from completely embedded in the matrix, to fibre pull-out. In Figure 2.16, the ascending branch OA, is associated with the fibre debonding from the surrounding matrix, until full debonding occurs (AB). Part BC occurs when the fibre hook begins to straighten out. Once the mechanical anchorage begins to slip and the second hook of the fibre begins to straighten, the second peak at D is reached. Finally, after the second hook straightens out (DE), and the mechanical anchorage has been pulled out, the frictional decay occurs (EF).

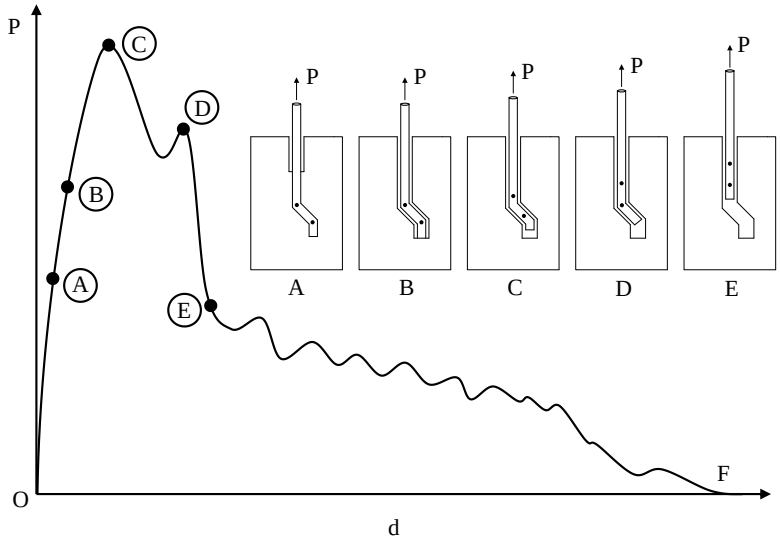

Figure 2.16: Typical fibre pull-out relationship between fibre end slip and load (based on (Deng, Ding, Chi, *et al.*, 2018; Ghoddousi *et al.*, 2010; Löfgren, 2005))

The behaviour of straight fibres differs from that of hooked-end fibres and the models used to predict the pull-out behaviour of hooked-end fibres are more complex, since it is dominated by the mechanical anchorage (Cunha *et al.*, 2007). Models to predict the pull-out behaviour of hooked-end fibres have been developed by Ghoddousi et al. (2010), Cunha et al. (2007), and Deng et al. (2018).

2.2.5.3. Combined aggregate and fibre bridging

In plain concrete, the aggregates play a role in crack bridging, albeit a relatively short working range. When fibres are added to concrete, they act as an additional bridging mechanism. The addition of fibres can increase the fracture energy and critical crack opening by a factor larger than 10 (Groth, 2000). The addition of fibres does not affect the linear-elastic behaviour of concrete, but it does affect the post-cracking behaviour. During the post-cracking behaviour of FRC, the maximum fibre bridging stress depends on the parameters described for the single fibre pull-out, as well as additional effects due to random fibre orientation (Löfgren, 2005). During the fracture process of FRC, there is a combined bridging behaviour from the aggregates and the fibres, as shown in Figure 2.17. As the crack opens, there are three distinct zones which describe the behaviour: (1) the large crack openings where there exists a traction free zone, (2) the bridging zone, where fibres and aggregates work to inhibit crack growth, and (3) the macrocrack and microcrack growth zone.

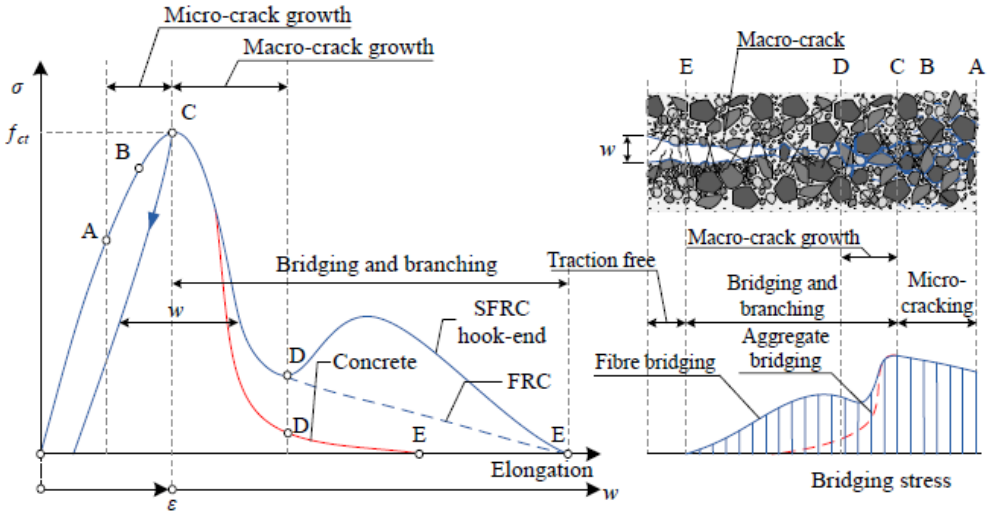

Figure 2.17: Schematic representation of the effect of fibres on the fracture process in uniaxial tension (based on (Löfgren, 2005))

In Figure 2.17, the stress-crack relationship is described schematically, and it is dependent on the fracture properties of the concrete. The stress-crack opening response begins at the descending branch (CD) for small crack openings, where $w < 0.1$ mm. The fibre bridging activity occurs gradually and contributes significantly only once the crack opening has reached at least 0.05 mm. Based on the fibre characteristics, the descending branch (DE) will gradually decrease to zero as the fibre slip increases. However, for fibres with mechanical anchorage, there will be an additional ascending branch where the stress increases due to the deformation and straightening of the mechanical anchorage. Eventually, the stress will decrease until zero (Löfgren, 2005).

2.3. Fatigue life prediction

The fatigue life prediction of plain concrete and FRC have been mainly done empirically. Lengthy fatigue tests are performed and the test data is usually presented as Wöhler curves, also known as S-N curves (Carlesso *et al.*, 2019; Lee & Barr, 2004). This is the most widely accepted approach in engineering practice. Goodman diagrams are also used, which represent the effects of minimum stress in the loading cycles. The abovementioned fatigue curves provide a graphical representation of the fatigue behaviour for various loading parameters (Lee & Barr, 2004).

Numerical simulations have also been developed and performed in order to predict the fatigue life of concrete. Finite element modelling (FEM) is generally employed to predict

the fatigue life. Although it is more demanding, it does provide insight into the fundamental underlying physical behaviour (Lee & Barr, 2004). The fracture mechanics approach may be incorporated into FEM. Various parameters or models may be required for FEM, which include material models, fatigue damage models, crack length, and stress intensity factor, among others (Banjara & Ramanjaneyulu, 2018). Literature discussing FEM of concrete under fatigue loading has been published by (Dobromil, Jan & Radomir, 2010; Hatzigeorgiou, Beskos, Theodorakopoulos, *et al.*, 2001; Wang, Shen & Ma, 2012).

Statistical modelling may also be incorporated into fatigue life prediction. This is usually used to incorporate fatigue failure probability into S-N curves (Singh & Kaushik, 2000). The probabilistic approach is required to ensure that the prediction of fatigue life remains consistent (Carlesso *et al.*, 2019; Do *et al.*, 1993). Statistical modelling may use various approaches, however, for mathematical convenience, the logarithmic-normal (lognormal) distribution function is generally used. The Weibull distribution is another approach which is preferred for the statistical description of fatigue data, since the Hazard function of the lognormal distribution violates the physical occurrence of the progressive deterioration of materials during the fatigue process (Carlesso *et al.*, 2019).

Various S-N expressions have been developed by researchers to estimate the fatigue life of plain concrete and FRC and are described in Sections 2.3.1 and 2.3.2.

2.3.1. Expressions describing the fatigue life of plain concrete

Aas-Jakobsen's S-N expression:

Aas-Jakobsen (1970) developed the S-N equation for plain concrete as shown in Equation (2.2).

$$\frac{\sigma_{max}}{f_s} = 1 - (1 - R)\beta \log N \tag{2.2}$$

Hsu's S-N expression:

Hsu (1981) incorporated the effects of loading frequency on compression fatigue behaviour and developed two equations by modifying Equation (2.2). Equation (2.3) was developed for low-cycle fatigue ($N < 10^3$), such as structures which are subjected to earthquakes. Equation (2.4) was developed for high-cycle fatigue ($10^3 < N < 10^7$), such as airport pavements, highways, and bridges.

Low-cycle fatigue:

$$\frac{\sigma_{max}}{f_s} = 1 - 0.0662(1 - 0.556R)\log N - 0.0294\log T \quad (2.3)$$

High-cycle fatigue:

$$\frac{\sigma_{max}}{f_s} = 1.20 - 0.20R - 0.133(1 - 0.779R)\log N - 0.053(1 - 0.455R)\log T \quad (2.4)$$

Zhang, Phillips and Wu's S-N expression:

The expression of Equations (2.2) to (2.4) were modified by Zhang, Phillips & Wu (1996), who accounted for the effects of loading frequency and stress reversal on the flexural fatigue behaviour of plain concrete. Their modified expression is showed by Equation (2.5)

$$\frac{\sigma_{max}}{f_s} = \left(ab^{-\log f} + c\right)[1 - (1 - R')\beta \log N] \quad (2.5)$$

Banjara and Ramanjaneyulu's expression:

Banjara & Ramanjaneyulu (2018) proposed an expression based on experimental results of flexural fatigue behaviour in plain concrete, using the abovementioned expressions to derive a unified S-N expression in Equation (2.6)

$$\frac{\sigma_{max}}{f_s} = 1.1268 - 0.0776\log N \quad (2.6)$$

2.3.2. Expressions describing the fatigue life of FRC

Cachim's S-N expression:

Research on flexural fatigue of FRC was performed by Cachim (1999) at various frequencies and stress levels. The S-N expression in Equation (2.7) was proposed after a regression analysis was performed.

$$\frac{\sigma_{max}}{f_s} = \left(\frac{20.156\log N}{18.708}\right) \quad (2.7)$$

Naaman and Hammoud's S-N expression:

Naaman & Hammoud (1998) performed flexural fatigue tests on high performance FRC using hooked-end steel fibres, at three different stress levels. The expression in Equation (2.8) was developed.

$$\frac{\sigma_{max}}{f_s} = 93 - 3.68\log N \quad (2.8)$$

Singh and Kaushik's S-N expression:

The S-N expression in Equation (2.9) was developed by Singh & Kaushik (2003), after performing experimental investigations on the flexural fatigue life of FRC at different stress levels and ratios.

$$\frac{\sigma_{max}}{f_s} = c_1 N^{-c_2(1-R)} \tag{2.9}$$

Banjara and Ramanjaneyulu's expression:

Banjara & Ramanjaneyulu (2018) developed two expressions for the flexural fatigue behaviour of FRC, where Equation (2.10) considers the fatigue life of FRC with an average effect of the steel fibres. Equation (2.11) is proposed for the fatigue life of FRC of any fibre volume dosage.

$$\frac{\sigma_{max}}{f_s} = 1.1633 - 0.0783 \log N \tag{2.10}$$

$$\ln N = 244.1\left(\frac{\sigma_{max}}{f_s}\right) - 179.4\left(\frac{\sigma_{max}}{f_s}\right)^2 + 3.106V_f - 1.2V_f^2 - 70.29 \tag{2.11}$$

Where,

σ_{max} – maximum applied stress

f_s – flexural static strength of specimen

R – stress ratio

R' – reversed stress ratio

β – material parameter = 0.0685

N – fatigue life (number of cycles to fatigue life)

T – time period of the repeated loads

a, b, c – material parameters

f – loading frequency

c_1, c_2 – coefficients based on stress ratio

V_f – fibre volume fraction

3. Experimental framework

In this chapter, the experimental framework of the study is outlined. The study focuses on the fatigue testing of pre-slipped steel fibre reinforced concrete (SFRC) specimens at a single fibre level, and pre-cracked specimens at a macroscopic level. The loading conditions as well as data acquisition are outlined.

3.1. Concrete material properties and mixing procedure

3.1.1. Concrete material properties

The concrete mix constituents used for this study, apart from the steel fibres, were all locally sourced. The steel fibres were supplied by BEKAERT in Belgium, and are displayed in Figure 3.1. The cement was CEM II/A-S 52.5 N, which contained between 6-20% ground granulated Corex® slag (GGCS) extender, and was supplied by Pretoria Portland Cement (PPC). The coarse aggregates used in the concrete mix were a crushed 13 mm greywacke stone, and a natural pit sand (known locally as Malmesbury sand) was used as the fine aggregate. Chryso®Fluid Optima 206 was a high range water reducing superplasticiser used in the concrete mix. The concrete mix constituents and proportions are displayed in Table 3.1. The steel fibres used in all the concrete mixes were the DRAMIX 3D-65/60-BG hooked-end fibres, as shown in Figure 3.1. The fibre properties are displayed in Table 3.2.

Table 3.1: Concrete mix composition

Material type	**Relative density**	**kg/m³**
Cement (CEM II/A-S 52.5 N)	3.14	450
Sand (Malmesbury – FM = 1.88)	2.56	880
Stone (Greywacke 13 mm)	2.74	820
Water	1.0	194
Superplasticiser (1.4% by weight of binder)	1.05 (± 0.02)	6.3
Fibres (0.8% by volume)	7.8	65

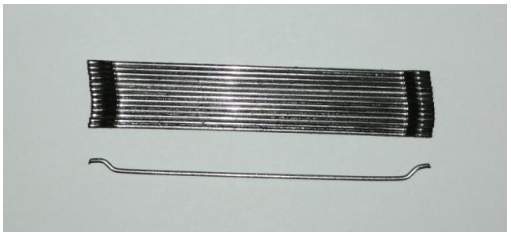

Figure 3.1: Hooked-end steel fibre

Table 3.2: Fibre properties (DRAMIX 3D-65/60-BG) ("Dramix® steel fiber concrete reinforcement - Bekaert.com", 2018)

Tensile strength	1 160 MPa
Modulus of elasticity	200 GPa
Length (*l*)	60 mm
Diameter (*d*)	0.9 mm
Aspect ratio (*l*/*d*)	67

Initially, two types of fine aggregates were considered for the mix design – fine and coarse Malmesbury sand – and the sieve analyses were performed for both. Figure 3.2 illustrates the grading curves for the two types of sand. The coarse sand was better graded as there was a better distribution of particle sizes in comparison with the fine sand, which had a large quantity of fine particles. The coarse sand was selected as it required less water and resulted in a viscous but flowable mix before fibres were added. This was an important factor to take into consideration since the addition of fibres decreased the workability of the concrete in the fresh state.

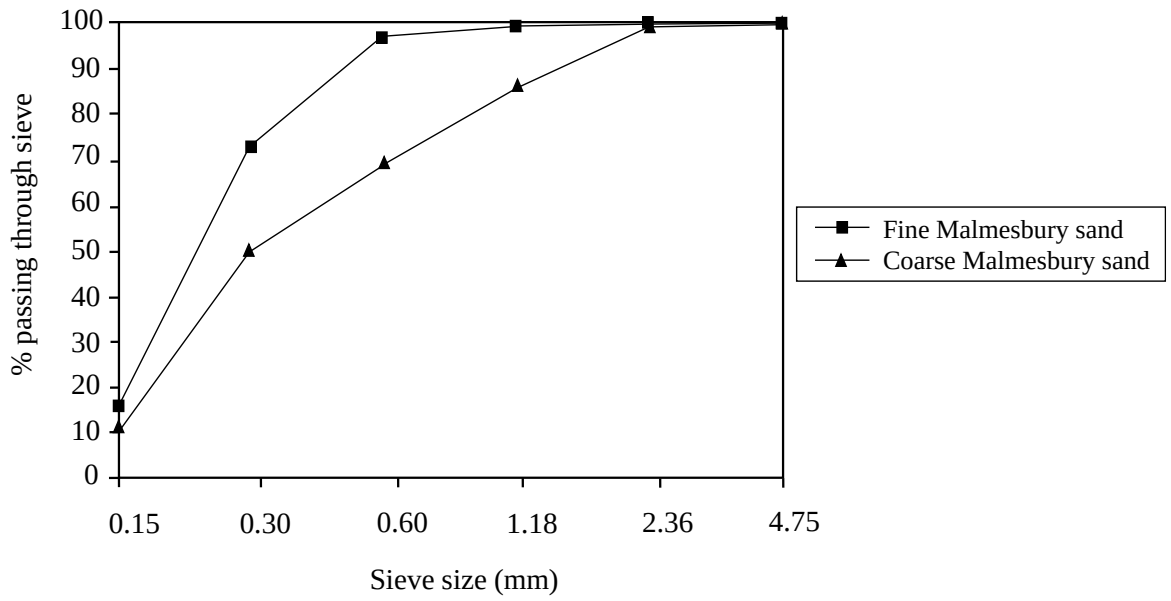

Figure 3.2: Grading curve for fine and coarse Malmesbury sand

3.1.2. Concrete mix procedure

The concrete was mixed in two different mixers for the single fibre specimens and the beam specimens. The single fibre specimen concrete was mixed in a 25-litre pan mixer, and the beam specimen mixes in a 120-litre pan mixer. The mix composition provided in Table 3.1 was proportioned accordingly for each mix. The mixing procedure was as follows:

1. All materials were weighed off using the same scale to ensure consistency.
2. The moulds required for a particular cast were assembled and greased with a thin layer of demoulding oil for easy removal of specimens.
3. The inner surface of the drum mixer was dampened, and excess water was removed with tissue paper.
4. All dry materials were added to the pan mixer, starting with the fine aggregate, cement, then followed by the coarse aggregate. The dry materials were mixed for at least 30 seconds to ensure that all the materials were uniformly mixed.
5. The water was then added and mixed for a further 60 seconds for the single fibre mix and 180 seconds for the beam mix.

6. The superplasticiser was then slowly added to the mix and mixed for an additional 180 seconds.

7. For the single fibre specimens, the mixing was stopped at this point and a slump test was performed. No fibres were added to the fresh mix, only a single fibre was embedded in each specimen mould after casting.

8. The beam specimen mixes had fibres added to the fresh mix. The fibres were added over a period of 30 seconds and the concrete was then mixed for a further 120 seconds to ensure uniform fibre dispersion. A slump test was then performed.

9. The specimens were then cast in their respective moulds as discussed in Section 3.1.3.

3.1.3. Specimen casting

After the completion of the fresh concrete mix, the specimens were cast. The preparation for casting the single fibre specimens and the beam specimens differed, and is discussed in Section 3.1.3.1. and 3.1.3.2.

3.1.3.1. Single fibre specimen casting

After the fresh concrete was mixed, the single fibre specimens were cast in moulds created from cube moulds with dimensions of 100 × 100 × 100 mm. A wooden cross-shaped partition was placed in the centre of the cube mould, which divided it into four equal specimen moulds with dimensions of 40 × 40 × 100 mm each as shown in Figure 3.3. The interior of the mould, along with the partition, was coated with a thin layer of demoulding oil, which allowed the partition to easily slide in and out of the mould.

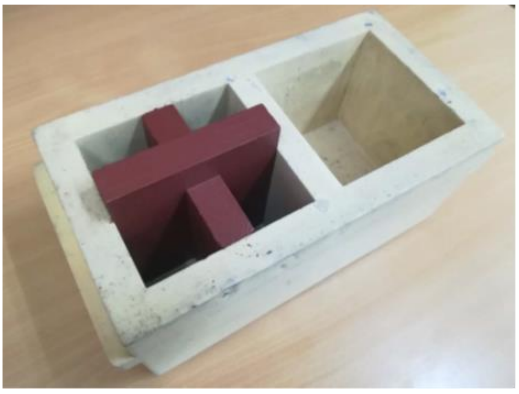

Figure 3.3: Single fibre pull-out mould

Due to the size of the specimens, the coarse aggregates were removed from the fresh concrete mix by sieving and only the mortar was used. Even though this was not ideal as it created a different material, it was the best way to keep the material as close as possible to the original concrete mix. This method allowed the single fibre to be inserted with ease to its required embedment length, without any interruption or damage caused by the coarse aggregates. The fresh concrete was poured into a 4.75 mm sieve and placed on the shaker table to filter the mortar through the sieve. This ensured that no coarse aggregates passed through. The moulds were then filled with mortar and placed on the shaker table for 30 seconds. Thereafter, a single fibre was inserted in the mortar of each specimen, to an embedment length of $l/2$ (30 mm). The moulds were then gently vibrated once more for 2-3 seconds to ensure that no voids remained after the fibre was inserted. The moulds were placed in an undisturbed area of the laboratory and were demoulded after 24 hours. After demoulding, the exposed part of each fibre was coated with wax to prevent any corrosion. The specimens were then submerged in water curing tanks, with a temperature of 24 ± 1 °C for an additional 26 days. The specimens were removed from the water on the 27^{th} day and prepared for testing on the 28^{th} day.

3.1.3.2. Beam specimen casting

The beam specimens were cast in steel moulds, with dimensions of 150 × 150 × 700 mm. The size of the moulds was adjusted to 150 × 150 × 550 mm by adding a 150 × 150 × 150 mm wooden spacer to one end of the mould as shown in Figure 3.4. Once the moulds were assembled to their required size, the interior was covered by a light film of demoulding oil. The moulds were then filled up to 90% of their height and then compacted individually on the shaker table for 30 seconds. The remaining 10% was added while the specimen was being compacted, as directed by BS EN 14651 (2005). The specimens were then placed in an undisturbed part of the laboratory. After 24 hours, the specimens were demoulded and placed in water curing tanks, at a temperature of 24 ± 1 °C for an additional 27 days.

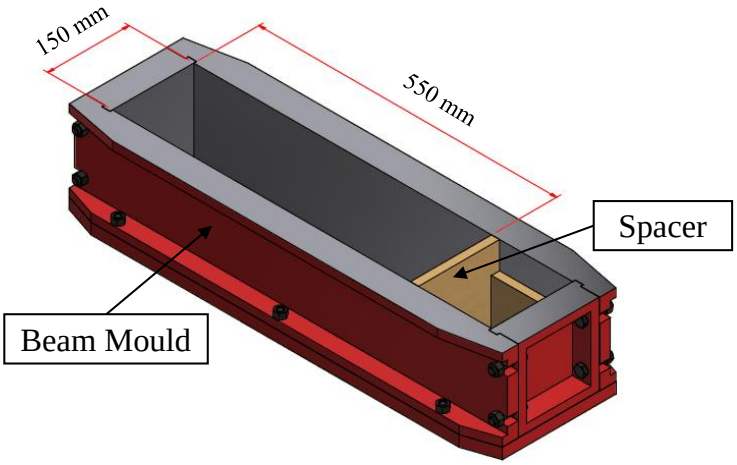

Figure 3.4: Beam mould

3.2. Single fibre pull-out test preparation

3.2.1. Specimen preparation

The single fibre pull-out tests were performed on individual specimens due to the sensitive nature of the test. As mentioned in Section 3.1.3.1, the specimens were cured in water curing tanks for 26 days. On the 27th day, the specimens were removed from the curing tanks and the excess water was dried using industrial grade tissue paper. The fibre, which was coated in a layer of wax, was thoroughly cleaned using tissue paper. The protruding hook of the fibre was carefully removed using pliers to allow the fibre to be clamped by the testing machine. Figure 3.5 illustrates the fibre before (a) and after (b) the hooked end was removed. The specimens were then left to air dry for 4-5 hours.

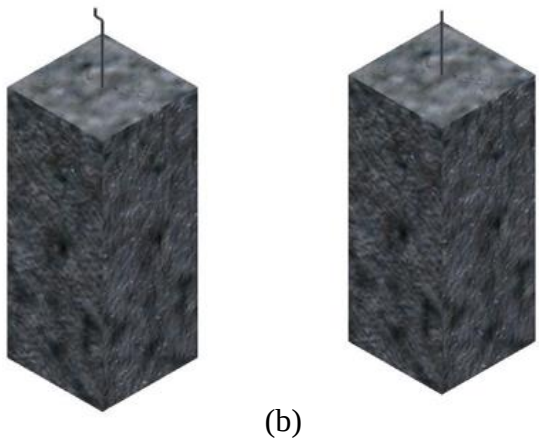

(a) (b)

Figure 3.5: (a) Specimen with hook on protruding edge, (b) Specimen with hook removed from protruding edge

Once the specimens were air dried, a two-part epoxy – Sikadur-30 – was used to bond the base of the concrete specimens to individual steel plates, which were then bolted onto the test setup. The epoxy required 24 hours to set and fully harden, after which the specimens were tested. The static tests were performed at 28-day strength of the concrete, while the fatigue specimens were tested between 28 and 40 days. This was done due to the lengthy nature of the fatigue tests – since four days were required to run the test to completion without failure.

Compressive tests were also performed on several 100 × 100 × 100 mm cube specimens to determine the 28-day strength. These samples did not contain fibres in the concrete mix, they did however contain coarse aggregates. The average compressive strength recorded over the duration of the study was 54 MPa.

3.2.2. Test setup

The single fibre pull-out static and fatigue tests were performed on the same testing machine. The test setup consisted of a stiff steel frame fixed to the concrete floor, and a 50 kN servo-controlled hydraulic Instron actuator, with a 250 mm stroke length, as shown in Figure 3.6. Based on similar tests performed previously on 3D fibres (Nieuwoudt, 2016), the loads were expected to be well below 50 kN, and therefore, a 5 kN external load cell was introduced to the setup to improve the resolution. An external linear variable differential transducer (LVDT) was also incorporated into the test setup to ensure the accuracy of the fibre pull out readings in comparison with the LVDT of the Instron. Figure 3.7 displays all the components of the test setup.

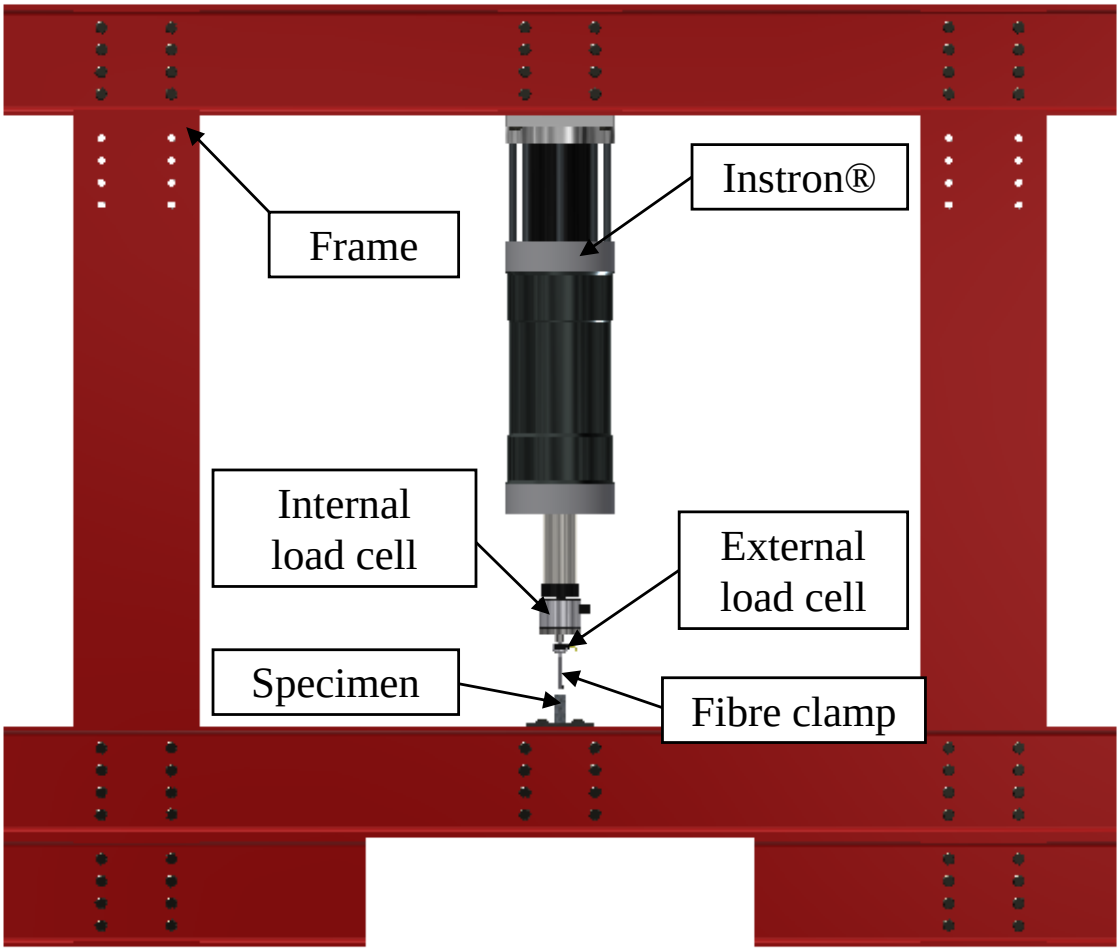

Figure 3.6: Single fibre pull-out test setup

After the epoxy was completely set, the steel plates were bolted onto the test setup as shown in Figure 3.7. Once the fibre was correctly aligned with the opening on the fibre clamp, the head of the Instron was slowly lowered into position to allow the fibre to slide completely into the fibre clamp. The fibre clamp was tightened by two grub screws which held the fibre firmly in place, so that no slippage would occur between the fibre and the clamp. After fixing the fibre in place, the external LVDT was positioned between the base of the test setup and the external load cell adapter to measure the crosshead movement of the Instron head in relation to the base of the specimen.

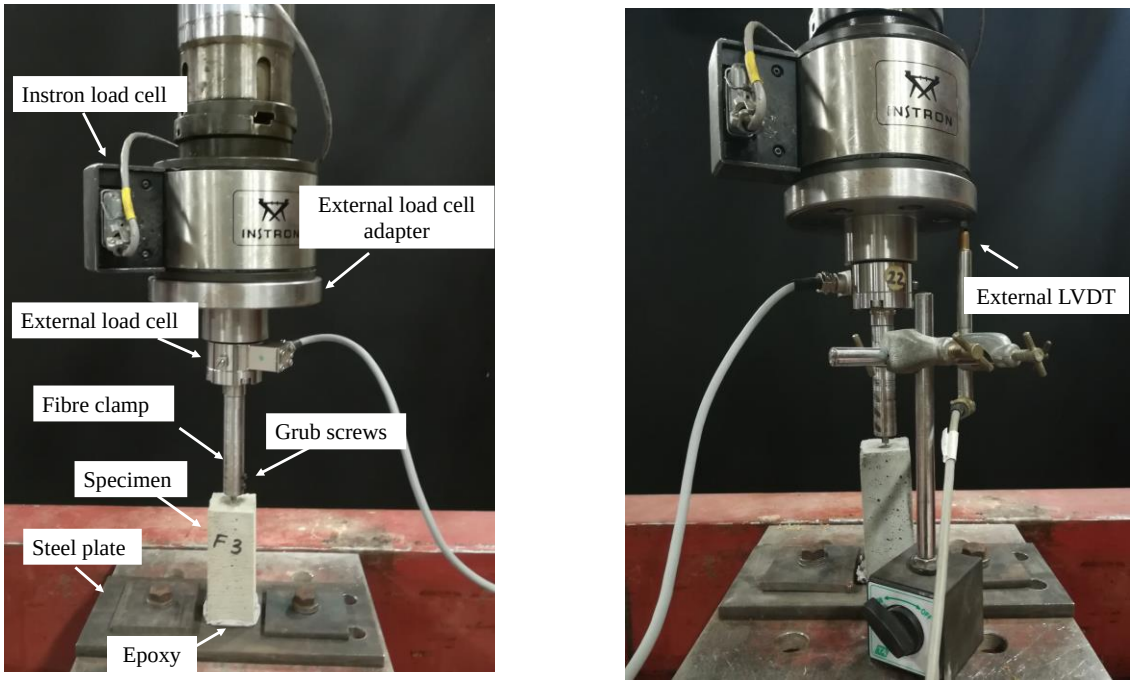

Figure 3.7: All components attached to test setup

3.2.3. Test programme

Throughout the experimental programme, only the DRAMIX 3D-65/60-BG fibre was used. The load levels were tested at 50%, 70% and 85% of the average maximum static pull-out load. Different pre-slips were tested, which included 0.6 mm, 1.2 mm, 1.8 mm, and 2.5 mm, to determine the fatigue capacity at different degrees of fibre hook deformation. At least 5 specimens were tested for the static tests, and at least 2 specimens were tested for each load level and pre-slip combination of fatigue tests. The pre-slips and load levels were chosen specifically to induce failure after various degrees of damage to the fibre in order to find the fatigue limit, since there was no prior literature on pre-slipped single fibre pull-out fatigue tests.

3.2.4. Loading regime

3.2.4.1. Static tests

In order to perform the single fibre pull-out fatigue tests, the average maximum pull-out load was required first. To obtain this, static single fibre pull-out tests were performed on several specimens. The static tests were displacement-controlled, with the fibre pull-out rate of 3 mm/min. The load was continuously recorded during the test and the test ended once the fibre was completely pulled out.

3.2.4.2. Fatigue tests

The fatigue loading was applied by a sine waveform load application as illustrated in Figure 3.8. The maximum load (A_{max}) was taken as a certain percentage of the average maximum load. The minimum load (A_{min}) was kept as a small positive value, generally between 20 N and 23 N. This was the lowest stable value the actuator could maintain to provide a smooth sine load application while simultaneously maintaining fatigue tensile loads at a frequency of 6 Hz.

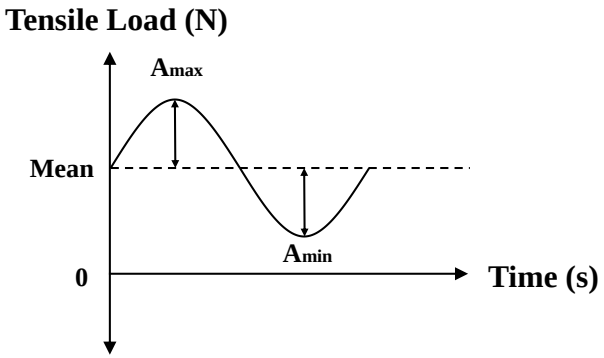

Figure 3.8: Tensile sine waveform loading application for single fibre pull-out fatigue tests

In order to achieve the control over the stable sine waveform load application, the proportional-integral-derivative (PID) controller needed to be tuned to suit the particular fatigue test. In order to tune the controller, the Instron Controller Console software had a built-in function to tune the controller automatically or manually. However, due to the intricate setup with the different stiffness in tension and compression, the external load cell could not be tuned automatically for the load control and the manual loop tuning tool was used. The manual loop tuning tool allowed the user to firstly, specify the shape of the waveform – e.g. square, sinusoidal, and secondly, input the PID parameters. Once the shape of the waveform was chosen – in this case, it was a sine waveform – the amplitude, mean, and frequency was required to plot the waveform.

The PID control tuning could be simplified by setting two of the three parameters to zero, depending on the complexity of the application. The proportional parameter was used to determine how rapidly the waveform reached the sine waveform input parameters. If the proportional parameter was increased too much, the system could overshoot, which could lead to oscillations and instability. The integral parameter was used to resist disturbances at low frequencies, but could also lead to overshooting. The derivative parameter was used to

eliminate the overshoot and oscillations (Ellis, 2012). A combination of these three parameters allowed the user to tune the controller for the required application.

Figure 3.9 illustrates the sine waveform when only a proportional parameter has been introduced. The Instron Console software provides an ideal sine waveform based on the input amplitude, frequency and mean as previously mentioned. The PID parameters must then be adjusted accordingly to fit the actual waveform in order to achieve the desired sine output. It was not always possible to achieve the ideal sine waveform due to inevitable noise, but it was adjusted as much as possible to attain a stable sine waveform loading.

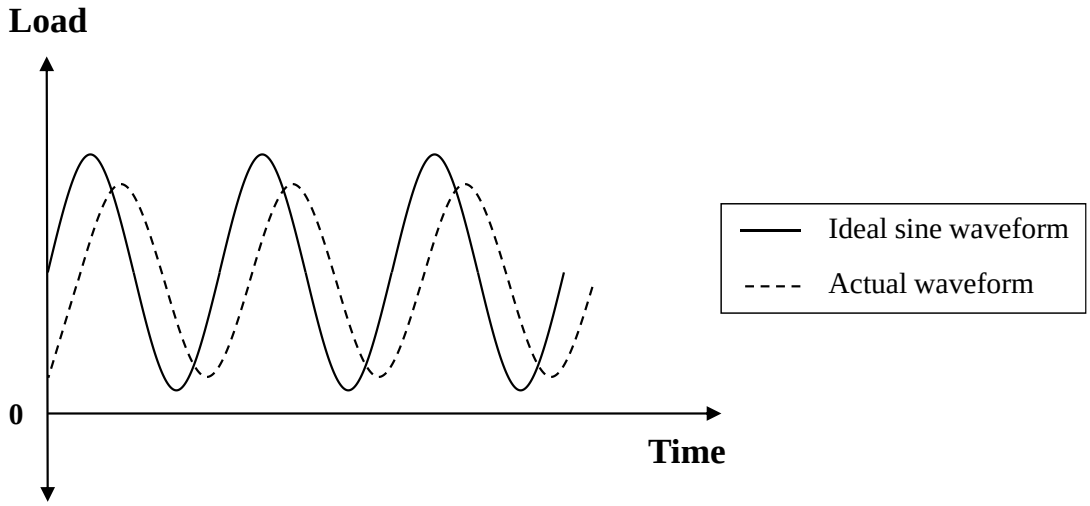

Figure 3.9: PID sine waveform load tuning

The single fibre pull-out fatigue tests consisted of three steps: (1) pre-slip; (2) load/unload; and (3) fatigue loading. The first step was displacement-controlled whereby the fibre was pulled out to the user-defined pre-slip at a rate of 0.6 mm/min, while the load was recorded. The pre-slip simulated the behaviour of a fibre in a cementitious matrix once a crack has formed. Once the pre-slip was reached, a load-controlled step by the external load cell commenced. The second step required the pre-slip load from the first step to either increase or decrease to reach the specified mean value of the sine waveform load in Figure 3.8. The loading rate was applied at 10 N/s and the step ended once the mean value was reached. The last step was the fatigue loading step and was load-controlled by the external load cell. The fatigue loading cycled from the mean value, to the maximum and minimum load until failure, or until the test had completed 2 million load cycles. The 2 million load cycle limit is a widely acceptable limit for terminating fatigue tests in

literature. This limit may also be indicative of the typical loading experienced by structures such as airport and highway pavements. The flow diagram displayed in Figure 3.10 illustrates the fatigue loading regime.

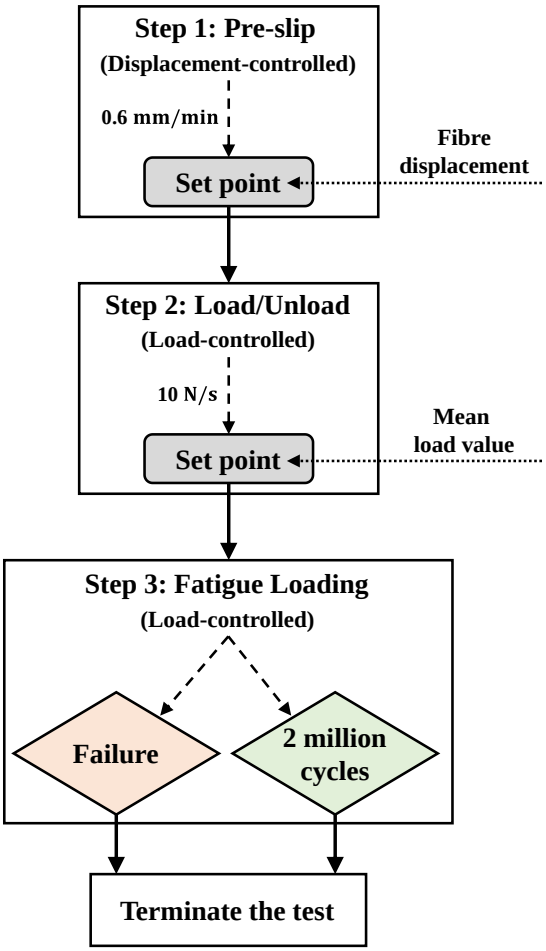

Figure 3.10: Loading regime for single fibre pull-out fatigue tests

3.3. Beam test preparation

3.3.1. Specimen preparation

After 27 days of curing in water curing tanks, the beam specimens were removed and prepared for testing according to BS EN 14651 (2005). Each specimen was rotated 90° on its longitudinal axis and a 25 mm notch was sawn at mid-span over the width of the specimen as seen in Figure 3.11. The notch allowed for a controlled crack to form at the mid-span of the specimen. The specimen was notched at least 3 hours prior to testing, and the notch width was no more than 5 mm, as specified by BS EN 14651 (2005).

Once the notching of the specimens was completed, knife edges as shown in Figure 3.11 were glued onto the outside of the notch opening using Pratley Steel Quickset® epoxy. Once the epoxy had set, the specimens were ready for testing. Individual specimens were mounted onto the test setup, which is discussed in Section 3.3.2. A clip gauge was then attached to the knife edges to measure the crack mouth opening displacement (CMOD) during the test. The static tests were performed at an age of 28 days, whereas the specimens cast from each batch for fatigue tests were tested between 28 and 40 days. This was done to decrease the variations in results due to the lengthy nature of the fatigue tests.

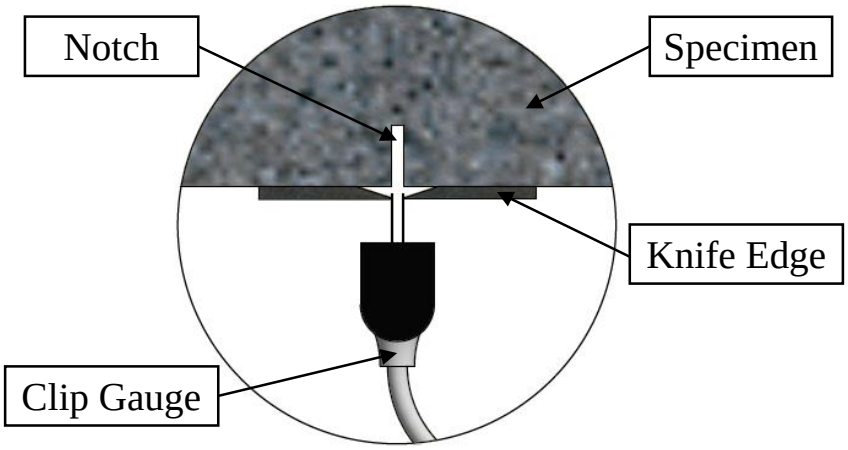

Figure 3.11: Notch on specimen with clip gauge

Compressive tests were performed at 28 days on 100 × 100 × 100 mm cube specimens. These samples contained 0.8% fibre dosage in the concrete mix, as well as coarse aggregates. The average compressive strength recorded over the duration of the study was 62 MPa.

3.3.2. Test setup

The flexural tests were performed on two separate setups – one for the static tests and the other for the fatigue tests. The static tests were performed on the 2 MN Instron Universal Material Testing Machine while the flexural fatigue test setup was configured.

The flexural fatigue test setup consisted of a 500 kN servo-controlled hydraulic Instron actuator mounted onto a stiff steel frame which was fixed into the concrete floor. The full setup for the flexural fatigue test can be seen in Figure 3.12. The Instron actuator had a stroke length of 50 mm when fully extended. The results from the static tests gave insight into the maximum loads to be expected from the specimens and it was well below the

500 kN capacity. As a result, a smaller 50 kN external load cell was fitted onto the test setup to provide a better resolution for the load-controlled tests.

The base of the test setup consisted of a steel I-beam which was bolted to the concrete floor. Two rollers were mounted on a frame which was fixed on top of the I-beam, spaced 500 mm apart as specified by BS EN 14651 (2005). A third roller was attached to the external load cell to complete the three-point bending setup. The test specimen was placed on top of the two base rollers, with 25 mm of the specimen overhanging on either roller. The clip gauge was then attached to the knife edges. The Instron head was slowly lowered until it just made contact with the specimen, after which, the testing commenced.

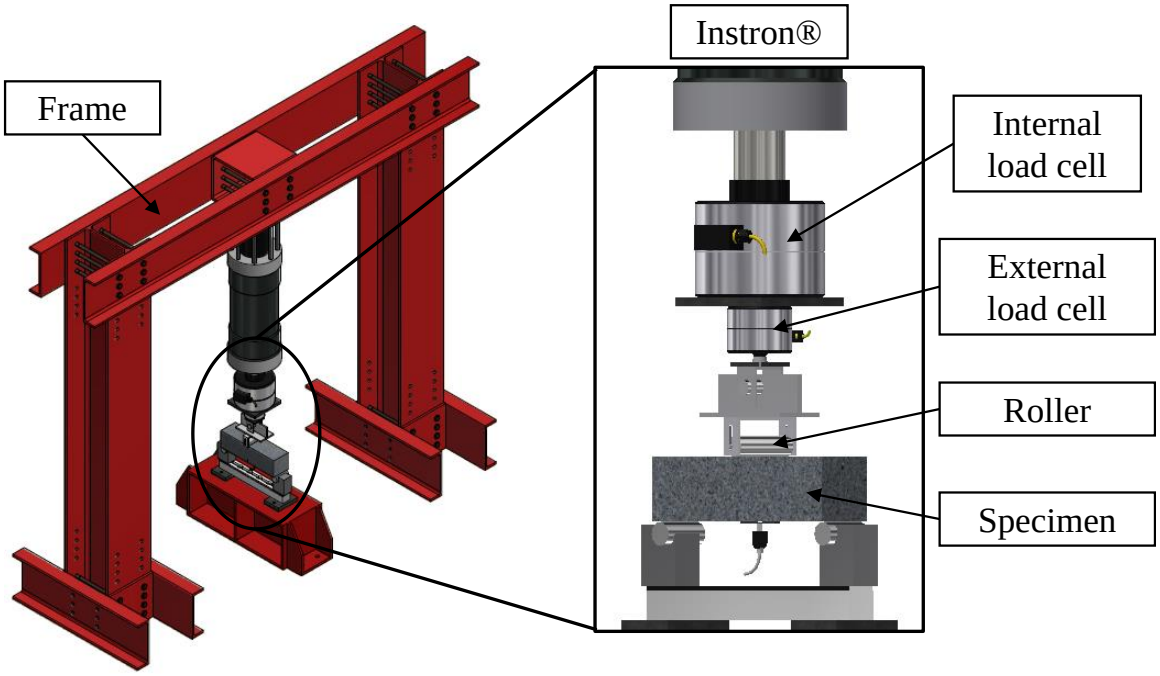

Figure 3.12: Full test setup for flexural tests

3.3.3. Test programme

The test programme for the flexural tests was similar to that of the single fibre pull-out tests. Three different static flexural tests were performed, each having a different fibre dosage. This was done in order to find the required fibre dosage to use for the flexural fatigue tests. At least five specimens were tested in flexure for each fibre dosage. Once the required dosage was found, the flexural fatigue test specimens were all mixed and cast with the same fibre dosage. DRAMIX 3D-65/60-BG steel fibres were used throughout the tests.

The load levels applied to the flexural fatigue tests were the same as the single fibre pull-out fatigue tests – 50%, 70% and 85% of the average maximum static load. The specimens were also pre-cracked to different CMODs, including 0.6 mm, 1.2 mm, 1.8 mm and 2.5 mm.

3.3.4. Loading regime

3.3.4.1. Static loading

The static flexural tests were performed in order to obtain the average maximum flexural load. The static tests were displacement-controlled according to the CMOD extension, and was loaded according to BS EN 14651 (2005). Initially, the CMOD was increased at a constant rate of 0.05 mm/min, until the CMOD reached 0.1 mm. Thereafter, the CMOD extension was increased to a constant rate of 0.2 mm/min for CMOD > 0.1 mm. The test was terminated at a CMOD of 3.5 mm.

3.3.4.2. Fatigue loading

The flexural fatigue loading was applied similar to that of the single fibre pull-out fatigue loading. However, the sine waveform loading was applied in compression to perform the three-point bending action, shown in Figure 3.13. The maximum load (A_{max}) was determined as the various load level percentages previously discussed in Section 3.3.3. The minimum load (A_{min}) was taken as a small non-zero value – generally between 3 kN and 3.5 kN in compression. To maintain stable loads, the PID controller was tuned according to the test required, as discussed in Section 3.2.4.2.

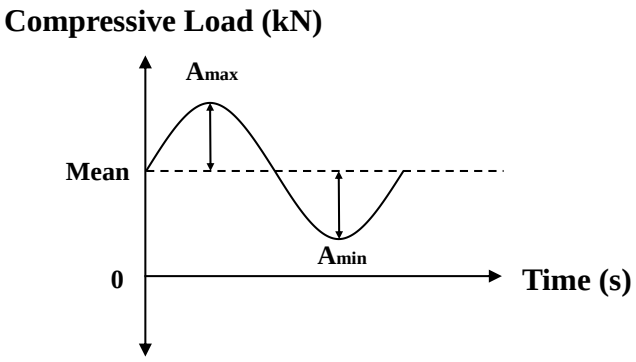

Figure 3.13: Compressive sine waveform loading for flexural fatigue tests

The first step of the fatigue loading was to pre-crack the specimen to the defined CMOD extension, see Figure 3.14. This was a displacement-controlled step, applied at a CMOD

extension rate of 0.6 mm/min. Once the defined CMOD was obtained, the second step commenced, which was load-controlled by the external load cell. This step required the load to either increase or decrease at a rate of 0.5 kN/s to reach the mean load from the load obtained in the first step. The last step, which was the fatigue loading, could begin after the mean load was reached. This was a load-controlled step by the external load cell, and loading was applied at a frequency of 5 Hz until 2 million load cycles were completed or until the CMOD reached a width of 3.5 mm.

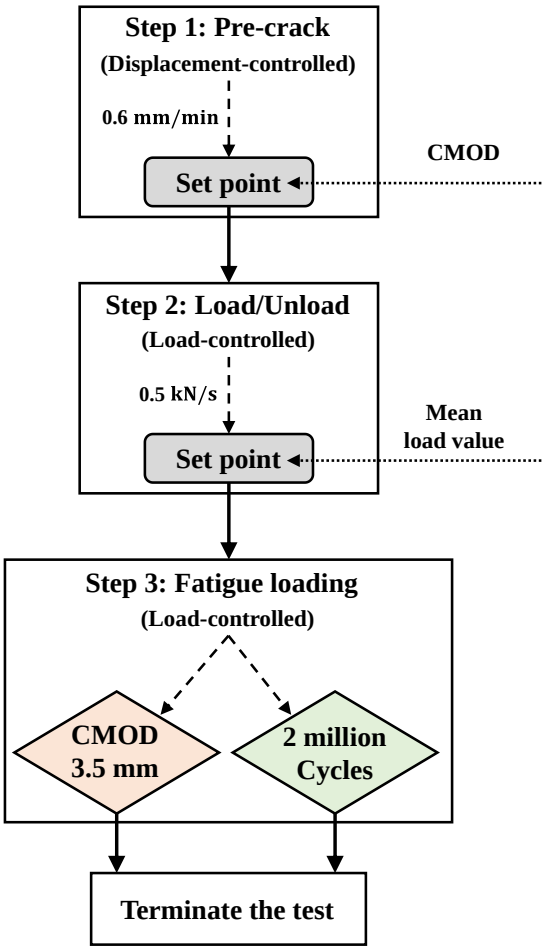

Figure 3.14: Loading regime for flexural fatigue tests

3.4. Data acquisition

All the information received from the actuator was saved and organised according to the user. The single fibre pull-out fatigue tests as well as the flexural fatigue tests followed a similar three-step loading regime. During each step, the data was saved and exported to a spreadsheet. During the first two steps, every data point was saved. However, for the

fatigue tests, the data points for each cycle could not be saved due to the lengthy nature of the tests. Thus, a data reduction method provided by the Instron WaveMatrix software allowed the user to specify which cycle's data points to save in order to provide the best results.

The data was then saved into three different spreadsheets. The first spreadsheet tracked and saved every data point for all the parameters of each of the reduced load cycles. The second spreadsheet saved only the specified parameters' maximum and minimum data points for the reduced load cycles. The final spreadsheet allowed the user to increase the saved data closer to the termination of the test. The fatigue cycle test data was saved as follows, with n being the number of cycles:

1. When $N \in [1; 100]$, save every cycle.
2. When $N \in [101; 1\,000]$, save every 10^{th} cycle.
3. When $N \in [1\,001; 10\,000]$, save every 100^{th} cycle.
4. When $N \in [10\,001; 2\,000\,000]$, save every 1000^{th} cycle.

3.5. X-ray Computed Tomography (CT) scanning specimen preparation

X-ray CT scans formed an integral part of the study. It provided a non-destructive method of analysing the interior of the specimens (du Plessis, le Roux & Guelpa, 2016). The X-ray CT scans were performed on the General Electric V|Tome|X L240 MicroCT scanner, which could accommodate samples up to 250 mm in diameter, depending on the material properties.

Both the single fibre pull-out test specimens, as well as the beam specimens, were sent for X-ray CT scans either before or after testing. The X-ray CT scans were performed in order to determine whether the concrete as well as the fibres were damaged before and after fatigue loading. Since concrete is a dense material, certain specimens were required to be resized in order to obtain a better resolution from the X-ray CT scans. The single fibre pull-out specimens were small enough for the X-ray CT scanner to penetrate it and obtain good resolution scans. However, the beam specimens were required to be cut smaller to focus on the cracked section as shown in Figure 3.15. The full crack throughout the depth

of the specimens was retained, however, the 25 mm notched section, and 45 mm from the top of the cracked section was removed. The final dimensions of the beam specimens which were sent for X-ray CT scans were 60 × 80 × 150 mm.

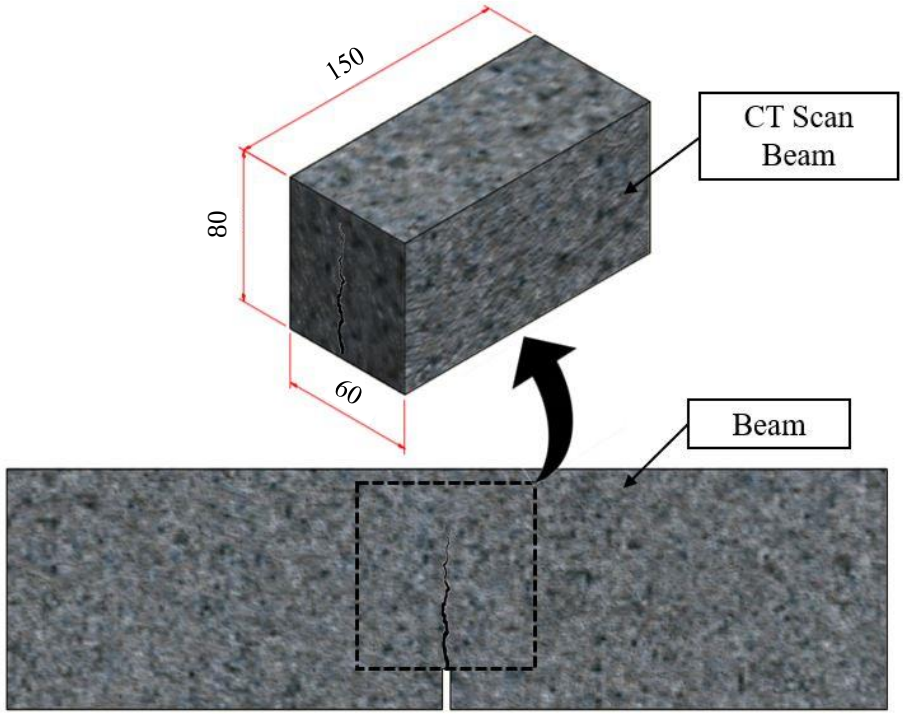

Figure 3.15: Sample cut from beam specimen to send for X-ray CT scan

3.6. Concluding summary

In this chapter, the layout for the experimental work was presented. A description of the mix design and procedure, followed by the specimen casting and preparation was discussed. All the test methodologies and test setups to perform the single fibre pull-out tests, as well as the macroscopic tests, were presented in detail. All the fatigue test load levels varied, as well as the pre-slip for the single fibre pull-out tests, and the pre-crack for the macroscopic tests.

Static and fatigue tests were conducted at a single fibre level. The same mix design was used for single fibre pull-out tests and macroscopic tests. To cast the single fibre pull-out specimens, the coarse aggregates were sieved out and the mortar was used. A fibre embedment length of $l/2$ was used for all single fibre pull-out tests. The static tests required

complete pull out of the embedded fibre. The fatigue test load levels were based on various percentages of the average maximum pull-out strength of the embedded fibre.

For the macroscopic tests, flexural static and fatigue tests were performed, and the concrete mix included the coarse aggregates, as well as a 0.8% dosage of hooked-end steel fibres. The beam specimens cast for the macroscopic tests were all notched prior to testing, which forced the crack to occur at a preferred location. The static tests were performed in order to obtain the average maximum load which could be sustained up to a crack mouth opening displacement (CMOD) of 3.5 mm. The fatigue tests were then based on certain percentages of the average maximum static load.

Specimens tested in static and fatigue loading were also sent for X-ray CT scans. This was done to determine any damage which could have been caused by the fatigue loading, as well as determining the failure mechanisms under fatigue load.

4. Mechanical investigation at a single fibre level

In this chapter, single fibre pull-out tests are described. In order to fully understand the mechanisms of fibre pull-out of hooked-end steel fibres, static pull-out tests as well as fatigue tests were performed. The static tests provide the basis for performing the fatigue tests. The fatigue tests were performed on specimens at different pre-slip values, as well as varying load levels to determine the fatigue failure mechanisms of steel fibre reinforced concrete (SFRC) at a single fibre level. X-ray Computed Tomography (CT) scans were performed to further validate the results obtained from the static and fatigue tests.

Experimental results from this chapter were published in an article titled "An experimental study on the fatigue failure of steel fibre reinforced concrete at a single fibre level", in Construction and Building Materials journal, volume 299, page 123869, 2021.

4.1. Static test results

Before any fatigue tests could be performed, the static single fibre pull-out tests were conducted in order to determine the average maximum force required to completely pull out the embedded single fibre. This information provided insight into the static capacity of the fibre embedded in concrete, as well as the behaviour as the fibre pulled out.

4.1.1. Single fibre pull-out tests

In Figure 4.1, the results of six single fibre pull-out tests are displayed. The test results all followed a similar trend. As the load increased, the fibre debonded from the surrounding matrix at a pull-out of 0.1 mm or less, with the corresponding load ranging from 100 N to 170 N. Once the fibre was completely debonded, the load decreased slightly and the fibre hook was activated, which resulted in the load increasing. The load continued to increase steadily before it reached the global peak at a pull-out between 0.8 – 1.0 mm, and the load ranging between 350 N and 440 N. Thereafter, the load decreased as the pull-out increased. At a pull-out starting at 2.2 mm, the load began to increase slightly until it reached a secondary peak at 3.5 – 4.0 mm, with the load ranging from 275 N to 390 N. Thereafter, the load decreased steadily with several smaller insignificant peaks. The same trends have been reported in literature for static single fibre pull-out tests on 3D hooked-end steel fibres (Abdallah *et al.*, 2017; Beglarigale & Yazici, 2015; Ghoddousi *et al.*, 2010; Marković, 2006; Nieuwoudt, 2016).

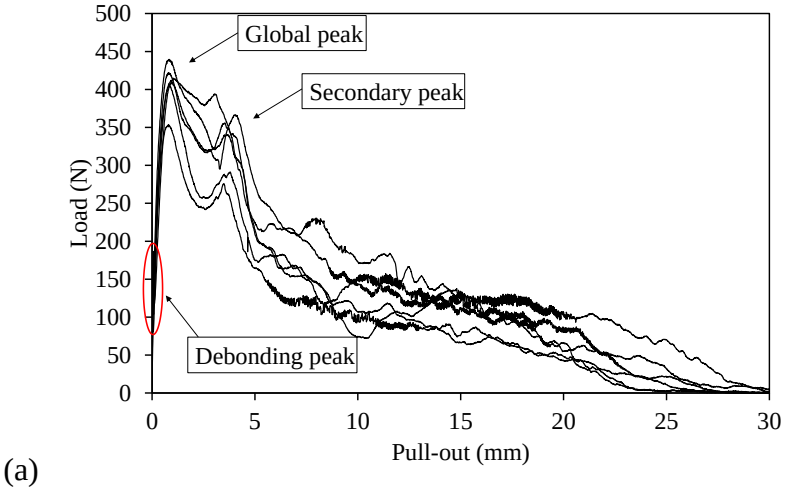

(a)

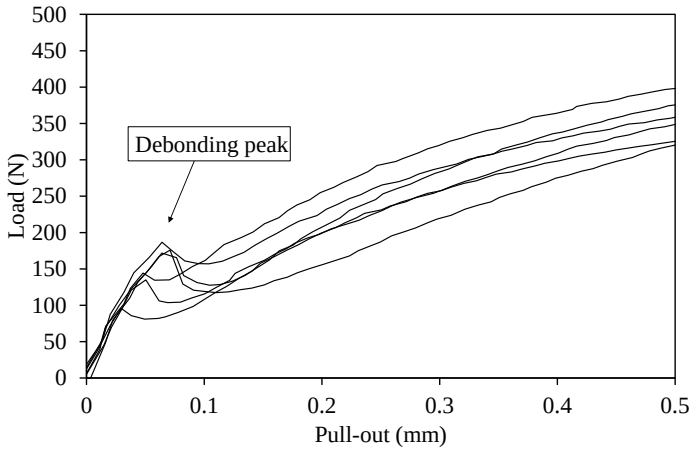

(b)

Figure 4.1: Static single fibre pull-out behaviour (a) complete pull-out (b) debonding

In addition to the complete static pull-out tests, partial pull-out tests were performed on several specimens, which were pre-slipped to varying degrees. These pre-slip values ranged from 0.3 mm to 4.0 mm, and were chosen due to the significant load-displacement results found within this range. These results are displayed in Figure 4.2. The global peak results showed a larger degree of variability compared to the complete static pull-out in Figure 4.1, ranging from 260 N to 590 N, at a pull-out starting from 0.5 mm to 0.8 mm. It can be seen that the specimens with a pre-slip of 0.3 mm have not yet reached the global peak load, but have surpassed the debonding load. The 0.6 mm specimens are in the range of peaking. However, it cannot be stated for certain that the 0.6 mm specimens are at the global peak load yet. The load then decreased up to a pull-out of 2.5 mm, after which it increased to reach the secondary peak.

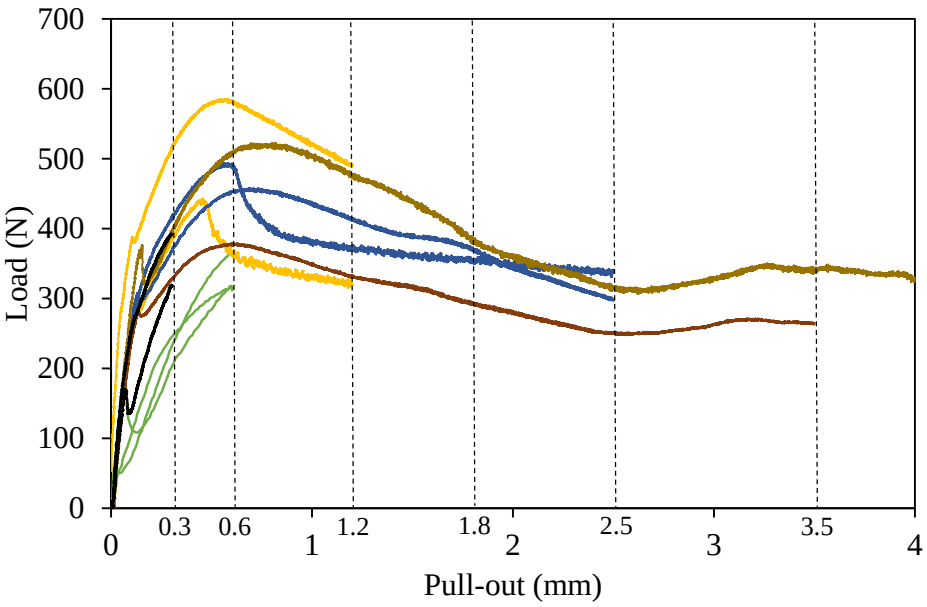

Figure 4.2: Load-displacement curve for pre-slipped specimens

Based on the trends found in the load-displacement curves in Figure 4.1 and Figure 4.2, a theoretical single fibre pull-out classification model, hereafter termed the single fibre model, was plotted and is displayed in Figure 4.3. It highlights the different phases of deformation the fibre underwent during the pull-out process, based on the expected load-displacement behaviour. During Phase 1, the load increased as the fibre started to debond from the surrounding matrix, until it fully debonded. Once the fibre has fully debonded from the surrounding matrix, it was classified into Phase 2. Additional increase in the fibre pull-out resulted in a higher load as the curves (A and B) of the mechanical hook of the fibre began to deform. The load required to overcome the initial fibre hook deformation was the global peak load (Phase 3). As the fibre deformation continued, the first curve (A) of the fibre hook deformed and straightened out to where curve B initially was, thereby resulting in the secondary peak (Phase 4). After Phase 4, both curves (A and B) of the fibre hook were fully deformed and straightened out and the fibre continued to pull out under frictional forces until it completely pulled out (Phase 5). Due to the hook deformation, the fibre was not perfectly straight in Phase 5, thus, the residual load consisted of increased frictional forces as the fibre pulled out.

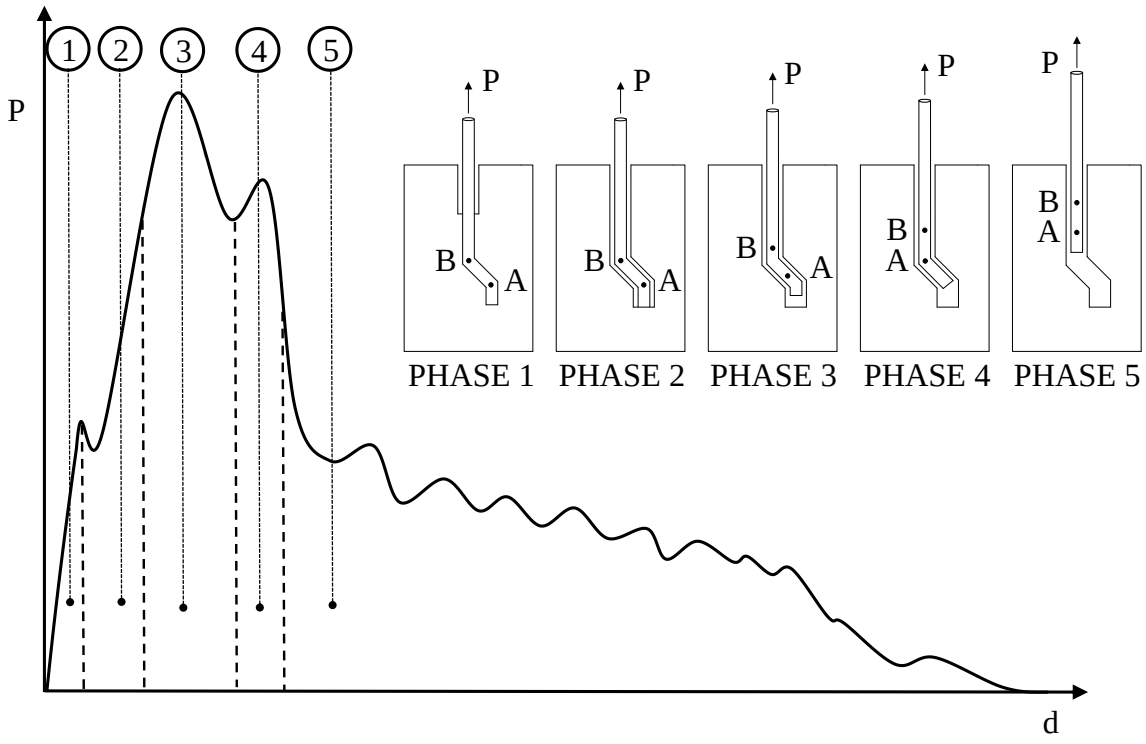

Figure 4.3: Theoretical single fibre pull-out classification model for pull-out of 3D hooked-end steel fibres

4.1.2. X-ray CT scans

X-ray CT scans were performed on the pre-slipped specimens tested in Figure 4.2. The tests were then classified into the different phases illustrated in Figure 4.3, and the CT scans were used to further corroborate the results found in Figure 4.2 and the model in Figure 4.3.

In Figure 4.4, the X-ray CT scans of the specimens pre-slipped to (a) 0.3 mm and (b) 0.6 mm respectively, are shown. In Figure 4.2, the load-displacement results for the 0.3 mm specimen illustrated that the load had not yet reached the peak load. It debonded from the surrounding matrix and the fibre hook was engaged. The X-ray CT scans show that there was no visible displacement at the end of the fibre, therefore, it was categorised into Phase 2. The scan in Figure 4.4 (b) shows that a 0.6 mm pre-slip resulted in a measured fibre end displacement of 0.31 mm, with the load ascending towards the global peak in Figure 4.2. Since the global peak load ranged between a pull-out of 0.45 mm and 0.8 mm in Figure 4.2, it cannot be stated for certain whether it had already reached the

peak or not. Subsequently, it was classified into Phase 2, where the fibre had fully debonded from the surrounding matrix and had been pulled out to a certain degree.

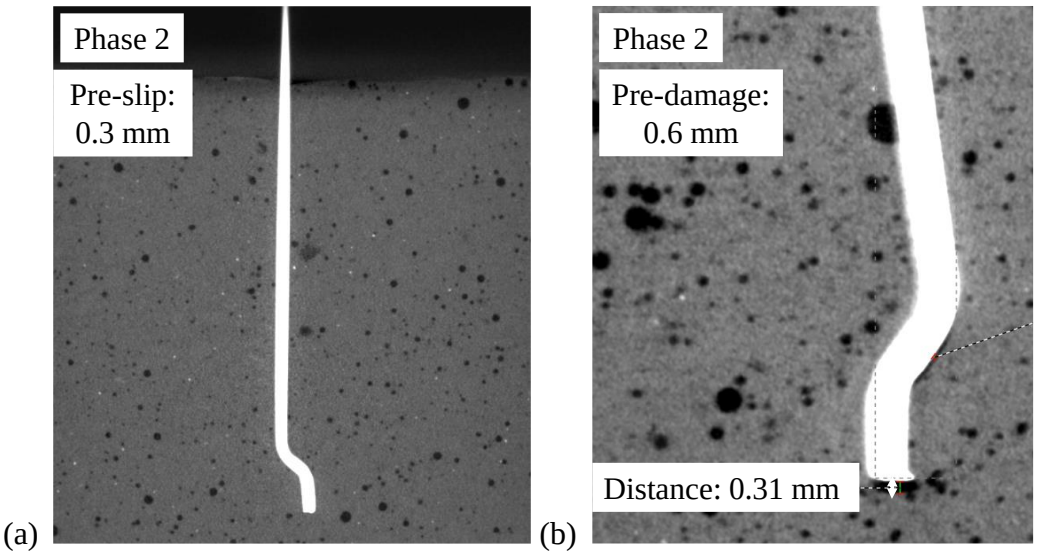

Figure 4.4: X-ray CT scans of pre-slipped specimens (a) 0.3 mm; (b) 0.6 mm

The pre-slip was then increased to 1.2 mm, 1.8 mm, and 2.5 mm. From the load-displacement curve in Figure 4.2, these test specimens were at different stages on the descending branch after the global peak had already been reached. All three pre-slips were placed into Phase 3. Figure 4.5 shows that the pre-slip of 1.2 mm and 1.8 mm resulted in measured fibre end displacements of 0.92 mm and 1.47 mm respectively. Figure 4.5 clearly illustrates the deformation of the fibre hooks. As the pre-slip increased, the fibre deformation became more progressive, which was suggested previously in Figure 4.3 for Phase 3 heading towards Phase 4.

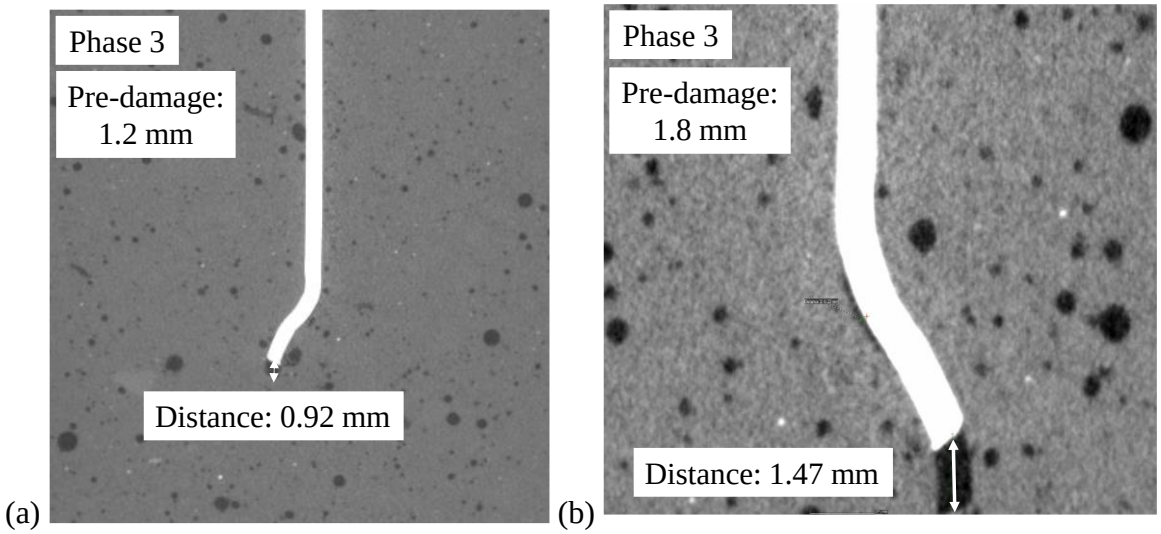

Figure 4.5: X-ray CT scans of pre-slipped specimens (a) 1.2 mm; (b) 1.8 mm

The specimens were also pre-slipped to 3.5 mm and 4.0 mm, and the CT scans are displayed in Figure 4.6. From Figure 4.2, after a fibre displacement of 2.5 mm, the load started to increase to reach the secondary peak. Both specimens in Figure 4.6 have large fibre hook deformations. The last curve of the fibre started to straighten out and as a result, both specimens were classified into Phase 4. Any further deformation of the hook would straighten it out and then it can be placed into Phase 5. At this phase, there was little to no resistance by the fibre and pull-out was imminent.

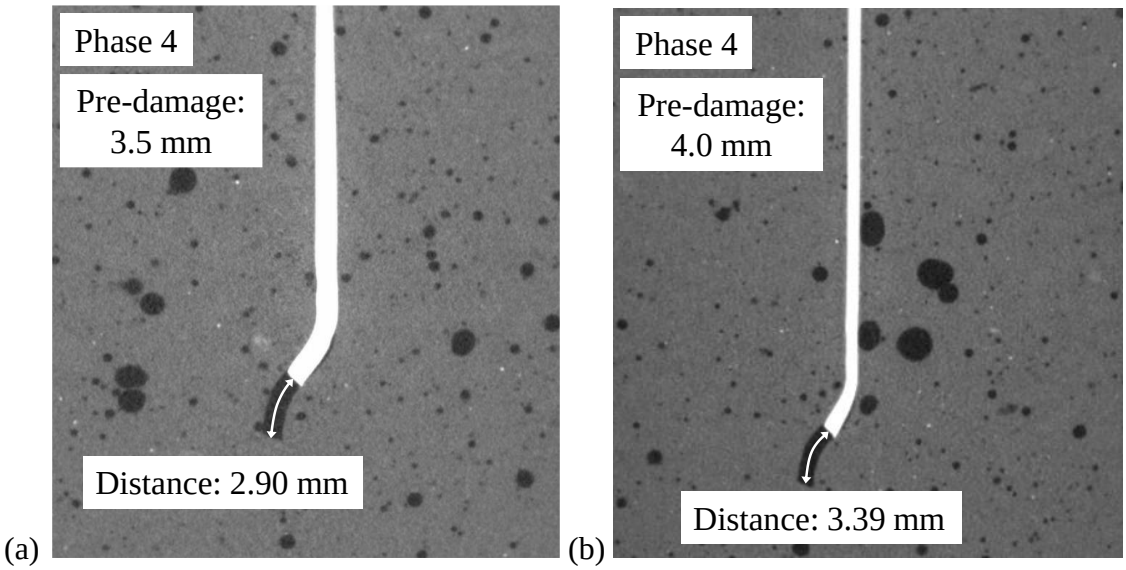

Figure 4.6: X-ray CT scans of pre-slipped specimens (a) 3.5 mm; (b) 4.0 mm

The measured pre-slip was plotted in comparison to the required pre-slip in Figure 4.7 for the six specimens as previously illustrated in Figure 4.4 to Figure 4.6. There was a clear trend in the offset between the pre-slip values. The offset remained nearly constant from the 0.3 mm pre-slip up to the 1.8 mm pre-slip, after which the offset started to increase. This could be as a result of elastic and/or plastic deformation of the fibre and/or system, fibre slippage at the clamp, or due to the fibre increasing in length as the fibre hooks started to straighten out at larger pre-slips, or as a combination of the factors. However, even though the measured pre-slip was not exactly the same as the required pre-slip, the results were still sufficient to classify the fibre pre-slips to the various phases in Figure 4.3.

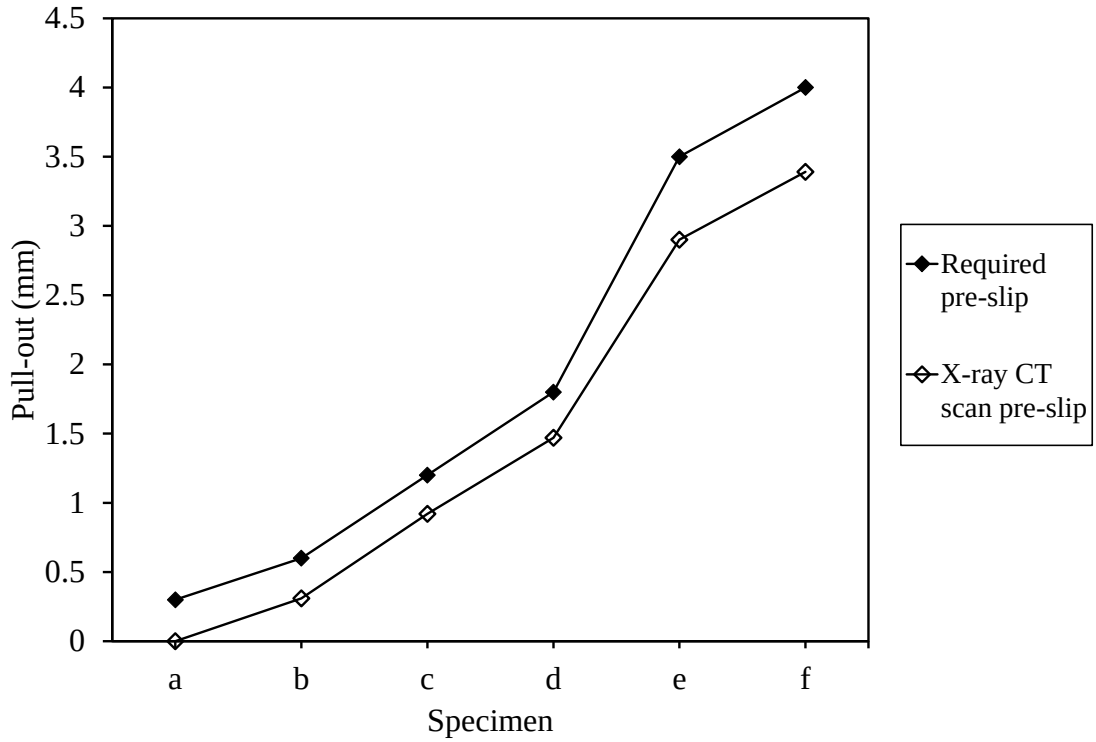

Figure 4.7: Difference between the required pre-slip and the X-ray CT scan measured pre-slip

4.2. Fatigue test results

4.2.1. Single fibre pull-out fatigue tests

The fatigue pull-out tests were performed on single fibre specimens, with three different load levels, as well as four varying degrees of pre-slip. The pre-slips were chosen based on the static pull-out results in Section 4.1.1, which ranged between 0.6 mm and 2.5 mm. This fibre pull-out range represented the region before and after the maximum pull-out load of

the fibre, and thus provided insight into the fundamental fatigue pull-out behaviour of pre-slipped specimens.

The results of the tested specimens are shown in Table 4.1. As previously mentioned, the tests were performed at a frequency of 6 Hz, until failure or up to 2 million load cycles. Each test was repeated three times on different specimens from the same batch, with the exception of the 50% load level test at pre-slips of 1.2 mm and 1.8 mm. Initially, the first two specimens tested at 50% load level and 0.6 mm pre-slip were only tested up to 1 million cycles. However, based on the performance of the tests, the test limit was increased to 2 million cycles for the rest of the tests.

The results in Table 4.1 indicate the number of load cycles sustained for each test performed, as well as the failure mechanisms. The number of cycles sustained for each test was rounded down to the nearest thousand, and specimens sustaining less than 1 000 cycles were not rounded. The 50% load level tests at pre-slips of 1.2 mm and 1.8 mm were terminated due to technical difficulties before the test could be completed. However, based on the fibre fatigue pull-out test results in Figure 4.9, it was assumed that the test would not fail and would reach 2 million load cycles.

Table 4.1: Fatigue life and failure mechanisms (green = no failure, orange = pull-out, red = rupture)

Pre-slip (mm)	**Specimen**	**Number of cycles**		
		Load level		
		50%	**70%**	**85%**
0.6	1	1 000 000	2 000 000	2 000 000
	2	1 000 000	2 000 000	1 109 000
	3	2 000 000	328 000	1 396 000
1.2	1	760 000†	2 000 000	889 000
	2	-	2 000 000	830 000
	3	-	2 000 000	50
1.8	1	1 352 000†	2 000 000	154
	2	-	1 800 000†	30
	3	-	566 000	24
2.5	1	2 000 000	2 000 000	34
	2	182 000	61	32
	3	56	37	29

† Test could not be completed

The number of load cycles in Table 4.1 illustrates a clear trend with regards to the load level as well as the pre-slip. A 50% applied fatigue load level resulted in no failures up to a pre-slip of 1.8 mm, after which, the pull-out failure mechanism dominated at a pre-slip of 2.5 mm. The 70% load level results were similar to the 50% load level results, however, fibre rupture as well as fibre pull-out occurred. The fibre rupture was present in the smaller pre-slip, whereas the fibre pull-out occurred at a pre-slip of 2.5 mm. At the 85% applied fatigue load level, the specimens presented minimal fatigue resistance, with only one specimen lasting the full 2 million load cycles. Fibre rupture failure was also more frequent, as well as fibre pull-out. Colour contours are used in Table 4.1 to show the failure mechanisms, with fibre rupture and fibre pull-out increasing in frequency as the pre-slip and the load level increase.

The test results plotted in Figure 4.8 illustrate the failure mechanisms as well as the fatigue capacity. The incomplete tests of the 50% load level (1.2 mm and 1.8 mm pre-slip) were assumed to last the full 2 million load cycles. For the 50% and 70% load levels, the specimens were able to provide a degree of fatigue capacity up to a pre-slip of 1.8 mm, with a possibility of fibre rupture for the 70% load level. Once the pre-slip increased to 2.5 mm, the fatigue capacity was severely compromised and pull-out failure was imminent regardless of the applied fatigue load level. The 85% load level fatigue capacity was substantially reduced as the pre-slip increased from 0.6 mm to 2.5 mm.

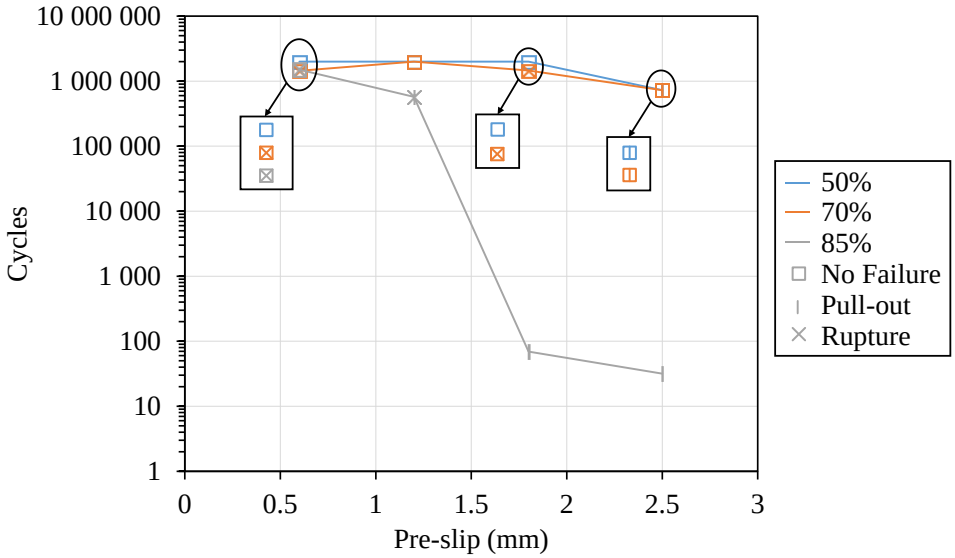

Figure 4.8: Fatigue failure mechanisms

4.2.1.1. Fatigue fibre displacement behaviour

For the duration of each test, the fibre displaced a certain amount based on the pre-slip and the load level. The graphs shown in Figure 4.9, Figure 4.10, and Figure 4.11 illustrate the behaviour of each fibre during the respective fatigue tests. The maximum pull-out displacement from each sine-cycle was used to plot the graphs in the abovementioned figures. Each graph isolates the load level, with the varying pre-slips for each test. After a fibre pull-out of 10 mm, the test represents complete pull-out of the fibre from the matrix in the abovementioned figures.

The 50% load level results in Figure 4.9 show the two complete pull-out failures, along with the other tests which did not fail. The one pull-out failure occurred at 56 cycles for a 2.5 mm pre-slip, and showed displacement to a pull-out of 3.0 mm within 10 fatigue load cycles. Pull-out failure occurred soon thereafter. The other pull-out failure test failed only at 182 000 cycles, and was the only specimen in the test series to pull-out completely after a significant number of applied fatigue cycles. After 10 000 load cycles, the pull-out increased slightly until it reached 3.0 mm, after which the failure was immediate. Based on the results in Figure 4.2, at a pull-out of 3.0 mm, the specimen is ascending to the second load peak, which means that the last curve (A) of the fibre hook is beginning to straighten out, thus making pull-out easier. All the other tests within the 50% load level did not fail. All the specimens which did not fail behaved in a similar manner, where the pull-out remained constant throughout the 2 million cycles, with little to no increase in the pull-out for the duration of the tests.

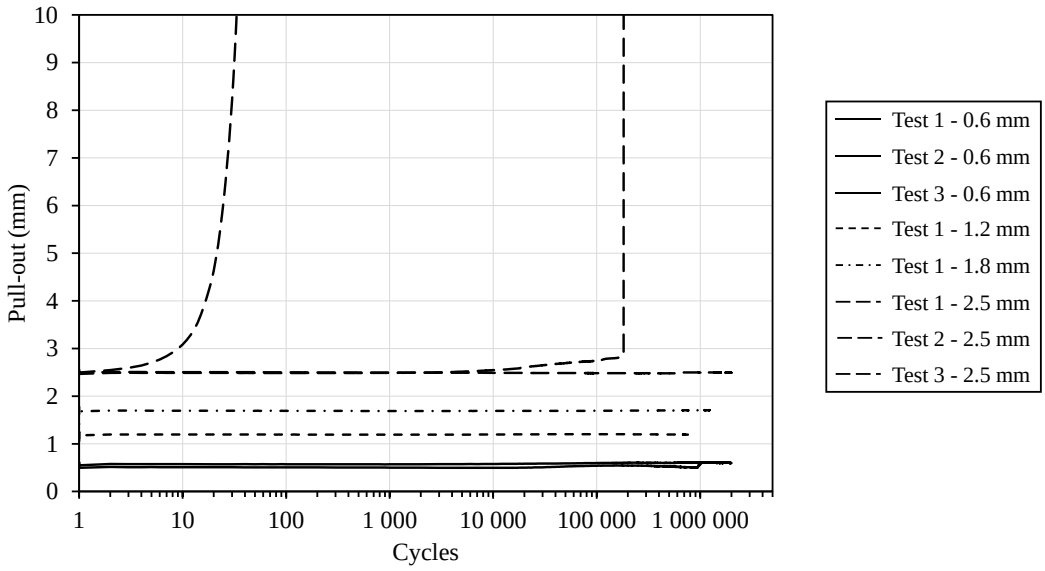

Figure 4.9: 50% load level fatigue test results

The 70% load level tests in Figure 4.10 show similar results to that of the 50% load level. There were however two ruptured specimens, the results of which are displayed in Figure 4.12. The two pull-out failures exhibited similar trends to that of the 50% load, with pull-out failure occurring within 100 load cycles for the 2.5 mm pre-slip test specimens. The third 2.5 mm test specimen which did not fail displayed different results to that of the other specimens which did not fail. After 10 cycles, the pull-out displaced to just above 3.0 mm, which would have generally resulted in pull-out failure. However, this was not the case. The test pull-out remained stable up to 10 000 load cycles, where it increased in pull-out once more to 3.5 mm. The fibre maintained this pull-out until the 2 million load cycles were completed. Based on the applied load level and the degree of pre-slip, the fibre should have pulled out. However, it was possible that this fibre still had its last curve (A) intact, or was at the initial stage of deformation, since the region of 3.5 mm is where the second peak occurs according to Figure 4.2. As a result, the fibre did not pull out.

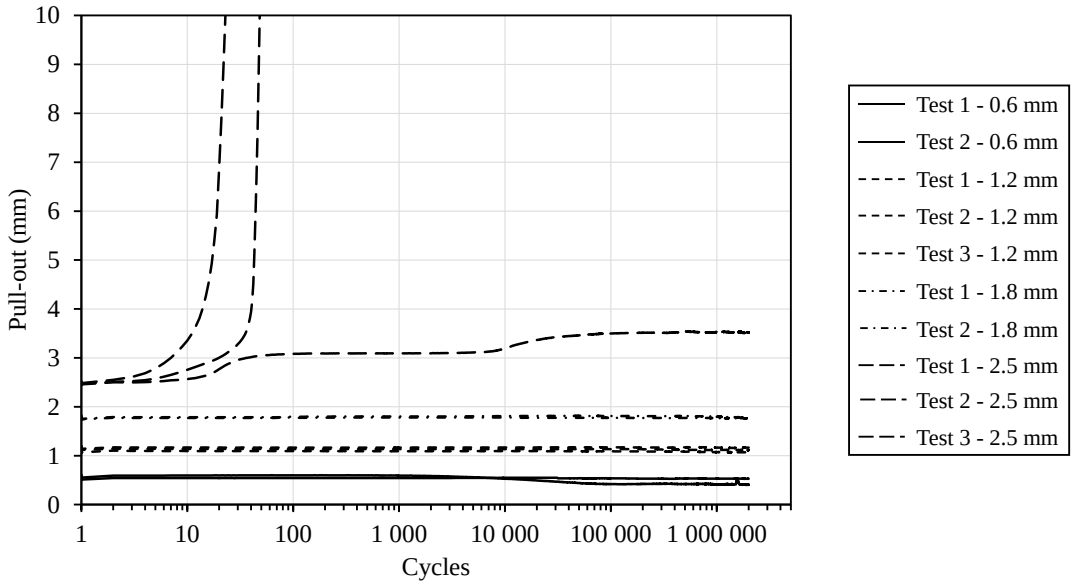

Figure 4.10: 70% load level fatigue test results

The 85% load level results in Figure 4.11 show more fibre pull-out failures than the previous two load levels. Specimens with pre-slips of 1.2 mm, 1.8 mm and 2.5 mm failed in pull-out with the 85% applied load level. Additionally, there were four specimens which also failed in rupture as displayed in Figure 4.12. The increased load level resulted in more failures in pull-out and rupture, with only one specimen lasting the full 2 million load cycles.

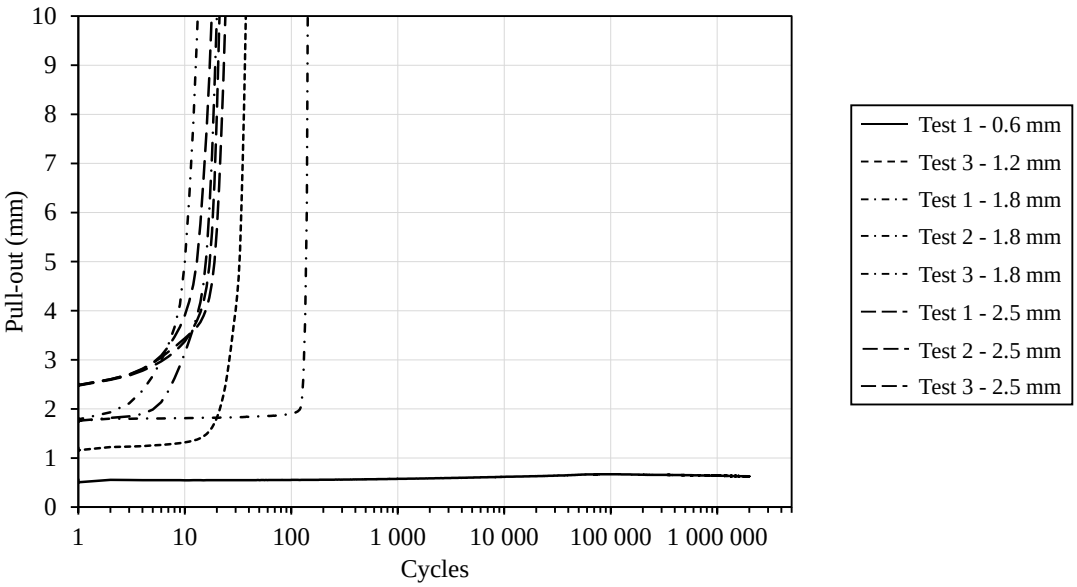

Figure 4.11: 85% load level fatigue test results

The individual ruptured specimen results for all load levels are plotted in Figure 4.12. The trend was the same throughout for all the ruptured specimens. A constant pull-out displacement was maintained for the duration of the test. When the fibre ruptured, there was no prior behaviour that would have indicated fibre rupture. The test results are almost identical to that of the specimens which did not fail. Only in this case, the fibre rupture occurred instantly and failed in a brittle fashion.

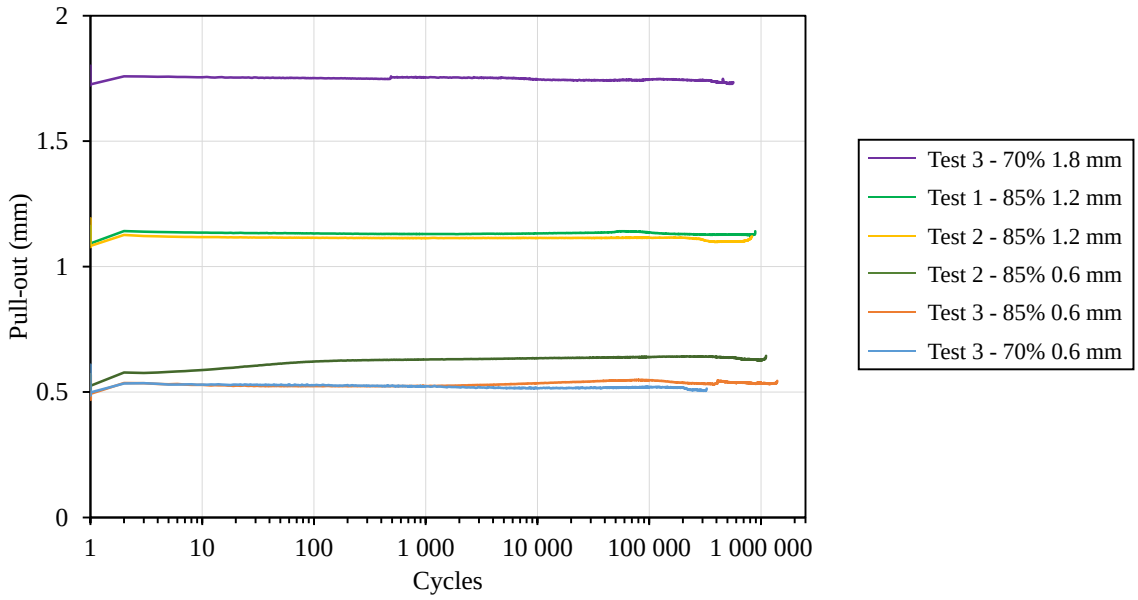

Figure 4.12: Isolated pull-out graph of ruptured specimens only

4.2.1.2. Pull-out failure

The failure mechanism results are plotted in Figure 4.13 for the different load levels and pre-slips, against the number of cycles each test specimen could withstand. The pull-out failure was found to be the most common failure mechanism, followed by fibre rupture.

As expected, the majority of the pull-out failures occurred at a load level of 85%, and decreased in frequency as the load level decreased. The pre-slip for the pull-out failures were mainly 1.8 mm and 2.5 mm, with one specimen at 1.2 mm pre-slip failing in pull-out. The pull-out failures occurred at high pre-slips, irrespective of the load level, and were largely determined by the phase the fibre was in prior to the fatigue loading. Once the fibre reached a certain phase, the load level then influenced the outcome of the test due to the fatigue loading.

At the lower pre-slip of 0.6 mm and 1.2 mm, the fibre was in Phases 2 and 3 respectively. With minimal fibre deformation, the load level then played the biggest role in determining the failure mechanism, if any. There were no pull-out failures for the 0.6 mm pre-slip at any of the load levels, and only one pull-out failure at 1.2 mm pre-slip at 85% load level. The 1.2 mm pre-slip just peaked or started on the descending branch of Phase 3 and Figure 4.5 (c) shows that the deformation to the fibre hooks was not significant. The load required to completely pull out the fibre was therefore dependent on the magnitude of the load from the respective applied load levels.

An increase of pre-slip to 1.8 mm and 2.5 mm, moved the fibre to various stages of the descending branch of Phase 3, where the 2.5 mm pre-slip was on the verge of heading to Phase 4. The deformation of the respective fibre hooks was more significant as the fibre pre-slip increased. The fibre then straightened out the curves A and B, which added additional length into the fibre cavity. When the curve A and B straightened out, the anchorage provided by the fibre hooks was diminished and fibre pull-out was imminent. The large fibre deformation, coupled with the high load level resulted in the pull-out failures experienced mainly by specimens with 1.8 mm and 2.5 mm pre-slip at 85% load level as shown in Figure 4.13.

The pull-out failures all exhibited the same trend with regards to the number of cycles it could withstand. With the exception of one specimen, Figure 4.13 shows that all the other specimens were only able to sustain less than 1 000 load cycles before pull-out failure. One specimen at 2.5 mm pre-slip and 50% load level, failed in pull-out at 182 000 load cycles. From Figure 4.9, the specimen is shown to follow the trend of no failure. Prior to the fatigue loading, the deformation caused to the fibre by the 2.5 mm pre-slip was likely to have been not as severe, with sufficient anchorage to hold the fibre in place during the fatigue loading. However, as the loading continued, the pull-out then slowly began to increase after 10 000 cycles until it deformed the fibre more, thus resulting in complete fibre pull-out.

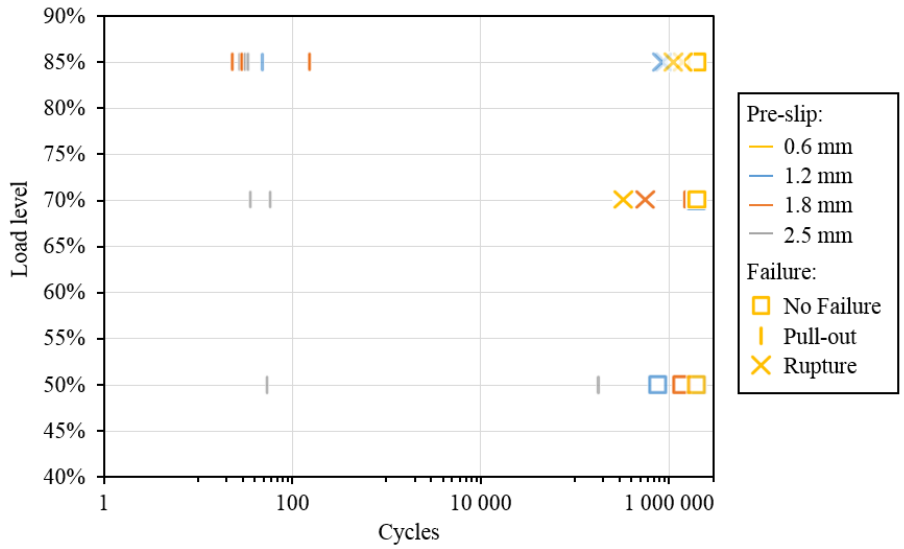

Figure 4.13: Fatigue life and failure mechanisms of all tested specimens

Figure 4.14 illustrates that the average static load-displacement curve formed an envelope for the fatigue behaviour. While the fibre was within Phase 3, the cyclic load-displacement graph remained stable with respect to the loading and the pull-out. However, once the fibre reached Phase 4, the pull-out displacements increased rapidly with each cycle and there was minimal fatigue resistance left since the remaining curve of the fibre hook had straightened out. As the fibre reached Phase 5, the fibre resistance was slightly more than that of the static pull-out curve as the fibre continued to displace until complete pull-out.

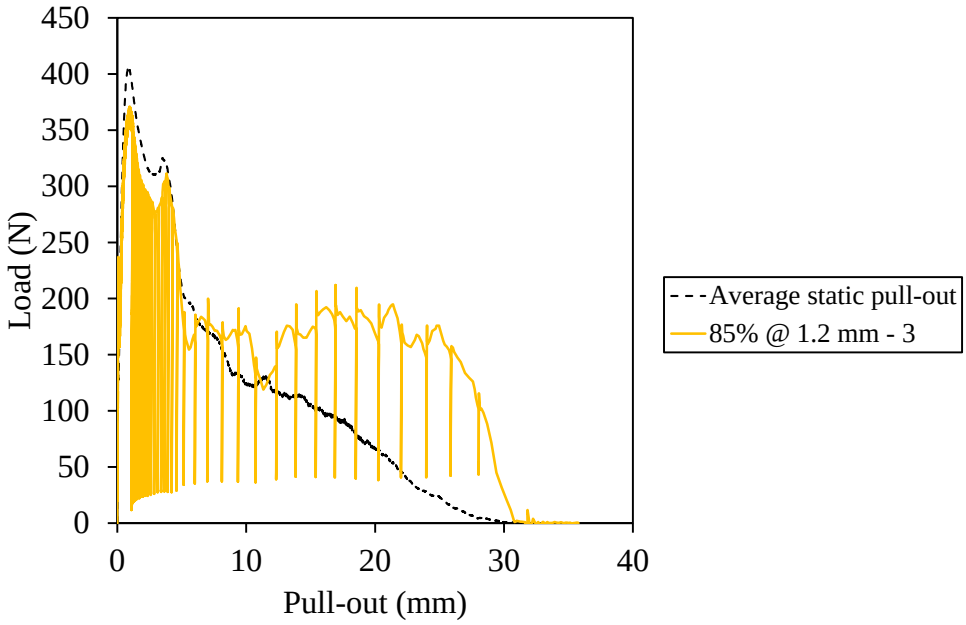

Figure 4.14: Envelope curve for fatigue pull-out

4.2.1.3. Rupture failure

The fatigue results presented in Figure 4.13 show that fibre rupture was a recurring failure mechanism. The ruptured specimens occurred more frequently at the 85% load level, followed by the 70% load level. There were no rupture failures at the 50% load level. Furthermore, the rupture failures only occurred at the lower pre-slip, namely 0.6 mm and 1.2 mm, with the exception of one occurring at a pre-slip of 1.8 mm.

All the ruptured specimen results are plotted in Figure 4.15, showing that they all failed within the same region, irrespective of the load level or the pre-slip. The 85% load level ruptured specimens showed a good correlation, with the 0.6 mm pre-slip sustaining marginally more load cycles than that of the 1.2 mm pre-slip. This is to be expected with the fatigue results. However, at the 70% load level, there was no clear trend in the failure, with the specimens sustaining even fewer cycles than at the 85% load level. The 0.6 mm pre-slip specimen also failed before the 1.2 mm specimen, which was not expected. However, the difference between the number of cycles sustained for each pre-slip was not significant. Furthermore, the fatigue fibre rupture results showed that a large number of cycles was sustained before the fibre failed in rupture. This is typical for fatigue behaviour and the results illustrate overall similar behaviour, with some deviation.

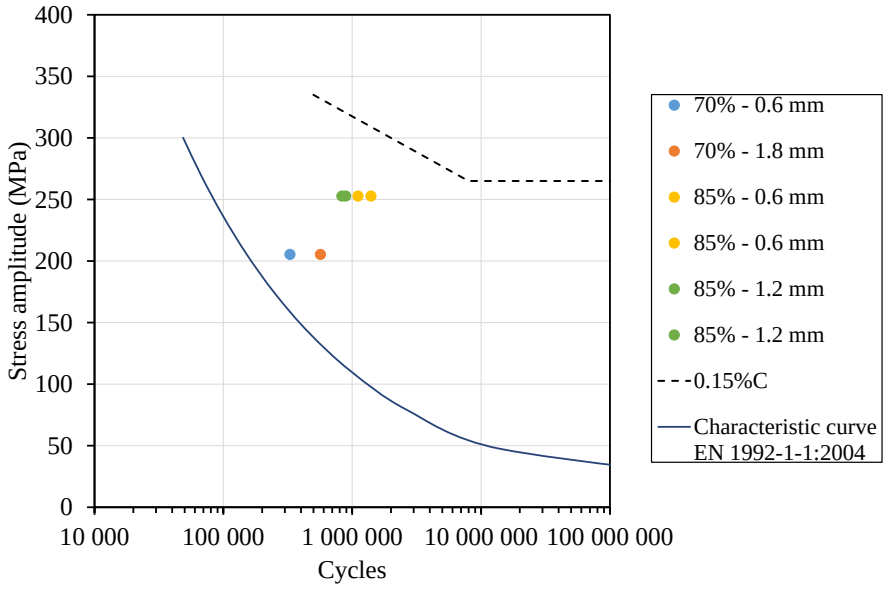

Figure 4.15: Fatigue rupture results compared with characteristic S-N curve of fibre based on BS EN 1992-1-1 (2004), and low carbon steel obtained from Mayer (2009)

The trend in results shows that at high load levels and small pre-slips, fibre rupture was the dominant failure mechanism. This may have been as a result of the minimal fibre deformation at the hooks during the pre-slip process, together with the high applied fatigue loading. The applied load may not have been sufficient to completely deform and pull the fibre out. Instead, the fibre hook provided resistance to the fatigue loading since it retained most of its shape, and the high fatigue load caused the fibre to rupture. This behaviour is illustrated in Figure 4.16.

The ruptured specimen results were then compared to the stress-number of cycles (S-N) characteristic curve for reinforcing wire fabrics based on the fatigue load applied to the fibre from BS EN 1992-1-1 (2004), and is illustrated in Figure 4.15. The S-N curve for low carbon steel, which is a similar type of steel to that used in fibres, is also plotted in comparison to the fatigue rupture specimen results. The low carbon steel contained 0.15% carbon, and was tested in fatigue tension and compression, with a stress ratio, R = -1. According to the characteristic curve, the 70% and 85% load levels should have sustained around 200 000 and 90 000 cycles, respectively. The ruptured specimen results were found to lie between the two S-N curves, with both the load levels' specimens enduring more fatigue load cycles than the characteristic curve and less than the low carbon S-N curve. However, due to the initial pre-slip performed, the boundary conditions of the tested specimens may differ to that of the characteristic curve. In contrast, the low carbon steel showed a significant difference in the expected number of cycles at the corresponding load levels. This could be due to the low carbon steel experiencing fully reversed fatigue loading (tension and compression), which could possibly result in an increased fatigue life expectancy (Musuva & Radon, 1979).

Three ruptured specimen results were plotted and were compared to the static load-displacement curve in Figure 4.16. After the pre-slips, all three specimens showed larger than average debonding strengths, as well as larger global peak strengths. This was likely to be indicative of rupture behaviour, since the load required to completely pull the fibre out could not be reached by the applied fatigue load. Even at the 85% load level, when the global peak strength was larger than the average peak strength, the load applied by the 85% load level may not have been sufficient to result in pull-out failure. This was further corroborated by Ghoddousi et al. (2010), who stated that specimens with lower

bond strength were likely to fail in pull-out, whereas a higher bond strength would result in fibre rupture.

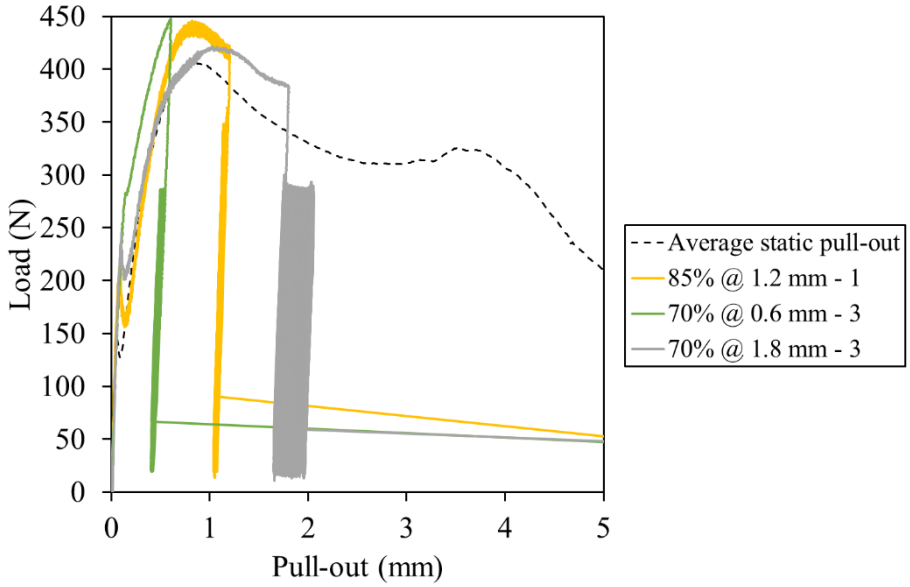

Figure 4.16: Fatigue rupture behaviour

4.2.2. Fatigue X-ray CT scans

X-ray CT scans were conducted on various specimens after the fatigue testing was completed to determine the failure mechanism in certain cases, or to illustrate the degree of damage caused by the fatigue loading.

Figure 4.17 shows the X-ray CT scan of a specimen which failed due to complete fibre pull-out. Even though the fibre had straightened out, some curves still remained where the fibre hook was. Since the fibre was not perfectly straightened out, the slight curves resulted in the increased residual loads shown in Phase 5 of Figure 4.1. This also caused the tip of the fibre to collect matrix particles during pull-out, which can also be seen highlighted in Figure 4.17. Furthermore, there was no visible damage caused to the matrix surrounding the fibre cavity after pull-out. Although not visible, the failure mechanisms were suspected to cause some damage to the matrix surrounding the fibre.

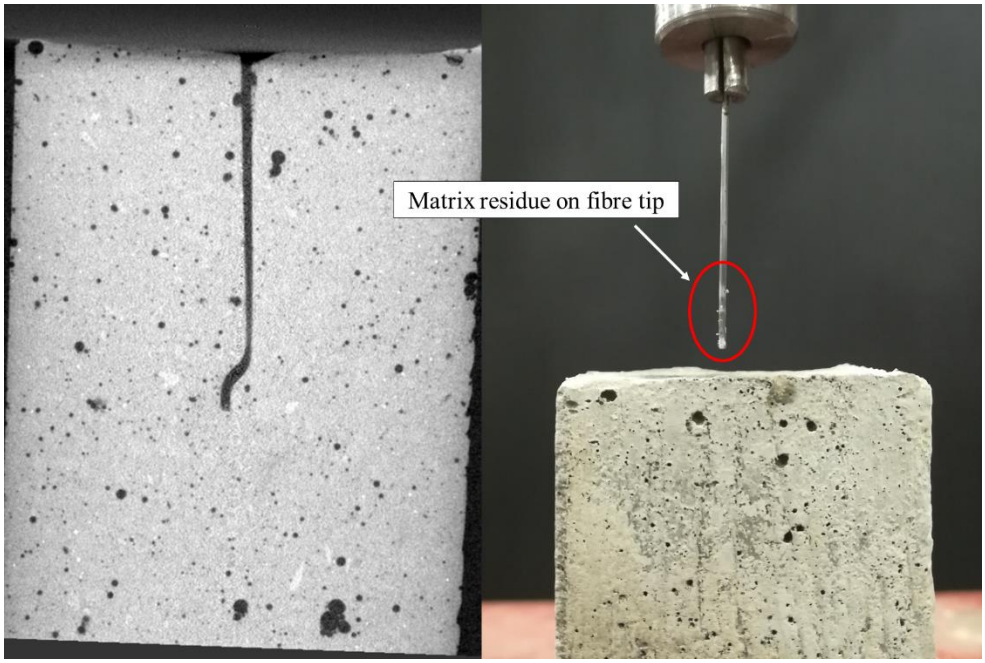

Figure 4.17: Specimen after complete fibre pull-out

The specimens which failed due to rupture were also sent for X-ray CT scans and the four specimens are displayed in Figure 4.18. The X-ray CT scans show that the fibres ruptured either at the hook or at the surface of the concrete. There was no clear indication of when the fibre would rupture and at which location, since the 85% load level tests with pre-slip of 1.2 mm shown in Figure 4.18 (a) and (c) both ruptured at different locations. The fibre which ruptured at the hook in Figure 4.18 (a) showed that the complete fibre hook was still intact, whereas the fibre in (b) showed that part of the hook remained embedded in the matrix only. However, the location of rupture was not of significant importance, since the failure was brittle and immediate at both locations.

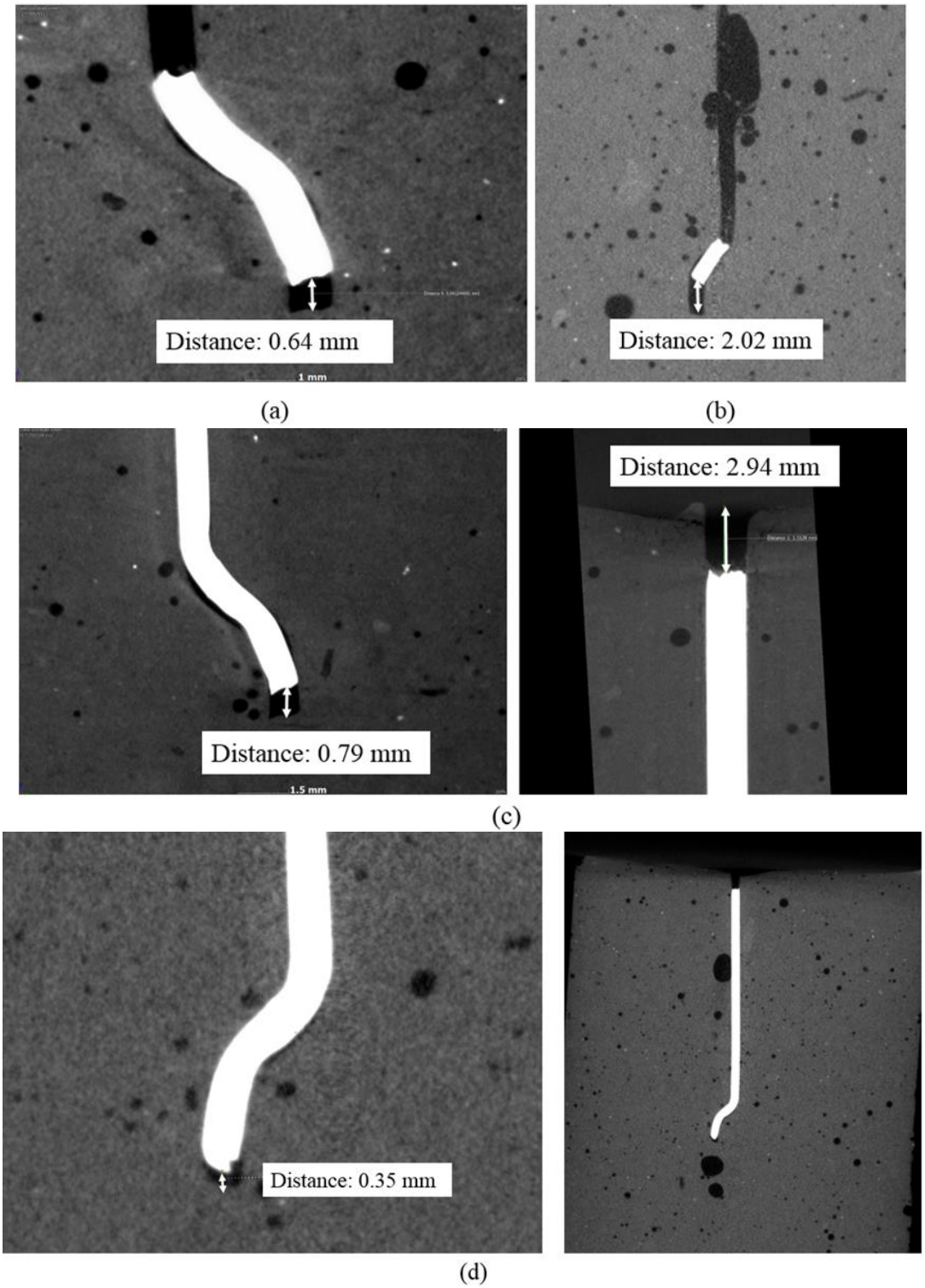

Figure 4.18: Post fatigue test X-ray CT scans of ruptured specimens (a) 85% at 1.2 mm Specimen 1, (b) 70% at 1.8 mm Specimen 3, (c) 85% at 1.2 mm Specimen 2 – illustrating the hook pull-out and fibre rupture location, (d) 85% at 0.6 mm Specimen 2 – illustrating the hook pull-out and fibre rupture location

The specimen shown in Figure 4.18 (c) was further analysed and altered to remove excess matrix material in order to obtain a better resolution on the X-ray CT scan, shown in Figure 4.19. A section taken through the mid-point of the fibre and matrix showed visible cracks at the top surface of the matrix, starting from where the fibre ruptured. Further analysis of the X-ray CT scans revealed the micro cracks started just before the fibre ruptured in Figure 4.20 (a) and spread outwards as the scans progressed to the surface of the matrix in Figure 4.20 (b) and (c). This indicates that the fibre sustained large stresses, which then transferred into the matrix causing cracks, and eventually, fibre rupture.

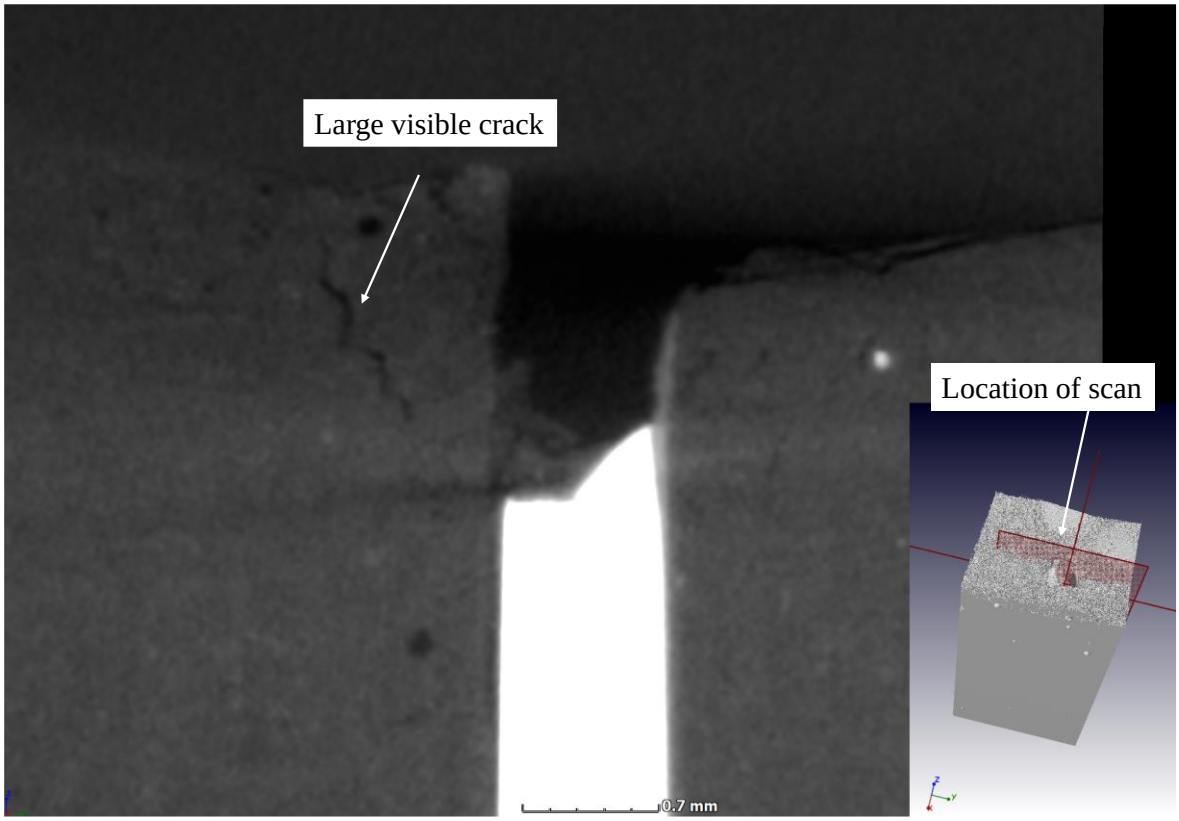

Figure 4.19: Cracks shown at the surface of Specimen 2 tested at 85% load level and 1.2 mm pre-slip

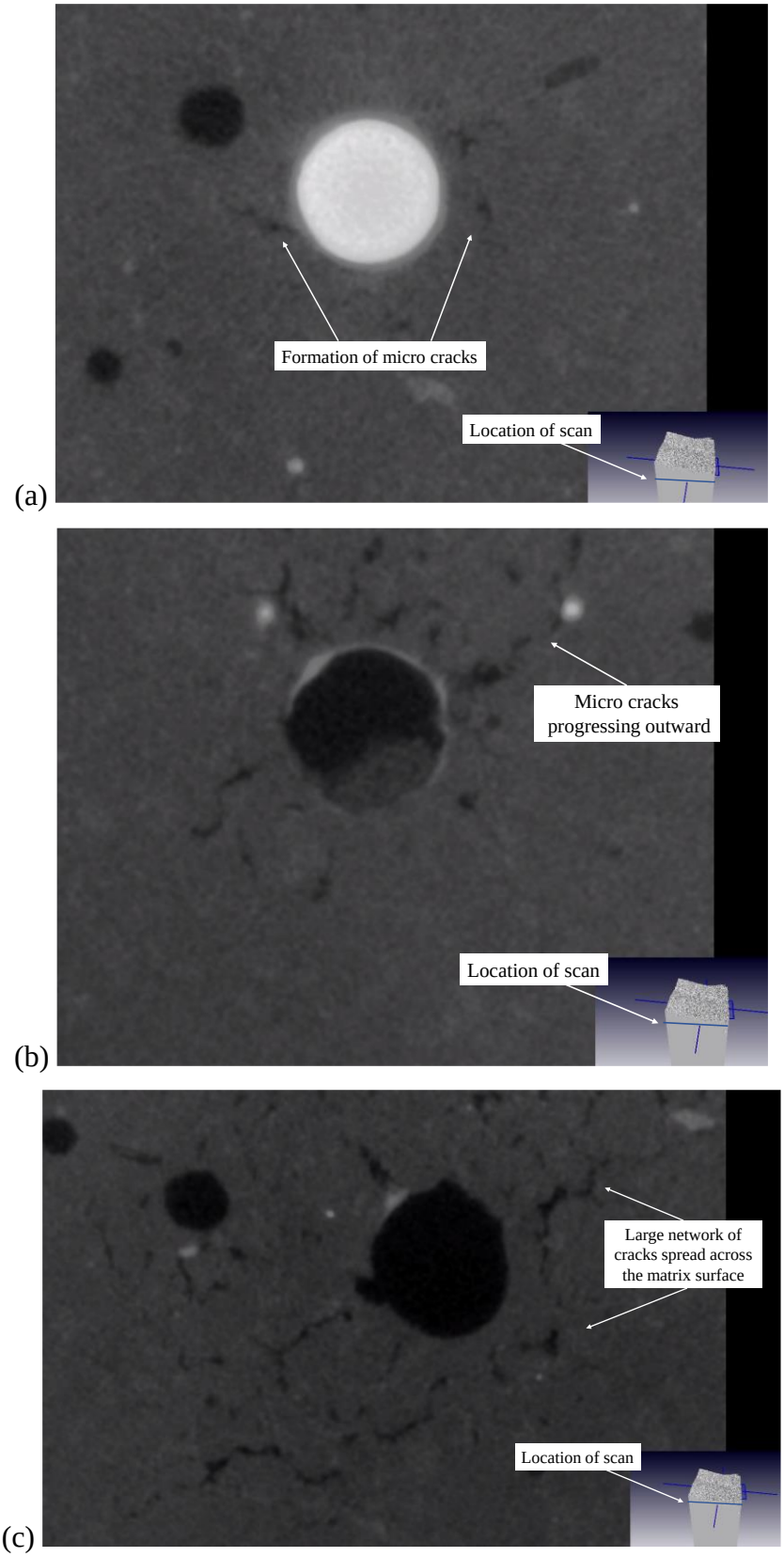

Figure 4.20: Spread of micro cracks at various locations along the ruptured fibre (a) before rupture (b) right after fibre rupture (c) at surface of specimen

An X-ray CT scan was also performed on a specimen which did not fail. The specimen was tested at a load level of 70% and pre-slip of 2.5 mm. Significant deformation of the fibre hooks can be seen in Figure 4.21. The fibre was isolated from the matrix and the indentations caused by the matrix to straighten the fibre out is clear in Figure 4.21 (b). The fibre curve B has already straightened out, with only a part of curve A remaining. In Figure 4.10, the graph illustrates the pull-out behaviour over the 2 million cycles for the specimen showing that the fibre pulled out up to 3 mm before the test ended at 2 million load cycles. The remaining curve A was able to withstand the fatigue loading throughout the test and provided anchorage. Since the fibre was in Phase 4 at the end of the test, any further fatigue loading may have resulted in fibre pull-out shortly thereafter.

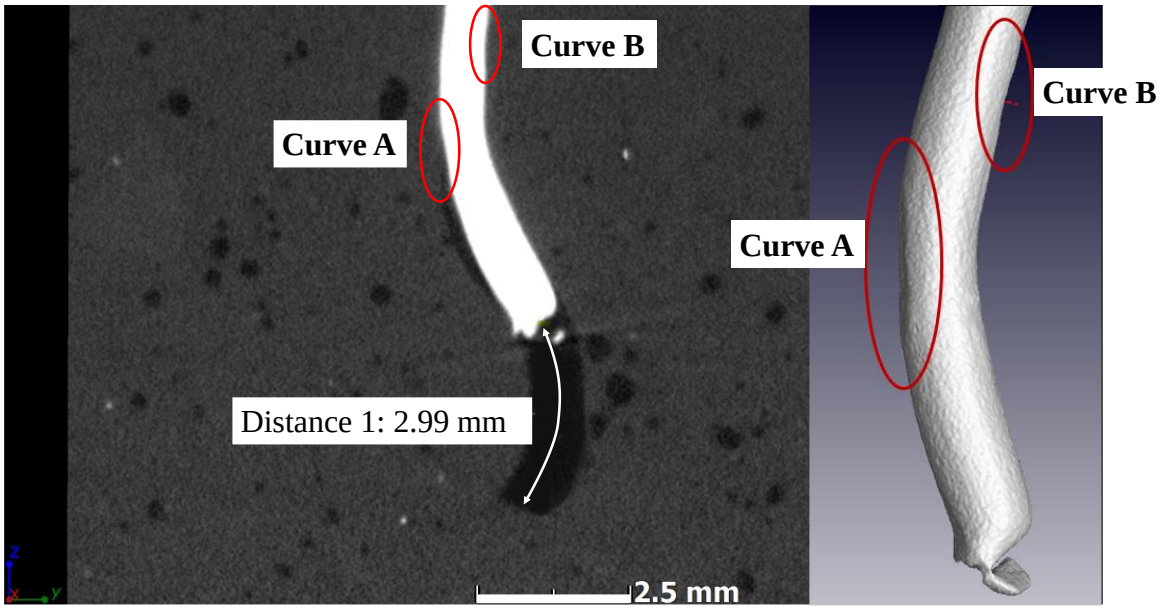

(a) (b)

Figure 4.21: Post fatigue test X-ray CT scan of 70% load level and 2.5 mm pre-slip Specimen 1 (a) full X-ray CT scan (b) fibre isolated from matrix

4.3. Concluding summary

In this chapter, the findings from the single fibre pull-out fatigue tests were presented for specimens that were pre-slipped to various degrees prior to fatigue loading. The fatigue tests were conducted at load levels of 50%, 70% and 85% of the average maximum static pull-out load. The pre-slips applied to the fibres prior to fatigue loading were 0.6 mm, 1.2 mm, 1.8 mm, and 2.5 mm.

Static pull-out tests were performed before any fatigue tests were conducted. Two types of pull-out tests were done, which included complete fibre pull-out, and partial fibre pull-out for the different stages of pre-slip. The complete fibre pull-out results were used to determine the average maximum static pull-out load, as well as to investigate the behaviour of the fibre as it pulls out of the matrix. The partial static fibre pull-out results were used along with the complete pull-out results to plot a theoretical single fibre model which classified the fibre pre-slips into different phases. X-ray CT scans were also performed on the partial fibre pull-out specimens to corroborate the proposed phases.

The level of deformation of the fibre hooks after the pre-slip determines which of the five phases the fibre is classified into. Phase 1 is the debonding process, where the load increases and the bond between the fibre and the matrix diminishes. This continues until the fibre completely debonds in Phase 2 and the fibre anchorage is activated. As the load increases, the fibre hooks begin to deform which occurs in Phase 3, where the fibre experiences the global peak load due to the deformation of the fibre hooks. In Phase 4, the last remaining curve of the fibre hook straightens out, which results in another peak in the load, followed by Phase 5 which is the frictional pull-out of the straightened fibre.

Based on the X-ray CT scans of the partially pulled out fibres, the pre-slip of 0.6 mm was found to be in Phase 2. The pre-slip of 1.2 mm, 1.8 mm and 2.5 mm are in Phase 3, and are each at different stages of the descending branch of the load-displacement curve. As the pre-slip increases, the deformation to the fibre becomes more severe, thereby diminishing the anchorage of the fibre hooks.

After the pre-slip, the specimens were tested in fatigue at 50%, 70% and 85% load levels, up to 2 million load cycles or until failure. Two failure mechanisms were observed in the results, predominantly fibre pull-out, followed by fibre rupture. The fibre pull-out occurs mainly with specimens whose pre-slip places it into the descending branch of Phase 3. This is due to the significant deformation on the fibre hook prior to fatigue loading. The 2.5 mm pre-slip predominantly fails in fibre pull-out, with only two specimens not failing at the 50% and 70% load level. As the pre-slip decreases, fibre rupture failure increases at the 70% and 85% load levels.

Based on the respective phase the fibre is in after the pre-slip process, as well as the load level applied to the specimen, the outcome of the fatigue tests could be predicted. At the

small pre-slip (0.6 mm and 1.2 mm) when the fibre is in Phase 2 or the beginning of Phase 3, and the load level is low, failure is unlikely. The curves of the fibre hook are reasonably intact, which provides sufficient anchorage. The load required to overcome the fibre deformation and result in pull-out is likely higher than the applied load level, thus the specimen is unlikely to fail. At the same pre-slip and larger applied load levels, the possibility of fibre rupture increases since the fibre deformation is minimal, but a high stress level is applied. As the pre-slip increases to a more severe Phase 3 (1.8 mm and 2.5 mm), coupled with a high load level, the fibre deformation increases, thereby resulting in fibre pull-out. The more the fibres deform prior to fatigue loading, the less resistance it provides and the quicker it fails under fatigue loading.

5. Mechanical investigation at a macroscopic level

In this chapter, fatigue behaviour at a macroscopic level investigation is discussed. Beam specimens were cast and tested under static and fatigue loading. The static tests were required in order to determine the performance of the composite material with various fibre dosages. They were also used as a basis for performing the flexural fatigue tests, which were conducted at different load levels and pre-cracks. X-ray CT scans were performed on pre-cracked specimens, as well as specimens that failed in fatigue in order to determine the extent of the damage caused by the fatigue loading.

5.1. Static flexural test

5.1.1. Static capacity

Before the fatigue tests could be performed, static tests were conducted. Three different fibre dosages were tested to establish the desired dosage, and then to determine the average maximum static load. The test was terminated when the CMOD reached 3.5 mm. The fibre dosages were tested at 0.6%, 0.8% and 1.0% by volume of concrete, and the results are displayed in Figure 5.1.

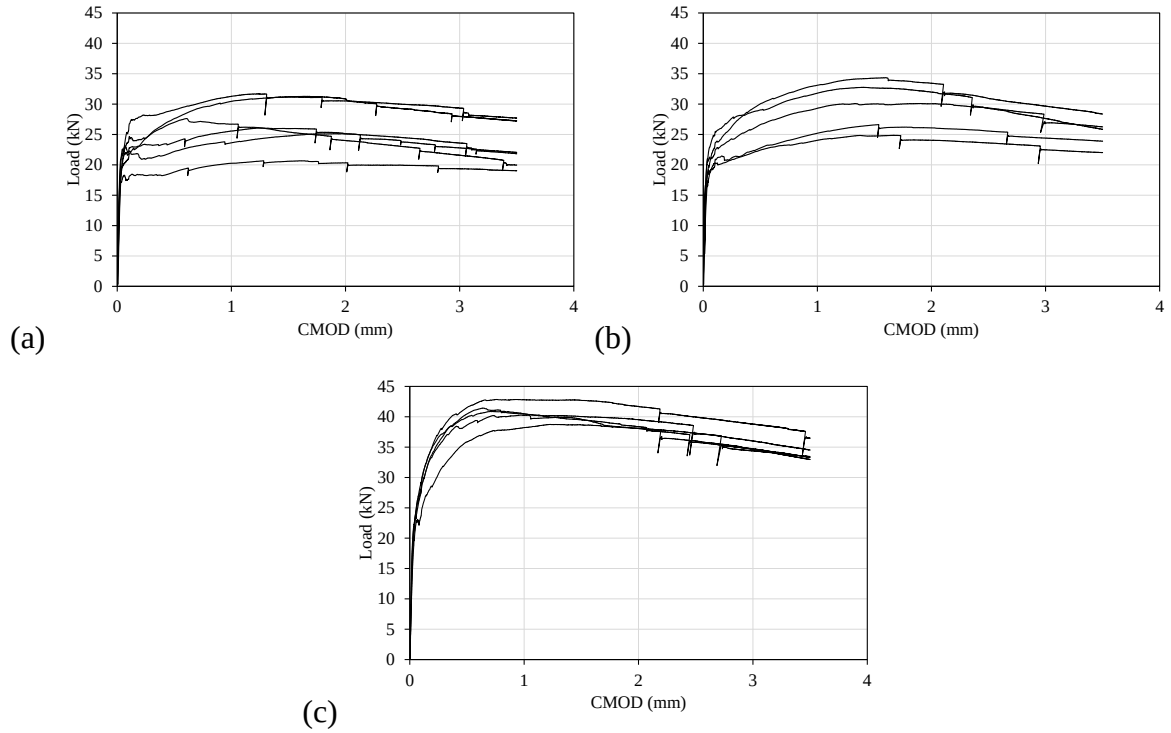

Figure 5.1: Flexural static tests with fibre volume dosage (a) 0.6%; (b) 0.8% and (c) 1.0%

At the 0.6% fibre dosage shown in Figure 5.1 (a), there was some variation in the load-CMOD results. The first crack strength ranged from 17 kN to 25 kN, followed by a gradual strength gain. Similarly, the 0.8% fibre dosage in Figure 5.1 (b) illustrated improved post-cracking behaviour, with a strength gain increasing at a steady rate after the first crack until it reached the peak, at a maximum of 35 kN. The 1.0% fibre dosage in Figure 5.1 (c) displayed the highest strength and showed good repeatability.

All the fibre dosages displayed deflection hardening behaviour. As expected, the post-cracking strength increased as the fibre dosage increased, thereby providing a more ductile post-cracking behaviour. As the tests progressed, there were numerous noticeable load reductions, followed by a quick recovery. This decreased in frequency as the fibre dosage increased. The load reductions were associated with the failure of fibres bridging the cracks, either in pull-out or rupture. At the lower fibre dosage, the fibres bridging the cracks were sparsely dispersed throughout the matrix, mainly due to the length of the fibre and the fibre dosage. As the load and CMOD increased, pull-out of fibres bridging the crack began. When the fibre hooks deformed, its ability to effectively carry its individual load decreased, thereby increasing the load in the neighbouring fibres (Abbas, Soliman & Nehdi, 2015). Due to the large inter-fibre spacing, these load reductions occurred more frequently, as fewer fibres were bridging the crack, thereby resulting in quicker fibre failure. An increase in fibre dosage correlated to more fibres bridging the crack and smaller inter-fibre spacing, since there were more fibres in the matrix.

After all the static tests were performed, it was decided to use the 0.8% fibre dosage as the overall results were good. The fatigue test results were also compared with similar tests performed by Hemmeter (2017) in the subsequent chapter, who also used the same fibre dosage and similar materials to perform fatigue tests.

5.1.2. X-ray CT scans

X-ray CT scans were performed on four specimens which were pre-cracked to 0.6 mm, 1.2 mm, 1.8 mm, and 2.5 mm. In order to obtain high resolution scans, the specimens were cut smaller as outlined in Section 3.5, and the full depth of the specimen along the crack was maintained for analysis. Since the specimens were cut smaller, and due to the random orientations of the fibres, it was not always possible to obtain images of a full fibre bridged across the crack. In the subsequent images, every effort was made to show the fibre hook

as well as part of the body of the fibre. Consequently, there may be fibres displayed with varying embedment lengths and orientations. However, it is used mainly for illustrative purposes. All the fibres discussed in this section refer to the highlighted fibre in the figures.

The CT scans are shown as they were tested, with the notch portion at the bottom, illustrating the largest crack opening, and the crack opening decreases as the crack progresses upwards. Each pre-crack is displayed on two figures, where the highlighted fibre in figures (a) represent the fibre deformation and pull-out a fibre closer to the notch and figures (b) show the fibre deformation and pull-out of a fibre further away from the notch. The CT scan images in Figure 5.2 to Figure 5.5 respectively for each pre-crack were taken on the same specimen, but at different locations throughout the depth of the specimen. As a result, the crack pattern on the images differs depending on the depth of the specimen.

At the 0.6 mm pre-crack in Figure 5.2, there is a noticeably small crack propagating from the bottom (notch) to the middle of the specimen. The 0.6 mm pre-crack is not large enough to create a crack up the full height of the specimen. Figure 5.2 (a) shows a fibre bridging the crack located close to the notch, where the largest crack opening occurs. No visible fibre pull-out can be seen, and it is assumed that the fibre has already debonded from the surrounding matrix, but the pull-out is too small to be visible. This fibre is similar to the fibres classified in Phase 2 in Section 4.1.2, where they are starting to pull out. In Figure 5.2 (b), the fibre shown is located further away from the notch, which ultimately results in less fibre pull-out. Fibres located further away from the notch bridges smaller cracks, which places the fibres in lower phases. The crack is too small to create any fibre deformation and at this pre-crack, there is still full potential for the fibres to resist loading, since the fibres have just been activated without any hook deformation.

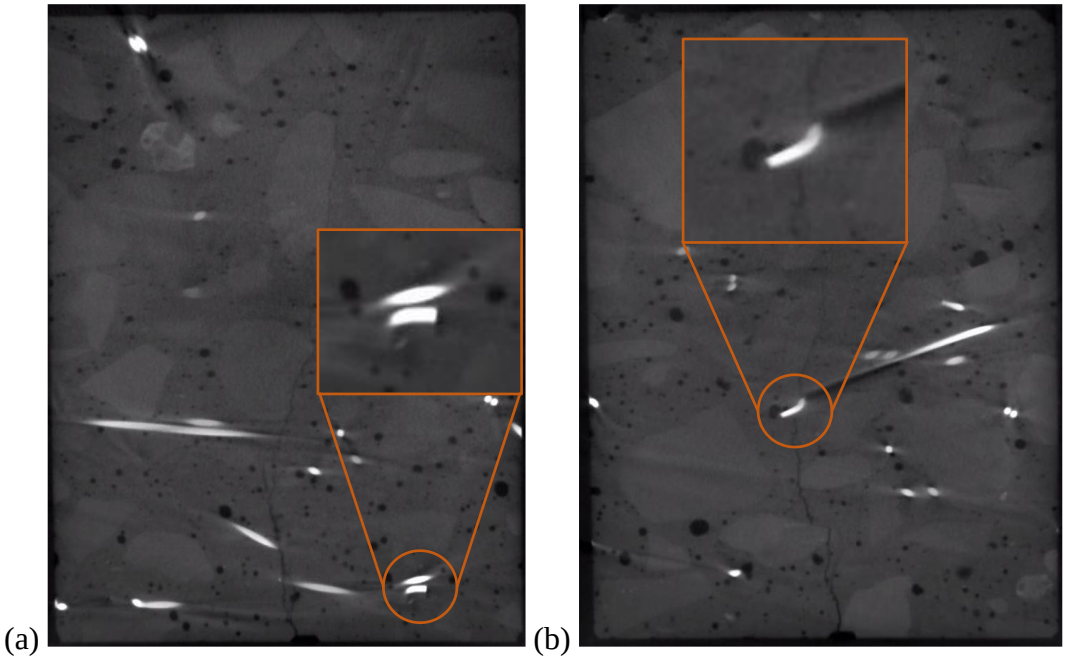

Figure 5.2: X-ray CT scan of specimen pre-cracked to 0.6 mm with fibres enlarged (a) fibre near the notch, (b) fibre away from the notch, (fibres indicated in orange)

In Figure 5.3, the specimen is pre-cracked to 1.2 mm, and the crack is seen to propagate over almost the entire height of the specimen. At the notch in Figure 5.3 (a), the fibre shows debonding and visible pull-out. For the fibre further away from the notch in Figure 5.3 (b), fibre pull-out is visible, but smaller than for the fibre closer to the notch.

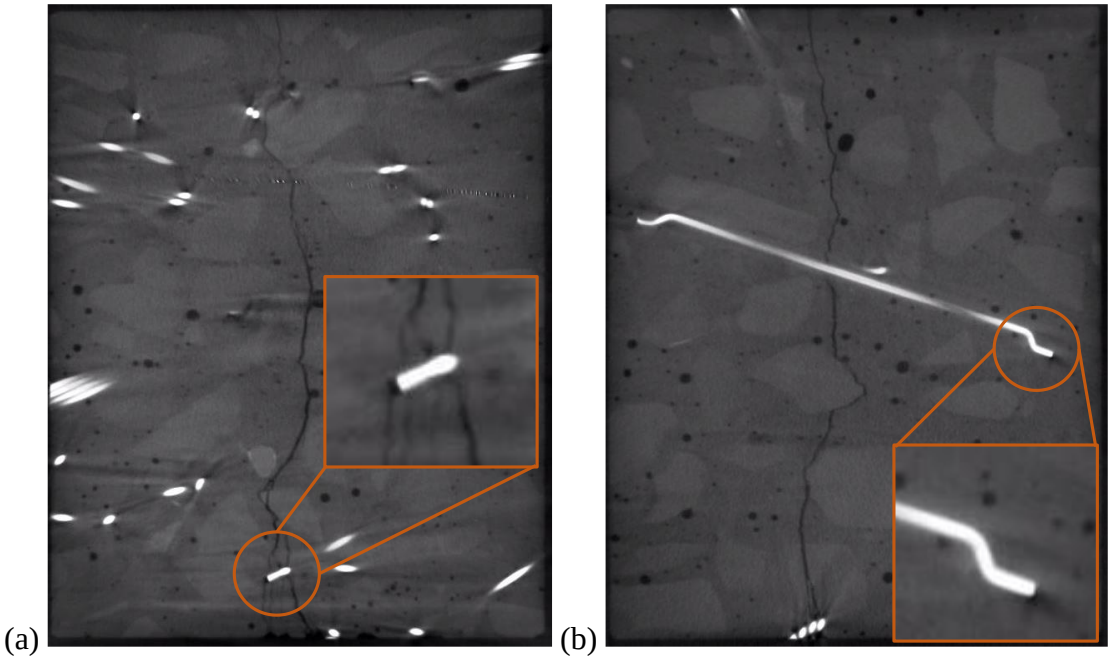

Figure 5.3: X-ray CT scans for specimen pre-cracked to 1.2 mm with fibres enlarged (a) fibre at the notch, (b) fibre away from the notch, (fibres indicated in orange)

For the 1.8 mm and 2.5 mm pre-cracks in Figure 5.4 and Figure 5.5, fibre pull-outs are larger, especially at the notch. Figure 5.4 (a) shows significant fibre pull-out, but no fibre hook deformation. As the fibres move further away from the notch, the fibre pull-out decreases. Figure 5.5 (a) illustrates fibre pull-out as well as fibre hook deformation at the 2.5 mm pre-crack. The fibre in Figure 5.5 (b) is further away from the notch and shows substantial fibre pull-out, since the crack opening at that point is relatively large as well. This is consistent with the fibre performance as the crack increases in size.

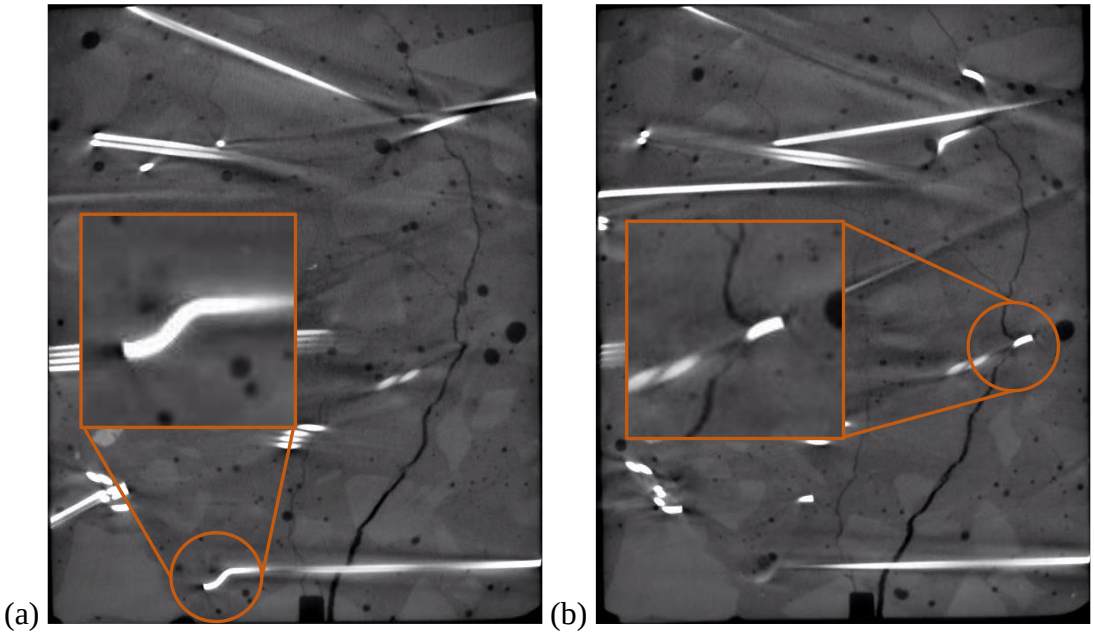

Figure 5.4: X-ray CT scans of specimen pre-cracked to 1.8 mm with fibres enlarged (a) fibre at the notch, (b) fibre away from the notch, (fibres indicated in orange)

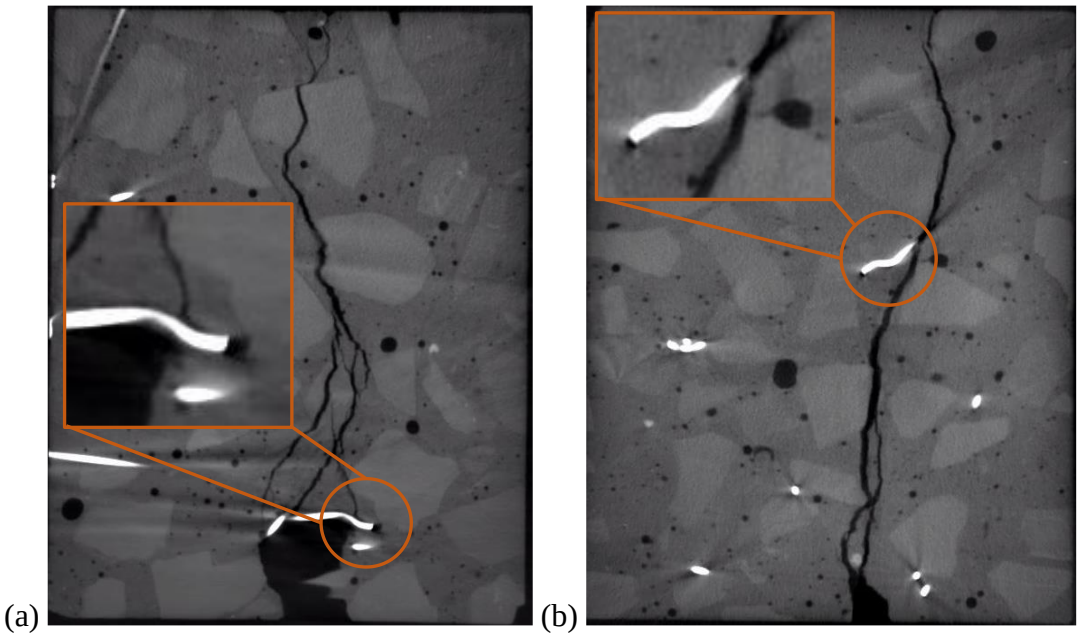

Figure 5.5: X-ray CT scans of specimen pre-cracked to 2.5 mm with fibres enlarged (a) fibre at the notch, (b) fibre away from the notch, (fibres indicated in orange)

5.1.3. Fibre classification phases – single fibre pull-out model

In Section 4.1.1, the single fibre pull-out model was developed, with different phases assigned to varying degrees of fibre pull-out as shown in Figure 5.6. In Phase 1, the fibre debonds, with no visible fibre end pull-out. Phase 2 is associated with a fibre pre-slip of

0.6 mm, Phase 3 with a fibre pre-slip of 1.2 mm, 1.8 mm and 2.5 mm, and Phase 4 with a fibre pre-slip of up to 4.0 mm. In Phase 5, the fibre pre-slip is greater than 4.0 mm, showing that the fibre hooks completely straighten out at this fibre pull-out.

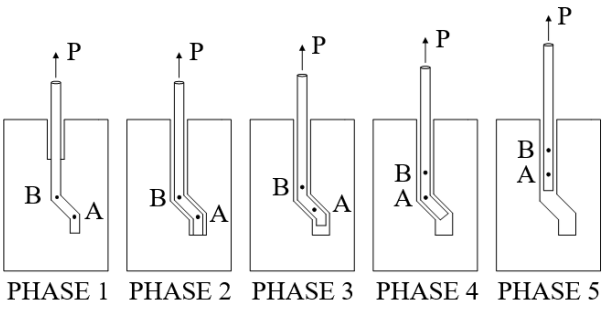

Figure 5.6: Phases for fibre pull-out

The beam specimens tested in flexure were pre-cracked to various CMOD's before being tested in fatigue. The pre-crack process resulted in different crack widths throughout the height of the specimen, with the largest crack opening at the notch and decreasing up the height of the specimen as illustrated in Figure 5.7. This resulted in fibres being pulled out to different degrees throughout the height of the specimen upon pre-cracking and therefore, the fibres were categorised according to the phases from Section 4.1.1.

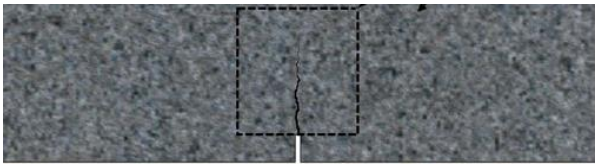

Figure 5.7: Cracked beam specimen

The X-ray CT scans performed on static test specimens in Section 5.1.2 showed how the fibres were pulled out to various degrees as the pre-crack changed. Based on the static X-ray CT scans, it was assumed that the fibres at the notch would be classified according to its pre-crack, prior to fatigue loading. Therefore, fibres at the notch of the 0.6 mm pre-cracked specimens were classified into Phase 2 as discussed in the single fibre pull-out model in Section 4.1.1. However, since the crack width decreased up the height of the specimen, the fibres located further away were classified into Phase 1, as there would be little to no crack opening further away from the notch.

For the 1.2 mm and 1.8 mm pre-cracks, the fibres at the notch were classified into Phase 3 as there was fibre pull-out at the hooks, but little to no hook deformation. The fibres

located further away from the notch were classified into Phase 2, since the fibre hook pull-out was small and the fibres were not fully engaged to cause hook deformation. However, at the 2.5 mm pre-crack, the fibres at the notch as well as throughout the height of the specimen was classified into Phase 3. There was large fibre pull-out and hook deformation at the notch, with fibre pull-out and deformation slightly decreasing further away from the notch. All the fibres were therefore classified into Phase 3, since the fibres further away from the notch were all fully engaged and active in carrying load due to the fibre end pull-out.

As the fibres moved further along into Phase 3 towards Phase 4, its fatigue capacity was severely compromised as seen from the results in Chapter 4. This, coupled with the load level, determined the fatigue outcome, as the fatigue capacity changed depending on the pre-crack and load level.

5.2. Flexural fatigue tests

5.2.1. Fatigue capacity

The fatigue tests were performed on specimens with four different pre-cracks and at three load levels, using a fibre dosage of 0.8%. Each test was repeated three times, unless otherwise specified, on different specimens. The test was terminated when the CMOD reached 3.5 mm, which was defined as a failure, or when 2 million load cycles were reached. The flexural fatigue test results are shown in Table 5.1. At the 70% and 85% load levels, all the pre-crack values were tested. However, the 50% load level tests excluded the 0.6 mm pre-crack tests. Two tests at the 50% load level could not be completed up to 2 million load cycles due to technical difficulties and were assumed to not fail based on their behaviour prior to the test ending.

The results from Table 5.1 show a decrease in fatigue capacity with an increase in load level and pre-crack, with the lowest fatigue capacity at the 85% load level. At the 0.6 mm pre-crack, the specimens were unable to withstand an average of 39 000 load cycles before reaching a CMOD of 3.5 mm. The failure was even more pronounced at the 2.5 mm pre-crack, where the average number of cycles sustained before failure was only 1 000 load cycles.

At the 50% load level, the test results show improved fatigue capacity when compared to the 70% and 85% load levels at the same pre-cracks. Based on the results from the 1.2 mm

pre-crack, the 0.6 mm pre-crack was assumed to last the full 2 million load cycles, and was not tested. The 50% load level results indicated an average of over 1 million load cycles for the 1.2 mm and 1.8 mm pre-cracks. At the 2.5 mm pre-crack, one test reached over 1 million load cycles, but could not be tested to 2 million cycles due to technical difficulties.

As expected, the 70% load level showed intermediate results when compared to the 50% and 85% load levels. The results were also most consistent in terms of coefficient of variation, and the number of cycles sustained for each pre-crack. Overall, the tests showed good repeatability regardless of the large coefficient of variation and this was expected from literature (Naaman & Hammoud, 1998; Nanni, 1991; Singh & Kaushik, 2003).

Table 5.1: Flexural fatigue test results

Pre-crack (mm)	**Specimen**	**Number of cycles**		
		Load level		
		50%	**70%**	**85%**
0.6	1	-	56 000	26 000
	2	-	75 000	38 000
	3	-	100 000	53 000
Average		**2 000 000***	**77 000**	**39 000**
Coeff. of variation (%)		**N/A**	**23.3**	**27.9**
1.2	1	1 700 000†	84 000	18 000
	2	2 000 000	208 000	20 000
	3	-	307 000	31 000
Average		**1 850 000***	**199 000**	**23 000**
Coeff. of variation (%)		**N/A**	**45.6**	**23.9**
1.8	1	746 000	43 000	6 000
	2	1 280 000	75 000	10 000
	3	-	-	29 000
Average		**1 013 000**	**59 000**	**15 000**
Coeff. of variation (%)		**26.3**	**27.3**	**63.7**
2.5	1	235 000	21 000	52
	2	888 000	26 000	651
	3	1 097 000†	37 000	2 300
Average		**740 000***	**28 000**	**1 000**
Coeff. of variation (%)		**49.6**	**23.4**	**95.9**

† Test could not be completed
* Assumed value

The average fatigue test results were plotted for each load level and pre-crack and are displayed in Figure 5.8. As mentioned previously, there was an overall steady decline in the flexural fatigue capacity as the load level and pre-crack increased, which can be clearly seen in Figure 5.8. The 85% load level showed an almost linear decrease in fatigue capacity as the pre-crack increased, up until the 2.5 mm pre-crack, where there was a drastic decrease in fatigue capacity. Similarly, the 70% load level also displayed a decrease in fatigue capacity as the pre-crack increased. However, the 1.2 mm pre-crack differed, since it sustained on average more load cycles than the 0.6 mm pre-crack at the same load level, and also had more variation in the test results. The standard deviation errors displayed in Figure 5.8 indicated more variation in the test results at the 1.2 mm pre-crack. It is possible that with a larger sample size, the average number of cycles sustained at a pre-crack of 1.2 mm and 70% load level would fit better within the general trend of a decrease in fatigue capacity as the pre-crack increased. The 50% load level showed the best fatigue capacity, with the 2.5 mm pre-crack sustaining on average 740 000 load cycles. The 1.2 mm pre-crack test results showed that there would possibly be no failure and would last the full 2 million cycles. Consequently, the 0.6 mm pre-crack test was not performed, and it was reasonable to assume that the 0.6 mm pre-crack at 50% load level would have also lasted at least the full 2 million load cycles without any failure. All the tests showed a general trend, where an increase in load level and pre-crack resulted in a decrease in fatigue capacity.

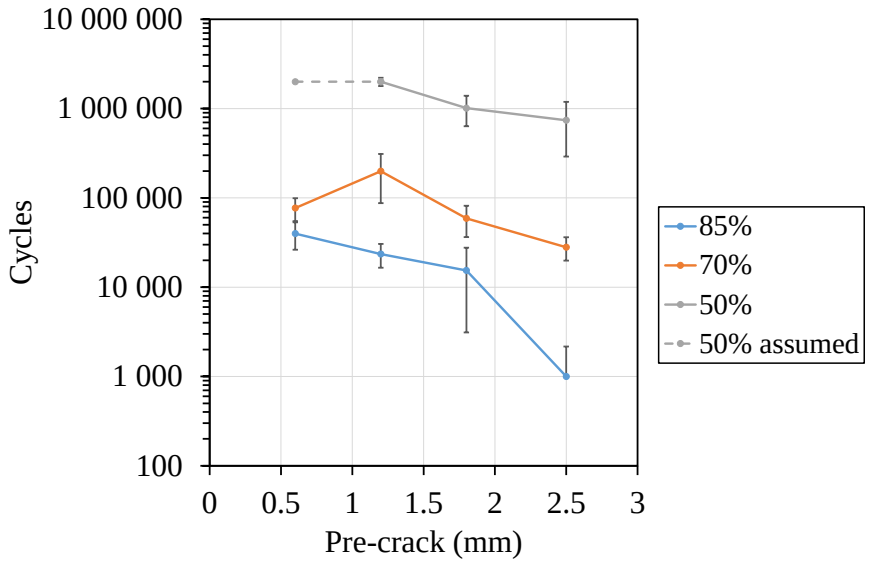

Figure 5.8: Average number of cycles sustained up to 3.5 mm CMOD or 2 million cycles

5.2.2. Effect of load level

After the pre-crack loading step, as shown in Figure 5.9, and prior to the fatigue loading, all the test specimens were subjected to an unloading to reach the mean load as outlined in Section 3.3.4.2. The mean load served as the starting point for all the fatigue sine waveform cyclic loadings, and was based on the applied fatigue load level. The fatigue load level was, in turn, taken as a percentage (50%, 70% or 85%) of the average maximum static load of the 0.8% fibre dosage specimens in Figure 5.1 (b). As the load level changed, so did the mean load, as well as the maximum load (A_{max}), while the minimum load (A_{min}) remained fixed at 3 kN as shown in Figure 5.9.

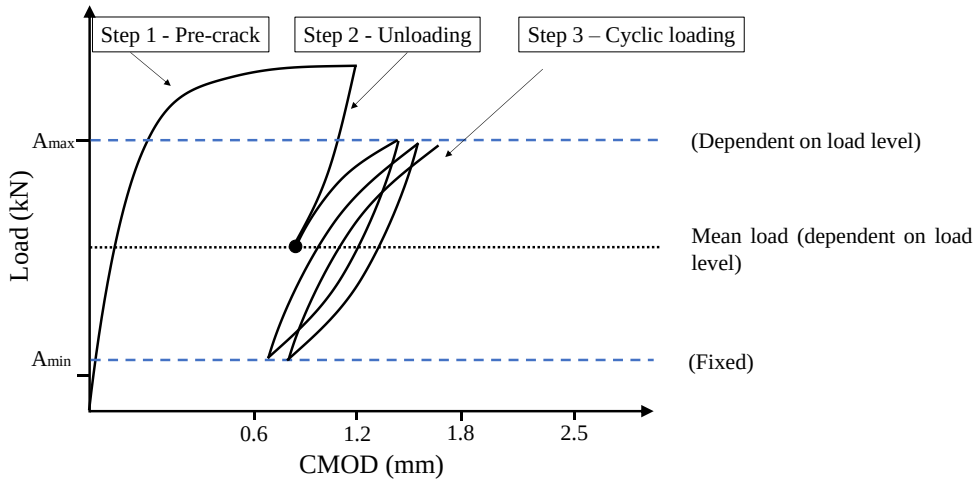

Figure 5.9: General loading steps of fatigue test based on 1.2 mm pre-crack and an exaggerated arbitrary fatigue load level

Depending on the applied load level, the magnitude of the unloading varied, as can be seen in Figure 5.9 and Figure 5.10. The lower the load level (50%), the more the load was required to unload in order to reach the mean load for the particular load level. In contrast, at a higher load level (85%), the unloading was less significant since the mean load was higher and generally closer to the pre-crack load. As a result, the crack closure varied depending on the applied load level. From Figure 5.10, it is clear that the 85% load level results in a smaller crack closure after the pre-cracking in Step 1, than the 50% load level. This is further illustrated in Figure 5.11, where the average crack closure for each load level and pre-crack was determined from the test results.

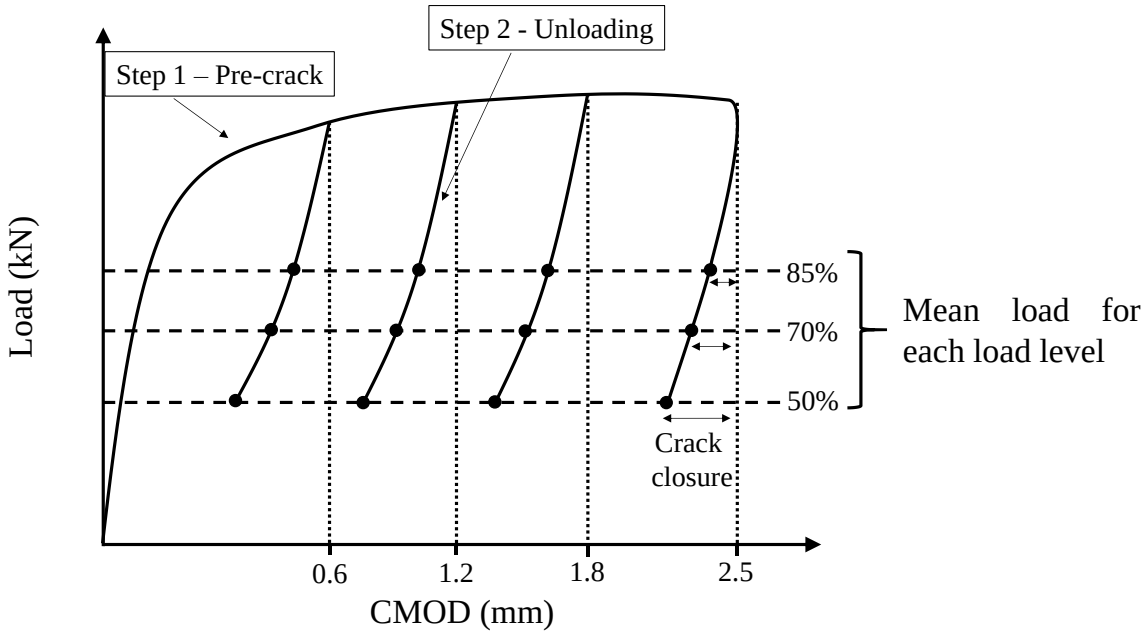

Figure 5.10: Loading/unloading (Steps 1 and 2) at different load levels and pre-cracks

In Figure 5.11, the average crack closure can be seen for all the pre-cracks and load levels. A general trend was observed, where the average crack closure increased as the pre-crack increased, followed by a decrease. The 85% load level showed the least crack closure overall, since the mean value was larger and closer to the pre-crack load. In contrast, the 50% load level showed more crack closure since the required unloading to the mean value was more substantial. The 70% load level showed results within the same range as the 50% load level. At the 1.8 mm and 2.5 mm pre-cracks, the 70% load level displayed more crack closure upon unloading. This was a result of a larger load experienced during the pre-cracking stage for the 1.8 mm and 2.5 mm pre-cracks at a 70% load level. Since the load had to decrease from the pre-cracking load to reach the mean load, more unloading was required, which resulted in the larger crack closing for the aforementioned pre-cracks and load level. Regardless of this discrepancy, the results were very close to the 50% load level results, and still followed the same general trend. Since the 50% load level at 0.6 mm pre-crack tests were not performed, the average crack closure was assumed to converge at the same point as the other load levels at 0.6 mm pre-crack.

The crack closure results show that there was a clear distinction between the 1.8 mm and 2.5 mm pre-crack. Between the 0.6 mm and 1.8 mm pre-crack, the trend showed that the increase in pre-crack resulted in more crack closure. However, at the 2.5 mm pre-crack, the

crack closure decreased when compared to the 1.8 mm pre-crack. This suggested that at all the pre-cracks, there was fibre debonding and pull-out, with a possibility of fibre rupture. Up to the 1.8 mm pre-crack, the fibre hook deformation from the pull-out was not significant as illustrated by the X-ray CT scans in Figure 4.4 (b) and Figure 4.5. The fibres would still have some degree of elasticity, as well as a small portion of plastic deformation in the fibre hooks. Once the 2.5 mm pre-crack was reached, there was increased fibre deformation caused by the fibre hooks deforming, which resulted in a larger permanent plastic deformation of the fibres, especially at the hooks. Thus, the crack closure decreased at the 2.5 mm pre-crack.

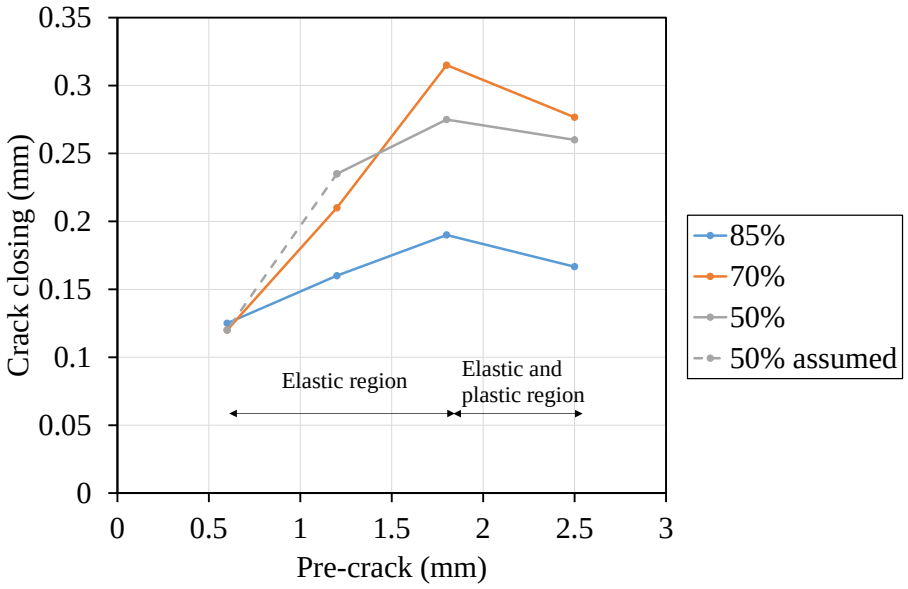

Figure 5.11: Average crack closure upon unloading for each pre-crack and load level

5.2.3. Effect of pre-crack

The CMOD progression for the full duration of all the test specimens based on the various pre-cracks and load levels are shown and discussed in this section.

0.6 mm pre-crack

In Figure 5.12, the 0.6 mm pre-crack is considered. Three tests were performed for only the 70% and 85% load levels. The results show that at the 0.6 mm pre-crack, all the tested specimens failed. The number of load cycles sustained for the 70% and 85% load levels were within close proximity to one another, ranging from the lowest of 26 000 cycles at 85% load level, to the highest of 100 000 cycles at the 70% load level as shown in Table

5.1. The 50% load level was assumed to endure 2 million load cycles, based on the projected test results in Figure 5.8.

Unlike all the 0.6 mm pre-crack behaviour, one 85% load level test quickly increased to a CMOD of 0.98 mm as soon as the test reached the 0.6 mm pre-crack as shown in Figure 5.13. The load application during the test was designed to switch to the unloading step once the set point of the pre-crack was reached, as outlined in Section 3.3.4.2. However, for this specific test, as soon as the CMOD reached the 0.6 mm pre-crack and the load-controlled unloading step started, an unstable crack opening occurred which increased the CMOD from 0.6 mm to 0.96 mm within 1 second, before unloading occurred. This data is presented in Appendix A. Based on the behaviour shown in Figure 5.13, as well as the distinctive sound of fibre failure observed as the set CMOD was reached for this specific test, this behaviour was attributed to a critical fibre slipping or failing in rupture as soon as the 0.6 mm CMOD was reached. Since the unstable crack opening occurred in Step 2, which was a load-controlled step, the CMOD could open or close to any magnitude as long as the mean load was reached within Step 2. The magnitude of the crack opening before stabilising, further suggested that the critical fibre failed, after which the surrounding fibres carried the load. Since the load quickly increased as the CMOD increased, followed by a stable load reduction further indicated that the testing machine quickly reacted to the rapid increased CMOD and subsequent downward vertical displacement. However, regardless of this anomaly, the specimen still behaved similar to the others in the same test group and was thus, not disregarded. Instead of the CMOD opening slowly over time like the other tests in the same test batch, it remained constant until 10 000 load cycles before the CMOD started to increase.

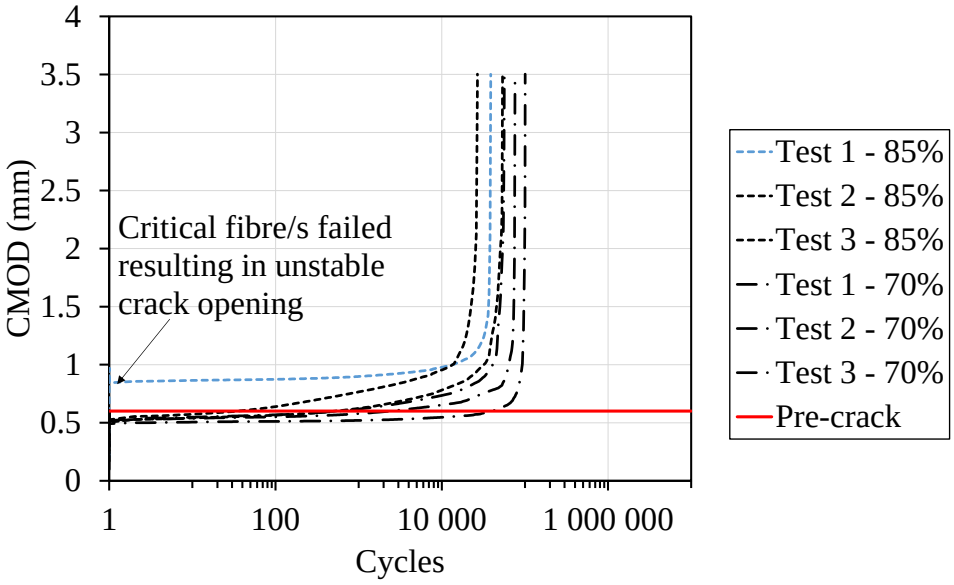

Figure 5.12: Fatigue CMOD results for 0.6 mm pre-crack

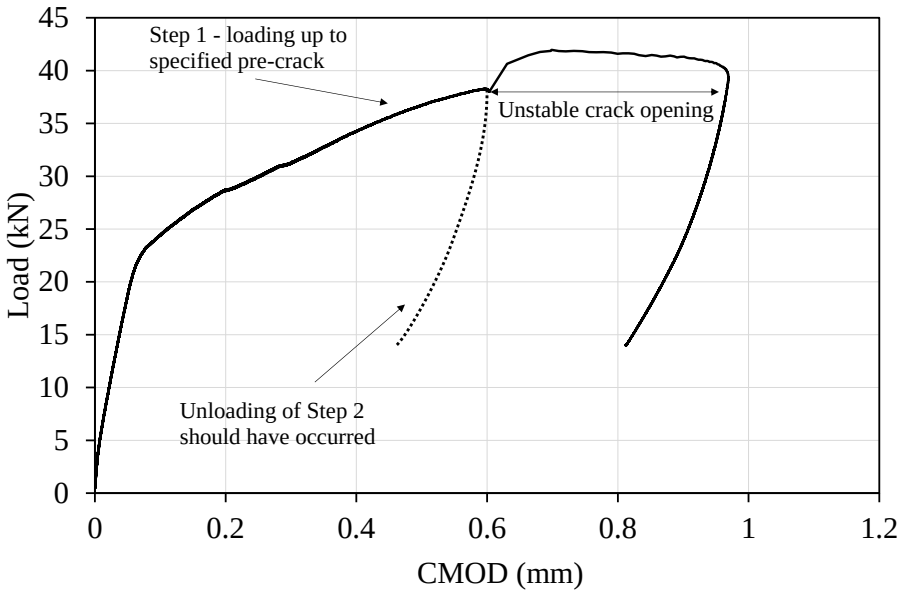

Figure 5.13: Loading/unloading (Step 1 and Step 2) of Specimen 1 for 85% load level at 0.6 mm pre-crack

1.2 mm pre-crack

For the 1.2 mm pre-crack shown in Figure 5.14, eight specimens were tested. Three were tested for the 70% and 85% load level each, whereas only two specimens were tested for the 50% load level. In order to test all the 50% load level specimens from the same batch,

one test was required to be forcibly stopped at 1.7 million cycles due to technical difficulties. This was only done based on the performance of the test specimen, which was well on the way to sustaining 2 million load cycles. As the other 50% load level test also sustained 2 million load cycles, it was justified to assume that the test would have reached 2 million load cycles without failure. At this pre-crack, the spread between the number of cycles sustained for the various load levels increased, however, the 70% and 85% were still in close proximity to each other. The 85% load level sustained the lowest number of cycles, only reaching 18 000 cycles, whereas the 50% load level could sustain 2 million load cycles.

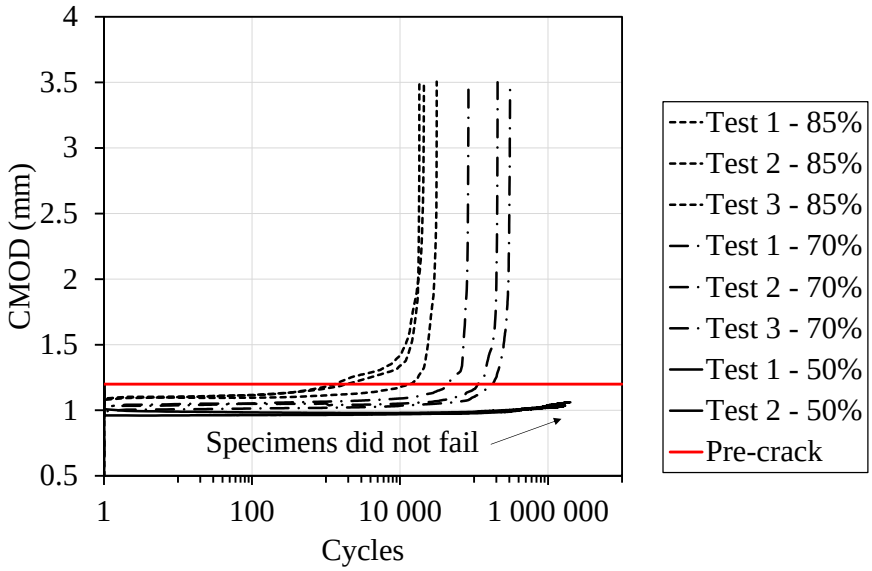

Figure 5.14: Fatigue CMOD results for 1.2 mm pre-crack

1.8 mm pre-crack

The pre-crack was then increased to 1.8 mm as shown in Figure 5.15. Only two specimens were tested for the 50% and 70% load levels respectively, whereas the 85% had three specimens tested. At the 85% load level, as expected, the increase in pre-crack decreased the fatigue capacity. In contrast, at the 50% load level, the fatigue capacity was highest when compared to the 70% and 85% load levels. However, when compared to the smaller pre-cracks (0.6 mm and 1.2 mm), the fatigue capacity was less due to the larger pre-crack.

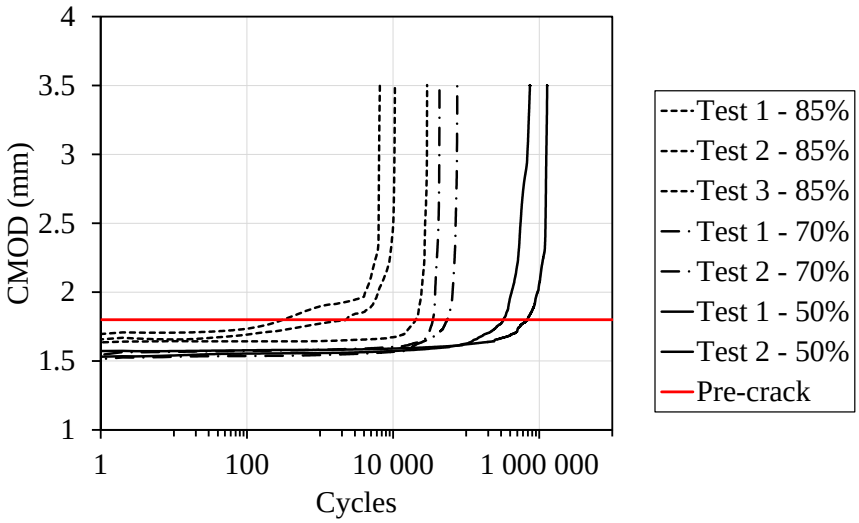

Figure 5.15: Fatigue CMOD results for 1.8 mm pre-crack

2.5 mm pre-crack

At the largest pre-crack (2.5 mm) as shown in Figure 5.16, the largest scatter of results was found. The 85% load level could barely sustain any load cycles, with specimens failing at 50 load cycles. At the 50% load level, the test results showed an increased fatigue capacity, with one specimen exceeding 1 million load cycles before the test was stopped due to technical difficulties. No signs of failure were shown for that specimen, and it cannot be assumed to complete the full 2 million load cycles based on the other two test results from the same test batch, as well as the large applied fatigue loading. The 70% load level tests showed an intermediate response, similar to that of all the other pre-cracks.

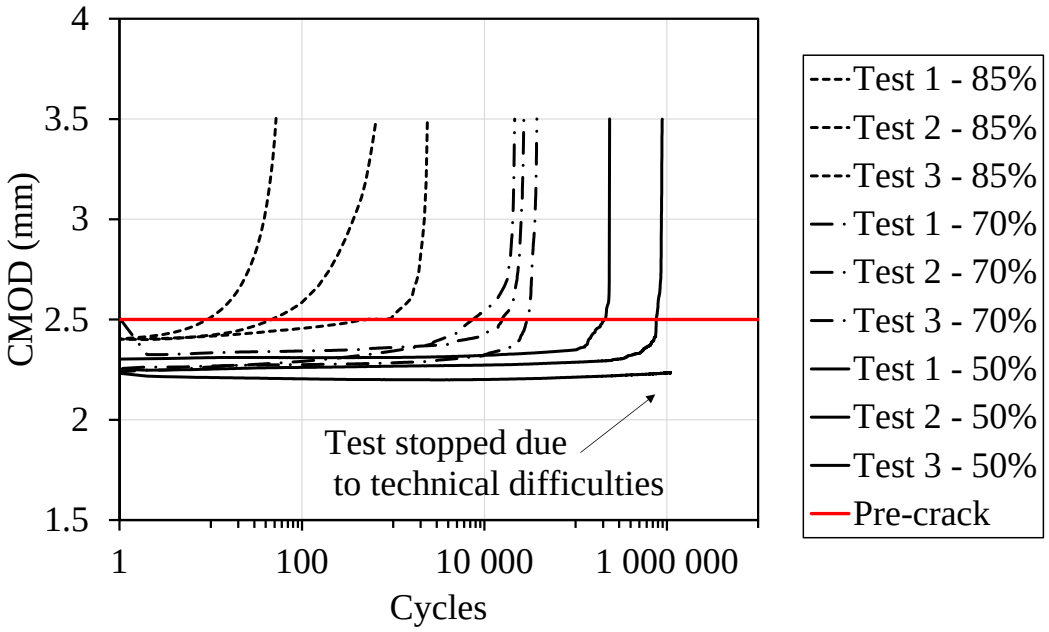

Figure 5.16: Fatigue CMOD results for 2.5 mm pre-crack

All the specimens tested at the various pre-cracks and load levels showed a similar failure trend where the CMOD started to increase rapidly, indicating imminent failure at a CMOD which was near the original pre-crack CMOD. This initial pre-crack point served as the marker as to when failure was likely to occur, since this behaviour occurred at every test performed, regardless of the pre-crack or load level. At the lower pre-cracks, more cycles progressed before the CMOD would reach the initial pre-crack, with failure occurring at a CMOD slightly larger than the pre-crack. However, at the larger pre-cracks, fewer cycles progressed until failure, which also occurred much closer to a CMOD similar to the pre-crack. This behaviour is discussed further in the next section.

5.2.4. Flexural fatigue behaviour observations

One trend observed throughout the fatigue tests presented in Section 5.2.3, was the significant increased CMOD just before failure. The CMOD increased gradually over time, followed by a rapid increase until failure. Figure 5.17 illustrates a generalised behaviour of the test specimens based on the fatigue test results. Initially, the crack closed to some degree after application of the pre-crack based on the load level and pre-crack as illustrated in Figure 5.11. The CMOD then slowly increased over time until it reached a critical CMOD, after which there was a rapid increase in the CMOD until failure. This critical

CMOD is described as the turning point after which the crack growth accelerated significantly, as highlighted in Figure 5.17. The initial pre-crack may serve as an indicator of the critical CMOD.

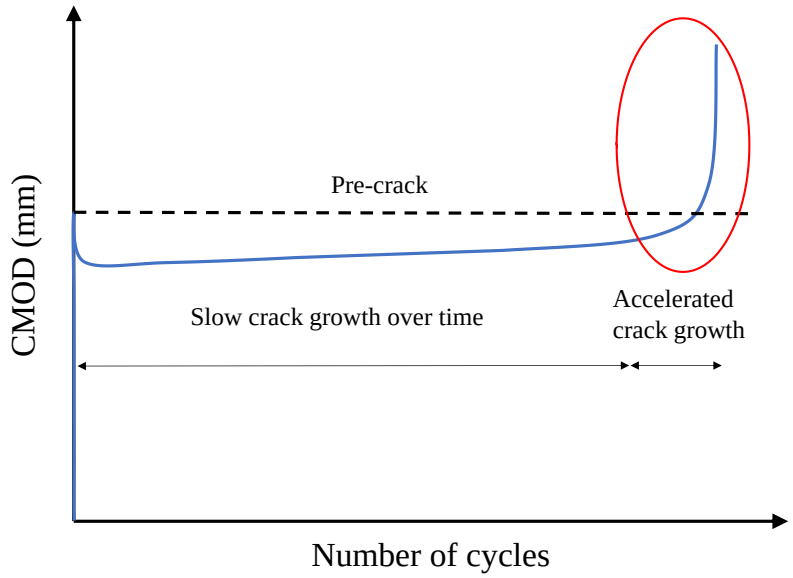

Figure 5.17: Generalised crack behaviour over time

At the 0.6 mm pre-crack in Figure 5.12, the crack growth over time for the 85% specimens occurs quicker than the other load level, and has a steeper slope before reaching the accelerated crack growth stage. At the 70% load level, the crack growth stage occurs more gradually, and thus takes longer to reach the accelerated crack growth stage. In all the cases, the accelerated crack growth occurs after passing the initial pre-crack level. This could be associated with the phases in which the fibres are in after the 0.6 mm pre-crack, since it was classified as Phase 2 for fibres at the notch. There was little to no fibre deformation and pull-out for the 0.6 mm pre-crack. As the crack closed to a similar CMOD for all the load levels before fatigue loading occurred in Figure 5.11, more fatigue loading was required to deform and pull out the fibres at the lower load level before the accelerated crack growth stage, since the fibres were in the initial part of Phase 2 during the pre-crack. At the higher load levels, the fibres' transition to higher phases occurred at a faster rate since the applied load level was larger, thereby generating more fibre deformation after every load cycle.

The 1.2 mm pre-crack in Figure 5.14 illustrated a similar behaviour to the 0.6 mm pre-crack specimens. Before fatigue loading, the initial CMOD was different for the

different load levels as highlighted in Figure 5.11, based on the crack closure. After the pre-crack, the fibres at the notch were classified into Phase 3 of fibre deformation. For the different load levels, there was a slight distinction in the length of the crack growth stage. The 85% load level crack growth occurs faster than the 70% and 50% load levels. This was mainly due to the fatigue deformation caused by the higher load level, as well as the original crack closure which was less than the other load levels. For the 50% load level, there was no failure for the two tested specimens. However, there was a noticeable increase in the crack growth stage at the time the test stopped. This was expected to increase gradually, past the 2 million load cycle limit. However, this study did not consider what happened after the 2 million load cycle limit.

The 1.8 mm pre-crack results in Figure 5.15 illustrate a more obvious distinction between the different load level results. As expected, the 85% load level failed quicker than the 70% and 50% load levels, since the crack growth was larger over a shorter period of time. This was due to the large pre-crack coupled with the large applied load level. The fibres were estimated to be within Phase 3 prior to fatigue loading, after undergoing fibre pull-out to a certain extent during the pre-cracking stage.

At the 2.5 mm pre-crack in Figure 5.16, the difference between the load levels was significant. The 85% load level specimens failed almost immediately after the fatigue load was applied. The fibres were classified to be in the latter parts of Phase 3, where they underwent deformation at the fibre hooks. The fibre deformation also resulted in an elastic and more plastic crack closure as shown in Figure 5.11, where the 2.5 mm pre-crack resulted in less crack closure due to plastic deformation in the fibres. The fatigue resistance decreased as the fibre deformation increased. This, coupled with the high load level resulted in the immediate failure. As the load level decreased, there was more resistance to fatigue loading, albeit limited.

5.2.5. X-ray CT scans

After performing the fatigue tests, several specimens were visualised using X-ray CT scans. All the specimens that were scanned, did not reach the 2 million load cycles, and failed by reaching the 3.5 mm CMOD during the fatigue testing.

After analysing the X-ray CT images, the most prominent failure mechanism was fibre rupture, as shown in Figure 5.18 to Figure 5.20. In contrast to the X-ray CT images of the

static tested specimens shown in Section 5.1.2, where there was mainly fibre pull-out, the fatigue test specimens showed many fibres failing due to rupture at the hooks, as well as fibre pull-out as seen in Figure 5.18. The ruptured fibres displayed a small degree of fibre pull-out at the ends before they ruptured, generally at the base of the hooks.

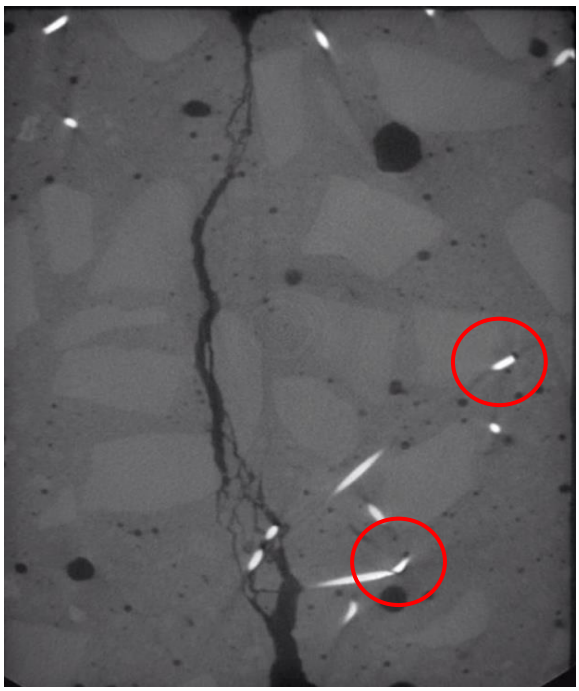

Figure 5.18: Post-fatigue test X-ray CT image of Specimen 3 tested to failure at 85% load level and 2.5 mm pre-crack showing fibre rupture and fibre pull-out

The rupturing of fibres can be attributed to the accelerated crack growth in Figure 5.17. The mechanism of failure changed from a ductile fibre pull-out, which was experienced in the static behaviour, as well as the slow crack growth period in Figure 5.17, to a brittle fibre rupture due to fatigue of the fibre. The ruptured fibres were mainly located at the notch region and decreased in frequency further away from the notch as the crack decreased in size. This suggested that the ruptured fibres were critical in carrying the load. Initially, the critical fibres pulled out to a certain extent during the slow crack growth period, then due to the fatigue load, they ruptured, and the load was transferred to other surrounding fibres possibly further away from the notch, which resulted in the CMOD increase.

After the static fibre deformation, the fibres underwent fatigue loading which resulted in the CMOD increasing up to the failure CMOD. As the fatigue loading continued, based on

the initial pre-crack, the fibres would have transitioned into different phases due to the crack increasing in width. Due to the fibre deformation at the hooks for fibres which pulled out, as well as the 3.5 mm CMOD upon failure, the fibres closest to the notch could be classified in Phase 3 nearing Phase 4. However, the fibres that failed in rupture could not be classified into any phases regardless of the fibre end pull-out prior to fibre rupture. This is as a result of the fibres not having any carrying capacity once they have already ruptured.

Although there was no complete straightening of the fibre hooks during pull-out, some fibres did experience fibre hook deformation as they pulled out as shown in Figure 5.19 (b) and Figure 5.20 (b). The 3.5 mm CMOD limit prevented the fibres from completely straightening and pulling out, since it required more displacement in order to straighten out. As a result, no fibres would have been classified in Phase 4 at any point during the fatigue test, as it required more fibre hook deformation, which required more displacement and thus a larger CMOD.

(a)  (b) 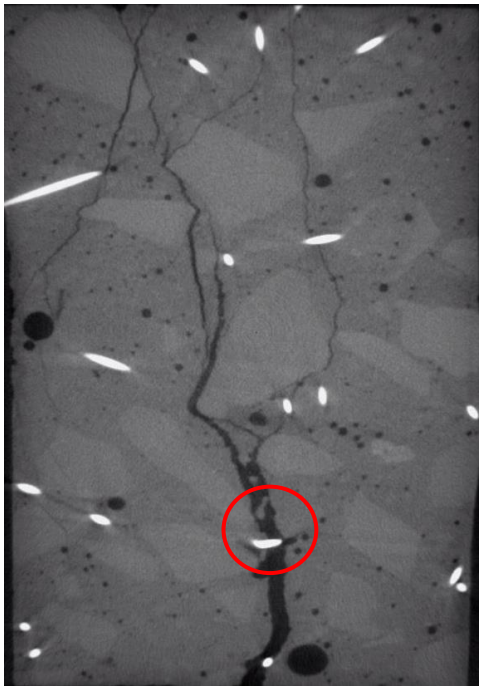

Figure 5.19: Post-fatigue test X-ray CT image of Specimen 3 tested to failure at 70% load level and 2.5 mm pre-crack (a) fibre rupture (b) fibre pull-out

(a) 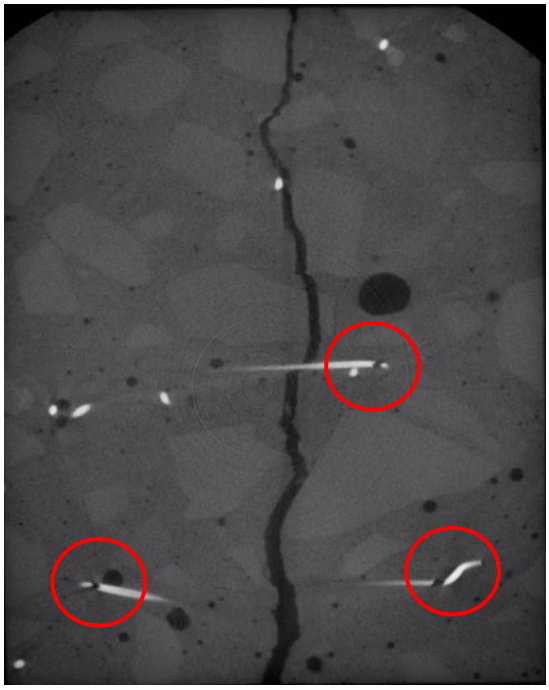 (b) 

Figure 5.20: Post-fatigue test X-ray CT image of Specimen 3 tested to failure at 85% load level and 1.2 mm pre-crack (a) multiple fibre ruptures (b) fibre pull-out

5.3. Concluding summary

In this chapter, the test results are presented and analysed for the pre-cracked flexural fatigue specimens. The fatigue tests were performed at load levels of 50%, 70% and 85% of the average maximum static load, with a pre-crack varying from 0.6 mm, 1.2 mm, 1.8 mm, to 2.5 mm. The tests were performed until reaching 2 million load cycles, or up to a CMOD of 3.5 mm, which was classified as failure.

Static tests were required before any fatigue loading could be applied. The static tests were performed on beam specimens with three different fibre dosages in order to determine the optimum dosage. The three fibre dosages tested were 0.6%, 0.8% and 1.0% by volume, and based on the static performance of the tests, the 0.8% fibre dosage was selected.

Additional static tests were performed on four specimens which were pre-cracked each to different pre-cracks. X-ray CT images were then produced to determine the degree of damage caused to the fibres prior to performing fatigue tests. The dominant failure mechanism was fibre pull-out. The fibres closest to the notch displayed the most fibre deformation after the pre-crack, since this was where the CMOD was the largest. At the 0.6 mm pre-crack, there was little to no fibre deformation, with no visible fibre end

pull-out. As a result, the fibres at the notch of the 0.6 mm pre-crack were classified as Phase 2 of the single fibre model in Figure 4.3. The fibres further away from the notch were classified into Phase 1 as there was little to no fibre pull-out or deformation. The 1.2 mm pre-crack illustrated a crack which propagated almost the entire height of the specimen. The fibres at the notch showed visible pull-out, with decreasing pull-out as the fibres moved further away from the notch. The 1.8 mm and 2.5 mm pre-cracks both showed fibre hook deformation for the fibres at the notch, as well as fibre pull-out. However, the fibre hook deformation was not present for fibres further away from the notch. Fibres at the notch of the 1.2 mm, and 1.8 mm pre-cracks were all classified as Phase 3 for the fibres visible in the X-ray CT images. Fibres further away from the notch were classified as Phase 2. All the fibres for the 2.5 mm pre-crack were classified as Phase 3 as there was significant fibre pull-out and deformation throughout the height of the crack.

The specimens were then tested at different load levels in fatigue, after applying the various pre-cracks. The test results showed good repeatability, although some tests presented higher variation than the others. The main trend established from the fatigue results was the decrease in fatigue capacity as the load level and pre-crack increased. This was expected, since the increase in load level and pre-crack resulted in more fibre deformations, which could ultimately lead to failure. The initial pre-crack served as an indicator as to when failure was likely to occur.

X-ray CT scans were performed on specimens which failed in fatigue. The dominant failure mechanism for the fibres changed from fibre pull-out in the static tests, to fibre rupture in the fatigue tests. Although fibre pull-out was a failure mechanism which contributed to the slow crack growth over time, the fibre rupture resulted in the accelerated crack growth until specimen failure. The majority of fibres which ruptured were located at the notch, and the fibre ruptures decreased in frequency further away from the notch.

6. Modelling framework for fatigue behaviour of steel fibre reinforced concrete

In this chapter, the steps towards modelling and predicting behaviour of pre-cracked steel fibre reinforced concrete (SFRC) under fatigue loading are discussed. The behaviour of pre-cracked FRC under fatigue loading at a single fibre level as well as at a macroscopic level was considered. The behavioural characteristics at a single fibre level were linked to the macroscopic level through the various phases in which the fibres are in after the pre-cracking process. A behavioural model and a fatigue life prediction approach were developed based on the flexural fatigue results, and steps towards analytical modelling of pre-cracked SFRC under fatigue loading were hypothesised.

6.1. Proposed flexural fatigue SFRC behavioural failure model

6.1.1. Background

Based on the fatigue test results presented in Chapters 4 and 5, a SFRC flexural fatigue behavioural failure model, hereafter called the fatigue model, was developed which considers the load level and pre-crack at the macroscopic level. The test results at the single fibre level serve as the basis for the fibre behaviour that could be expected at the macroscopic level.

Before the crack acceleration occurs in Figure 5.17, the fibres must undergo fatigue loading to ensure fibre deformation which results in fibre pull-out and/or rupture. During the slow crack growth stage in Figure 5.17, it is reasoned that the fibre failure mechanism is mainly pull-out, which results in the gradual ductile response of the CMOD increase. Since the largest crack opening at failure was 3.5 mm at the notch, the fibres will hardly ever straighten out completely. Thus, the fibre pull-out failure is classified as the fibre hook straightening partially or completely, which results in the fibres being unable to carry their maximum capacity anymore. From Table 4.1, it is clear that given a large load level, the fibre fatigue capacity is diminished once the pre-slip has passed a certain stage. However, in the macroscopic specimens, due to the limited crack opening when the fibre fails in pull-out, the fibres still contribute to the load-carrying capacity but to a lesser degree.

The fibres closest to the notch experiences larger loads and are assumed to be the initial critical fibres. This means that the fibres at the notch carry the largest portion of the loading, as they experience the largest deformation and stress. Further away from the notch, fibres also participate in the load-carrying capacity, but to a lesser extent. Once the initial critical fibres fail either in pull-out or rupture, the load is then transferred to other fibres which are possibly further away from the notch, and those fibres become the new critical fibres. This is assumed to have been the cause of the rapid CMOD increase previously shown in Figure 5.13.

This phenomenon is illustrated in Figure 6.1, where the fibres are assumed to be horizontal just for illustrative purposes. Initially, as the CMOD increases, all fibres bridging the crack are active in resisting the fatigue load. Fibres closest to the notch act as the initial critical fibres, which carry a larger fatigue load than the other fibres. However, fibres further away from the notch still sustain some degree of fatigue loading, but not to the same degree as the critical fibres. All the fibres active in bridging the crack undergo the same number of fatigue load cycles, but at different loads for each individual fibre. As the CMOD increases, the fibres pull out to some extent until the fatigue resistance of the fibre decreases by fibre failure in pull-out or rupture. Once this occurs, the load gets transferred to the surrounding fibres, thereby resulting in a new critical fibre, as shown in Figure 6.1 (b). The force experienced by the new critical fibre is then larger than before, which results in quicker failure due to the prior fatigue loading history experienced by the new critical fibre. Once this critical fibre fails, the load is transferred to surrounding fibres once more to find a new critical fibre. Each time a critical fibre fails, and the load gets redistributed to find a new critical fibre, the additional number of cycles to failure for the new critical fibre decreases due to its prior loading history in fatigue. This illustrates that the low fatigue loading in a fibre, followed by a sudden increased fatigue loading drastically reduces its fatigue capacity, resulting in the accelerated crack growth shown in Figure 5.17. This process continues until the CMOD reaches the failure CMOD as specified.

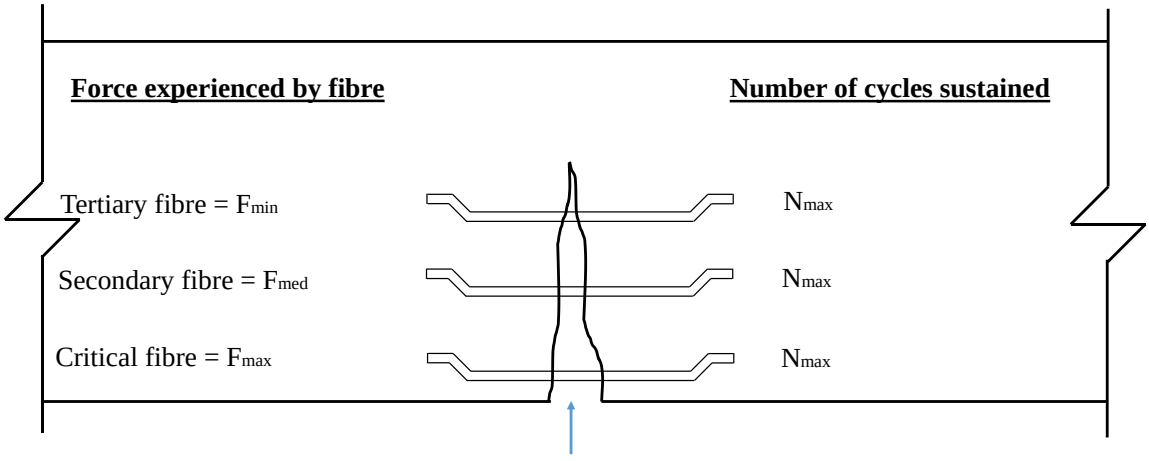

(a)

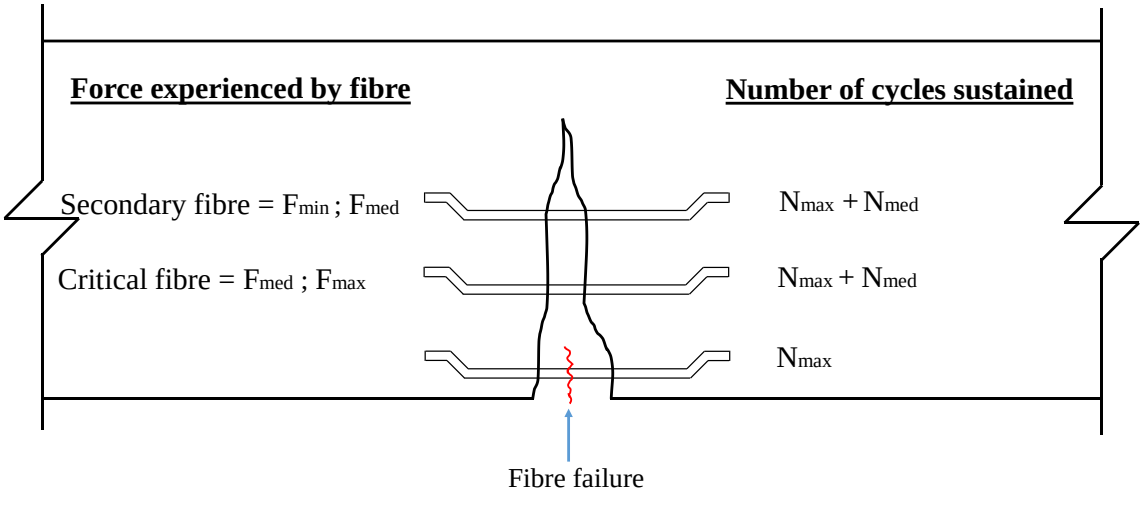

(b)

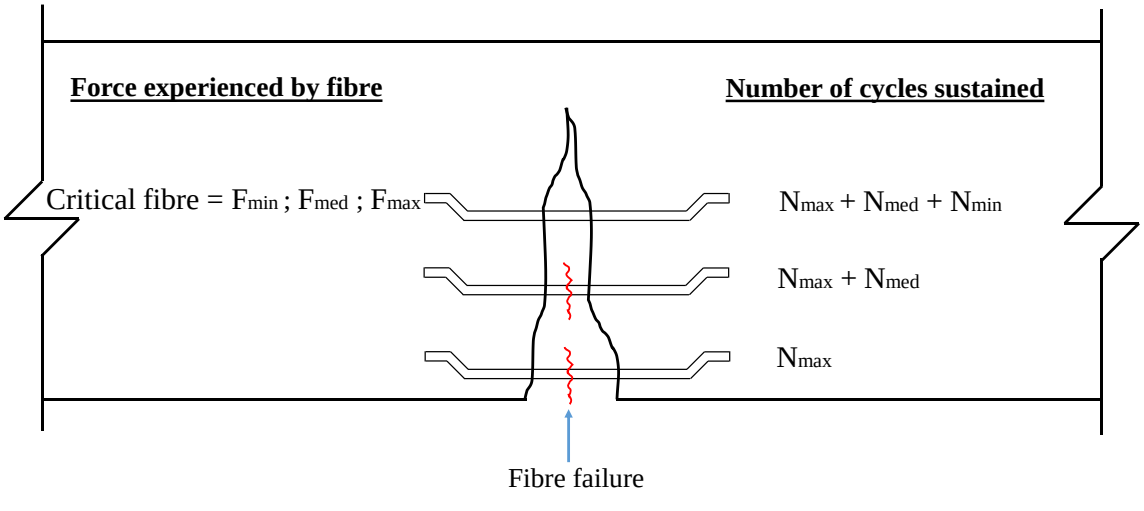

(c)

Figure 6.1: Fibre loading history (a) all fibres activated without failure, (b) fibre failure of initial critical fibre, (c) fibre failure of new critical fibre, (figure is not to scale, just for illustrative purposes)

6.1.2. Model development

As with the development of any model, a number of assumptions were made with regard to the limitations of the model. Based on the loading regime from Section 3.3.4.2, the loading for all tests followed three steps: (1) pre-crack (displacement-controlled); (2) load/unload to mean value (load-controlled); and (3) fatigue loading (load-controlled). The specimen is then loaded in fatigue until it reaches a CMOD of 3.5 mm or until 2 million load cycles are reached, which terminates the test.

The following assumptions are made:

1. The pre-crack load is always larger than the fatigue loading. Therefore, after pre-cracking, the load will decrease to reach the mean load, which is the starting point of the fatigue loading, resulting in crack closure prior to fatigue loading.
2. A non-failure event is limited to 2 million load cycles, and results after 2 million load cycles are not taken into account.
3. Complete specimen failure is classified as reaching a CMOD of 3.5 mm.
4. The fibres closest to the notch, where the CMOD is the largest, serve as the initial critical fibres.
5. The initial pre-crack CMOD serves as a guideline as to when CMOD acceleration will occur.

The generalised behaviour shown in Figure 5.17, as well as Figure 6.2, can be further divided into stages where significant events occur, and are classified as follows:

Stage I – pre-crack, followed by crack closure

Stage II – gradual increase in CMOD

Stage III – CMOD acceleration until failure

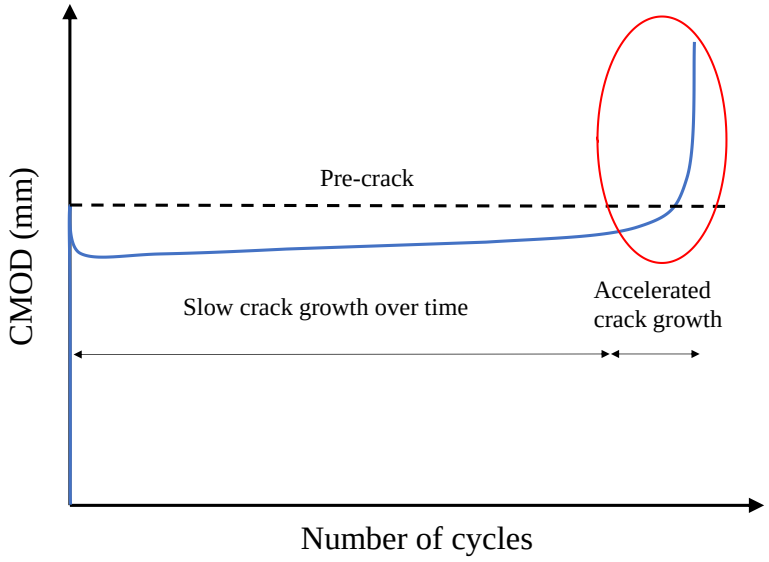

Figure 6.2: Generalised crack behaviour over time

Each of the abovementioned stages are affected by the load level and/or pre-crack. Based on the test results, the fatigue model is developed with three different outcomes, which are linked to the various load levels and pre-cracks, and directly influences the fatigue outcome.

Stage I occurs during the pre-crack (Step 1) and unloading (Step 2) steps from the loading regime outlined in Section 3.3.4.2. During this stage, a crack is initiated, and then depending on the load level and extent of fibre damage caused, the crack closes partially upon unloading. This stage is directly influenced by the pre-crack as well as the load level. As seen in Figure 5.11, the crack closure depends on the fibre deformation caused by the pre-crack. Since the pre-crack load decreases to reach the mean value prior to fatigue loading, the load level also influences how much the crack closes. This phenomenon was elucidated in Section 5.2.2.

Stage II is the crack growth stage over time due to the fatigue loading. This stage is dominated by the applied load level. The larger the applied load level, the more fatigue damage is done to the fibres after each loading cycle, which ultimately leads to fibre pull-out and/or rupture. The accumulation of fibre failure in pull-out and/or rupture, results in the accelerated fatigue crack growth. The larger load level directly leads to a steeper slope in the CMOD increase, which shortens Stage II, and vice versa.

Once Stage III has been reached, there is rapid CMOD acceleration. At this stage, the critical CMOD is reached, which is the point of no return. The fibres continue to fail in pull-out and/or rupture at an increased rate due to accumulated fatigue loading on various fibres as discussed in Section 6.1. Once this stage has been reached, failure occurs rapidly thereafter.

There are three different outcomes of the fatigue model depending on the load level and/or pre-crack, which are described as follows:

6.1.2.1. No failure

The no-failure outcome in Figure 6.3 describes the fatigue behaviour between 1 million and 2 million load cycles, as it was previously assumed that 2 million load cycles was the point of no failure. From the test results, it was found that after the 1 million load cycle mark, it was highly unlikely that failure would occur before 2 million cycles. Especially, not without prior indication during Stage II, where the slope of the CMOD would increase as the number of cycles increased. The 50% load level at 0.6 mm and 1.2 mm pre-cracks are associated with this type of failure. The pre-crack is too small to result in significant fibre deformations, and the load level is too low to result in significant fatigue pull-out or rupture of fibres which accelerates the crack growth. Consequently, the no-failure outcome only consists of Stages I and II. Due to the low load level, the slope of Stage II increases at a slow rate, which is not enough to reach Stage III within the limited 2 million load cycles.

Structures that experience the abovementioned load level and pre-cracks are able to last more than 2 million cycles under fatigue loading, provided the load level and loading frequency remain the same.

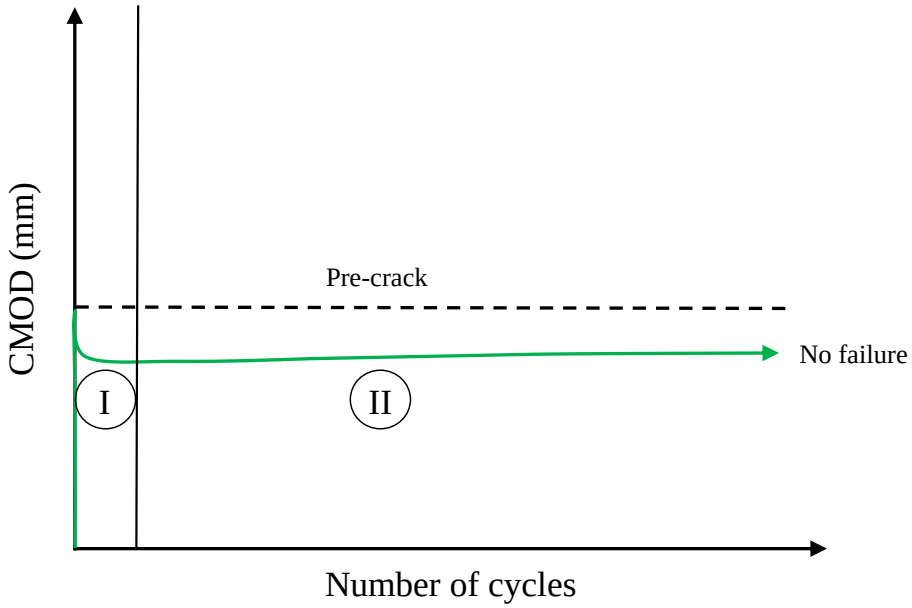

Figure 6.3: Proposed model for no failure

6.1.2.2. Gradual failure

The gradual failure outcome in Figure 6.4 suggests that there is some fatigue capacity, although, failure can be expected at some point. This outcome is associated with the following load levels and pre-cracks:

1. 85% load level at 0.6 mm pre-crack.
2. 70% load level at 0.6 mm, 1.2 mm and 1.8 mm pre-cracks.
3. 50% load level at 1.8 mm and 2.5 mm pre-cracks.

During Stage I, there is sufficient crack closing to allow for fatigue resistance as it moves to Stage II. The CMOD then increases gradually over time before reaching Stage III. For both the 70% and 85% load levels, Stage II increases at a steeper slope, and also decreases in duration. The failure criterion for the gradual failure is set between an average of 30 000 and 1 million load cycles. At the 85% load level and 0.6 mm pre-crack, there is less crack closure due to the load level, but more elasticity in the crack closing due to the pre-crack. As a result, even though there is a larger applied load level, more fibre deformation is required before fibre pull-out and rupture occurs, since there is little to no fibre deformation during the pre-cracking. The respective pre-cracks for the 70% load level exhibit elastic crack closure since the fibres are not significantly deformed to the point of

permanent deformation. This, coupled with the intermediate applied load level results in a gradual increase in the CMOD during Stage II, until it reaches Stage III. In contrast, the 1.8 mm and 2.5 mm pre-cracks at 50% load level result in large fibre deformations during pre-cracking, but the fatigue applied load level is low which results in slow but progressive fatigue fibre deformation over time.

Structures subjected to the abovementioned load levels and pre-cracks can be expected to last for a reasonable amount of time without failure, assuming that the load levels remain consistent. Given an increase in load level, fatigue failure is possible. Routine maintenance would be required throughout its lifespan to ensure its reliability.

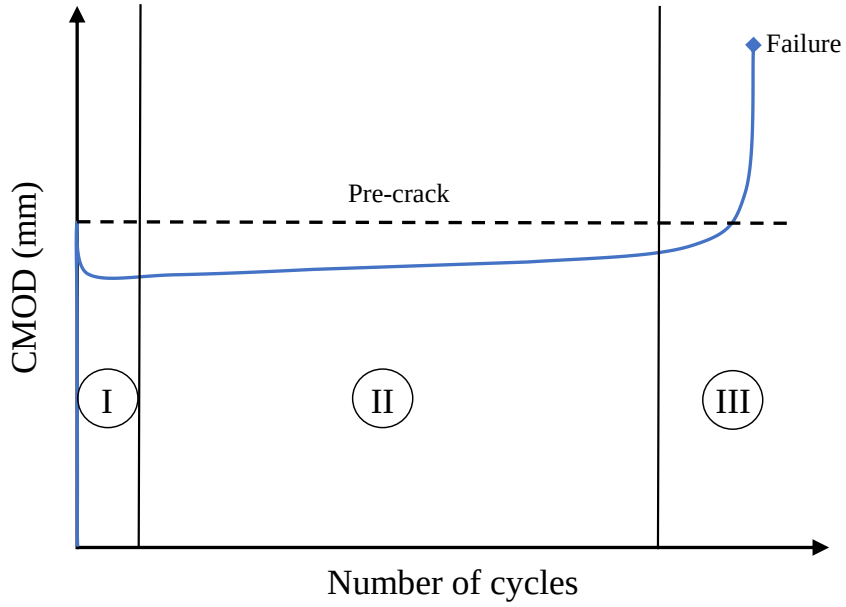

Figure 6.4: Proposed model for gradual failure

6.1.2.3. Immediate failure

The last outcome to be considered in Figure 6.5 is classified as “immediate failure”. As the name suggests, there is not much fatigue capacity after the pre-crack has been applied and failure is imminent once the fatigue loading has started. This outcome is linked to the high load level and high pre-crack. Typically, the crack closure in Stage I is lower since there is a large pre-crack as well as the high load level. As a result, the CMOD increases quickly in Stage II after critical fibres begin to fail due to the high applied load level. Stage II is generally short and thereafter, Stage III is soon reached where the CMOD quickly accelerates to the failure CMOD.

Immediate failure is classified as specimens able to withstand on average between 1 and 30 000 fatigue load cycles. The load levels and pre-cracks associated with the immediate failure include the 85% load level, at 1.2 mm, 1.8 mm, and 2.5 mm pre-cracks, as well as the 70% load level at 2.5 mm pre-crack. According to the test results, the typical number of cycles sustained before immediate failure occurs is on average between 1 000 and 28 000 load cycles. The fatigue capacity for the abovementioned load levels and pre-cracks is poor.

If a structure were to experience a single load event which would result in a large pre-crack coupled with large fatigue loadings, fatigue failure could easily be expected. Therefore, this situation should be avoided.

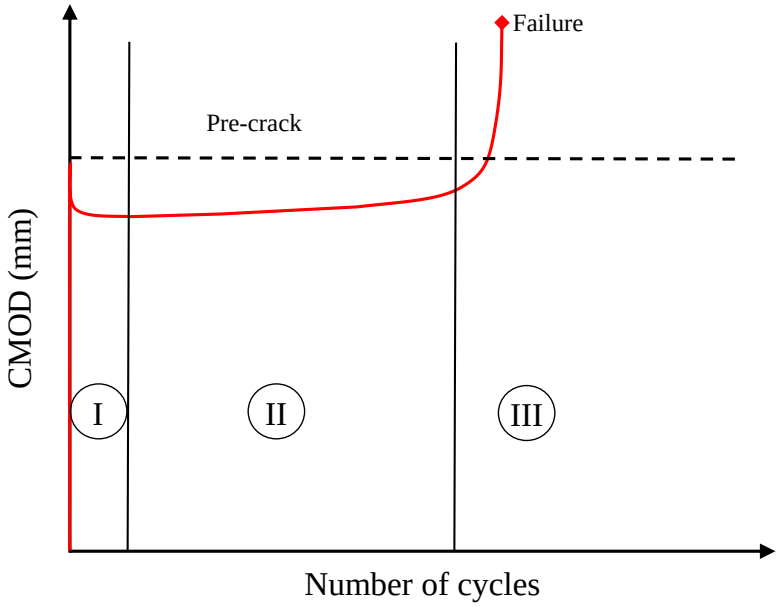

Figure 6.5: Proposed model for immediate failure

6.2. Flexural fatigue life prediction approach

The test results have shown that the initial fibre damage is a vital component in how the fibres deform, ultimately affecting the fatigue behaviour. Deformation to the fibre hooks may drastically decrease the fatigue life, showing that the fibre anchorage is necessary in resisting loads, especially fatigue loads.

Generally, S-N curves are used to illustrate and estimate the fatigue life of any material (see Figure 2.6). Using the experimental test results from Chapter 5, as well as the failure

criteria from the fatigue model in Section 6.1.2, a modified S-N curve was created, which incorporates the effects of the fibre damage through the initial pre-crack at the macroscopic scale. The modified S-N curve was developed as a general tool to estimate the number of cycles to failure at various fatigue load levels and pre-cracks.

The modified S-N curve includes the displacement from the CMOD, as shown in Figure 6.6. The average number of cycles sustained for each load level and pre-crack was plotted, and a curve was best fit through the points of each load level. All the data points plotted can be found in Appendix B. The failure criteria from the fatigue model were implemented in the modified S-N curve to illustrate the type of failure to be expected at each load level and pre-crack. All points on the border of a particular type of failure were classified according to the more conservative failure, since any change in fibre distribution may lead to lower fatigue capacity. This can be seen in the 50% load level at 1.8 mm pre-crack, which was classified as gradual failure. Also, the 70% load level at 2.5 mm pre-crack was classified into the immediate failure category. As the load level and pre-cracks increased, the average number of cycles to failure decreased progressively, thereby further substantiating the effect of the pre-crack and load level on the fatigue capacity of FRC.

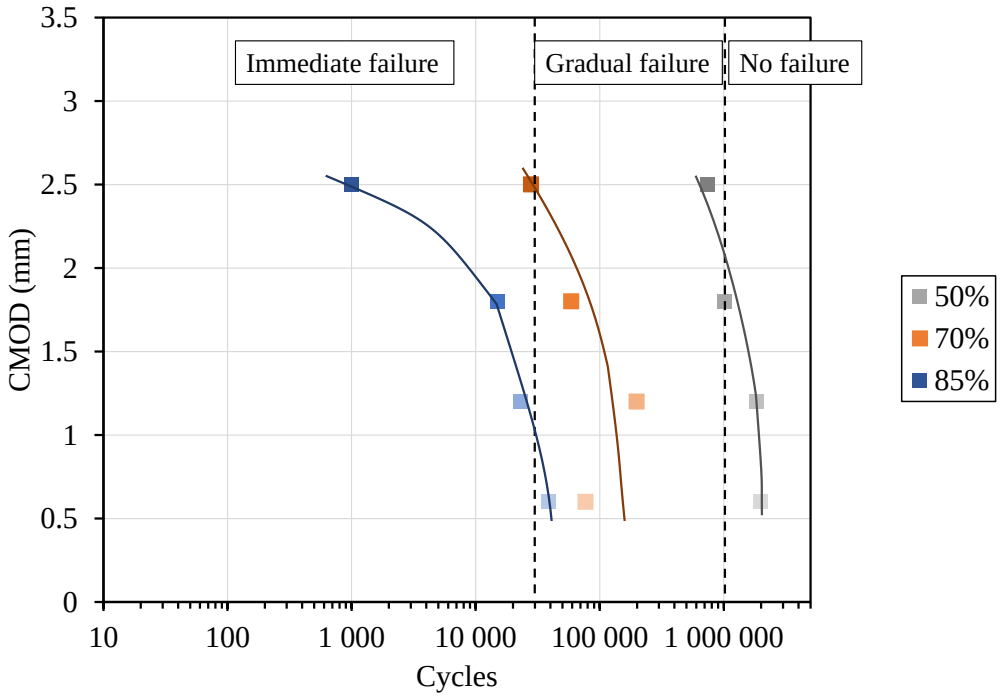

Figure 6.6: Modified S-N curve showing the average number of cycles sustained for all load levels and pre-cracks tested

Similar work performed by Hemmeter (2017) on the fatigue behaviour of pre-crack SFRC was considered. The same concrete mix composition, materials and fibres were used in both studies. However, the pre-crack levels differed slightly. The average results obtained from work performed by Hemmeter (2017) was plotted against the modified S-N curve created and is displayed in Figure 6.7. All the fatigue test results performed by Hemmeter (2017) can be found in Appendix C. The tests performed by Hemmeter (2017) only consisted of the 50% and 70% load levels at varying pre-cracks. The results show similar trends to the modified S-N curves. The fatigue capacity was however significantly lower when compared to the corresponding load levels and similar pre-cracks in Figure 6.7. This resulted in a shift to the left, and ultimately, being categorised into different failure categories than expected.

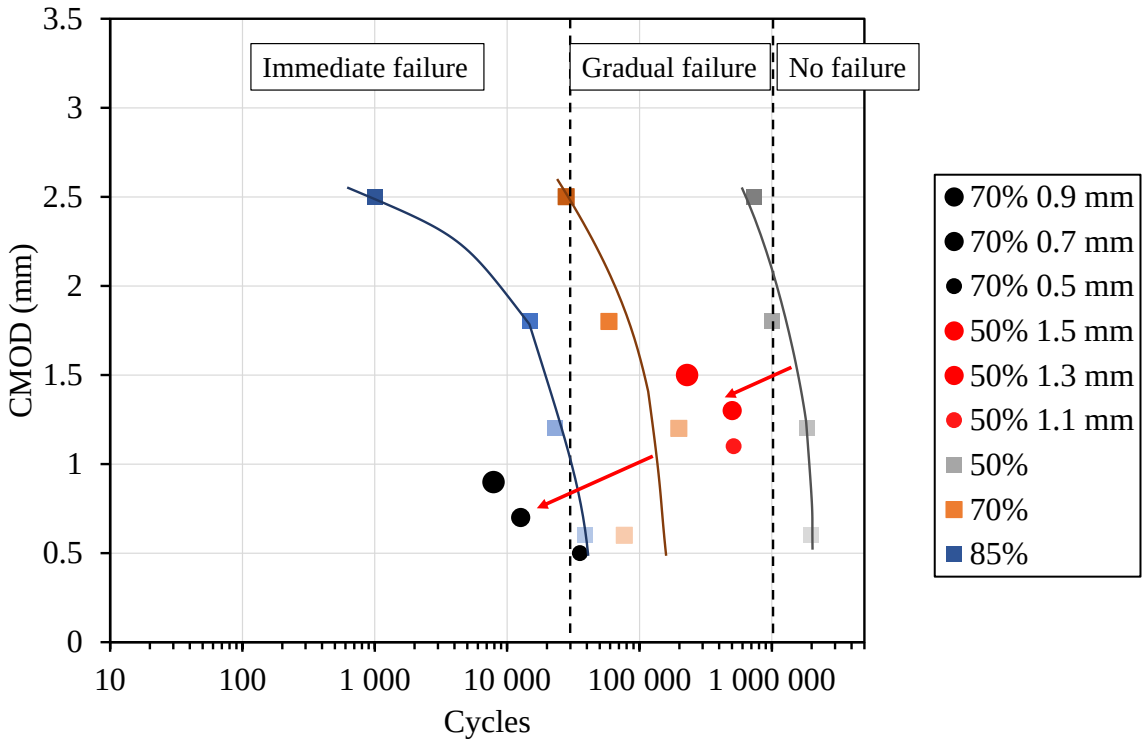

Figure 6.7: Comparison of average number of cycles sustained with Hemmeter (2017)

Investigating the mechanical behaviour of the SFRC produced by Hemmeter (2017) revealed that the post-cracking behaviour showed consistent deflection softening as seen in Figure 6.8. In contrast, the post-cracking behaviour of this study was deflection hardening, as illustrated in Figure 6.8. The fibre distribution and casting method could have a significant influence on the flexural behaviour of FRC, especially for highly flowable

mixes (Wille & Parra-Montesinos, 2012; Yoo, Yoon & Banthia, 2015). Furthermore, improved fibre alignment across the crack leads to better flexural strength (Stähli *et al.*, 2008). In FRC, especially SFRC, the number of fibres bridging the crack may show high scatter in various specimens with the same fibre dosage (Buratti *et al.*, 2011). All of the aforementioned factors could have resulted in the different post-cracking behaviour for the same concrete mix using similar materials.

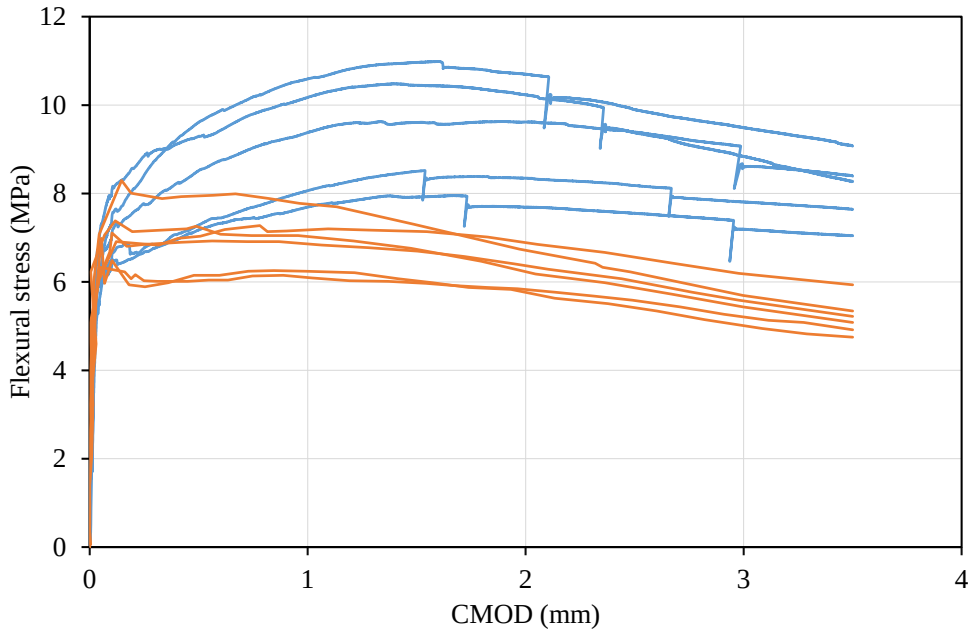

Figure 6.8: Post-cracking flexural stress of beam specimens with 0.8% fibre volume using Dramix 3D-65/60-BG fibres (orange represents work from Hemmeter (2017) and blue represents this study)

The post-cracking ductility could have a significant influence on the fatigue behaviour of pre-cracked FRC. The ability to withstand the fatigue loading would mostly depend on the ability of the fibres to withstand the applied loading, since the tensile capacity of concrete is assumed to be negligible. Based on the modified S-N curve in Figure 6.9, concrete with a deflection softening behaviour could result in an overestimation in the average number of cycles the FRC is able to withstand. In order to give accurate results, this approach should be applied to concrete with a similar mechanical performance. It may serve as a starting point for a prediction model; however, more work is still required before it can be implemented in design codes of practice.

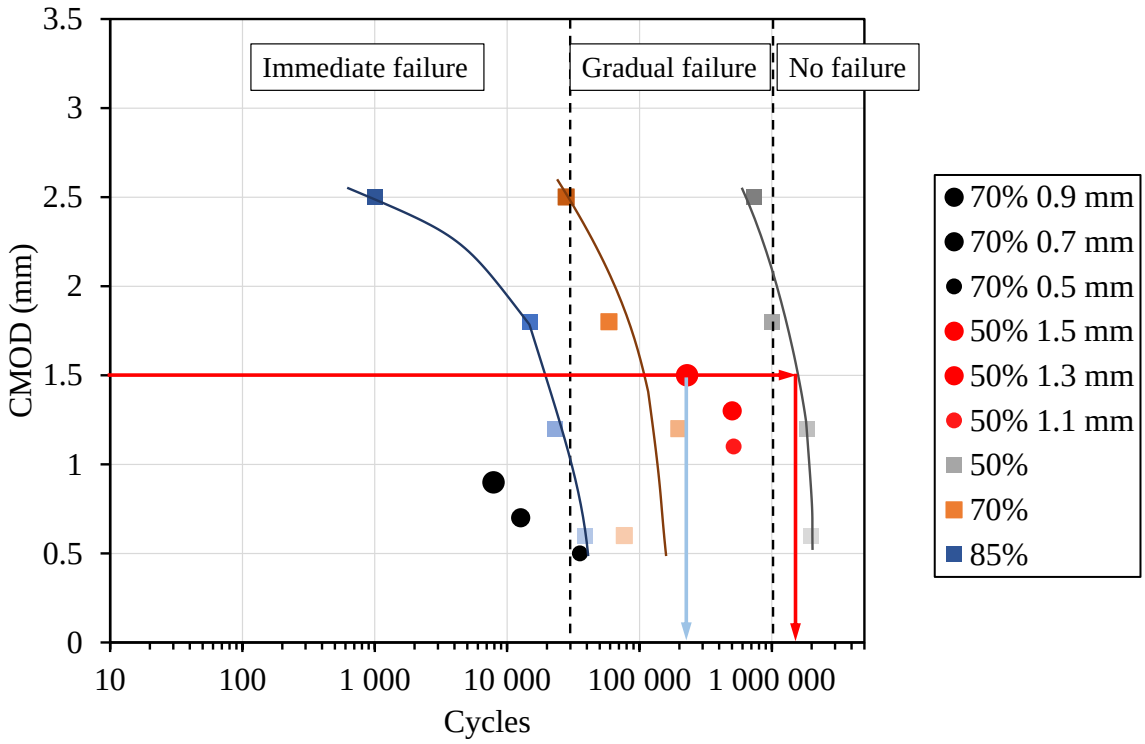

Figure 6.9: Overestimation of fatigue capacity for deflection softening FRC at 1.5 mm pre-crack (red vertical line illustrates the prediction and the blue vertical line illustrates the actual average number of cycles)

6.3. Flexural fatigue analytical modelling hypothesis

Based on the behaviour of the FRC under fatigue loading, and all the observations made, steps towards a flexural fatigue analytical model are hypothesised. The model considers the behaviour at a single fibre level and superimposes it on a macroscopic level. It accounts for the fibre behaviour, fibre-matrix interaction, and loading history. The following assumptions are made:

1. Due to the presence of the notch and initiating a pre-crack, flexural failure of the macroscopic specimens dominates.
2. All tensile loads are carried by the fibres across a crack.
3. The initial critical fibre is at the notch.

The abovementioned assumptions are general assumptions made. However, throughout the development of the model, several other assumptions and limitations to the model are made with respect to specific aspects at various steps.

6.3.1. Mechanisms influenced by the pre-cracking process

During the pre-cracking process, the composite experiences the largest loading throughout the test. This is based on the assumption made in Section 6.1.2, and is limited to the pre-cracks used only in this study. Smaller pre-cracks may not apply to this assumption. This is referred to as the "significant event" which causes the crack opening. In reality, the structure may experience a significant event over its lifespan which results in a large crack opening followed by fatigue loading. At this stage, all the tensile forces are assumed to be distributed to the fibres bridging the crack. The force distribution may not be even, as the fibres are randomly distributed throughout the matrix, as shown in Figure 6.10. However, since the largest opening of the crack would be at the notch, an assumption is made that the critical fibre/s is located closest to the notch. Fibres located further away from the notch will carry less force. Furthermore, an assumption is made that the crack height, *h*, is directly proportional to the crack width, *w*. As the crack width increases, the crack height increases, thereby mobilising more fibres.

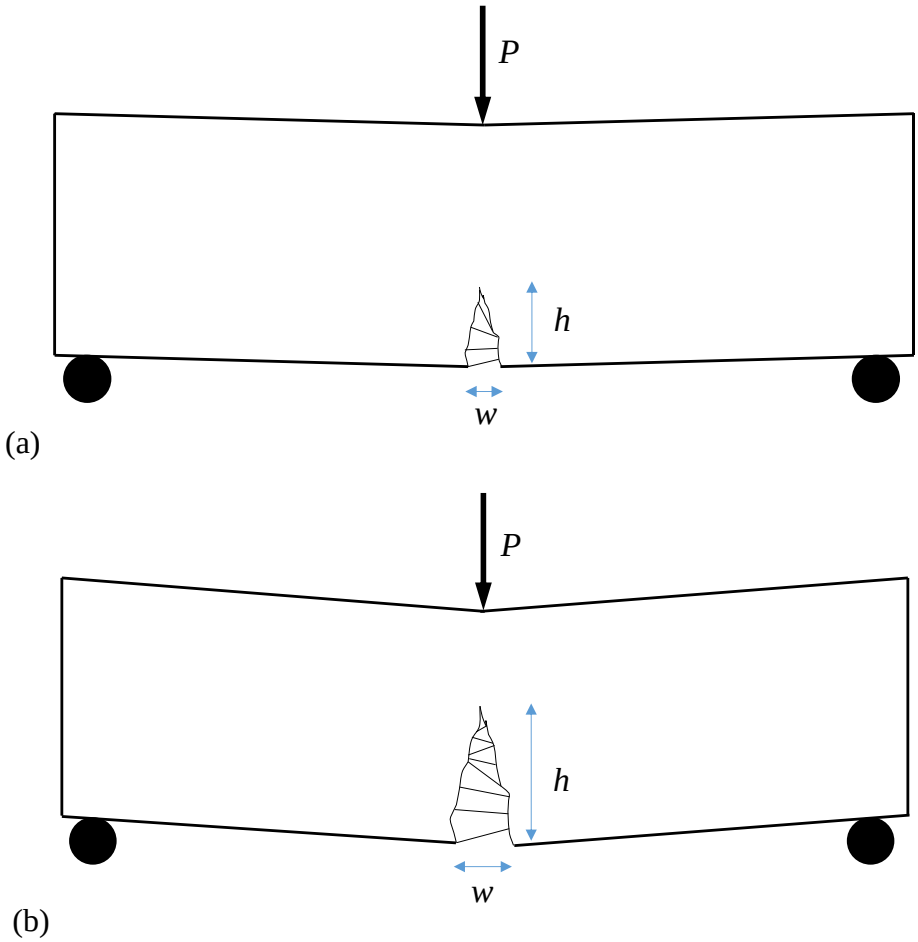

Figure 6.10: CMOD increases as load P increases (a) small CMOD, (b) large CMOD

An increase in the CMOD directly affects the fibre deformation. Since the fibres at the notch carry the largest force, it is assumed that the deformation of these fibres is the largest as well. The fibre deformation and force distribution were previously discussed in Section 6.1.1. Based on the results from Section 5.1.2, it is assumed that there is only fibre pull-out at this stage, since no ruptured fibres were found after static loading.

6.3.2. Effect of the fatigue loading and loading history

After the pre-crack or significant event, the crack closes to a certain extent due to the elastic behaviour of the fibres bridging the crack. As seen in Figure 5.11, the crack does not close completely, and the degree of crack closure depends on the fatigue load level applied as well as the magnitude of the pre-crack. All the fibres that have been activated to carry the tensile forces are in different phases according to their location relative to the notch, as discussed in Section 5.1.3.

As the fatigue loading commences, the tensile force in each fibre changes based on the fatigue loading level. Initially, the force in the fibre depends on the pre-crack load, then once the load changes from the pre-crack load to the mean load, the force decreases as well. The force in the fibre then cycles through the loads given by the fatigue loading. The first two loading applications (pre-crack load and unloading to the mean load) are both static loads, which deforms the fibres accordingly. Depending on the phase in which the fibres are in at the start of the fatigue loading, they have the ability to either pull-out or rupture. Based on the fibre hook deformation during the fatigue loading, it can be estimated whether the fibre is likely to fail in pull-out or rupture.

Fibre pull-out plays an important role in the fatigue capacity of FRC. In Section 5.1.3, all fibres are between Phases 1 and 3 during the pre-cracking process. Once the fatigue loading commences and w increases, the fibres can change to a different phase based on the fibre pull-out. Fibres in phases up to Phase 3 still have the potential to withstand loading. Once the fibre hook starts to deform and the peak load is reached, as shown in Figure 6.11, the fibre carrying capacity may decrease. Once the fibre hook has already deformed and it loses some of its load-carrying capacity, the fibre is likely to pull out under further fatigue loading. Figure 6.11 illustrates the average fibre pull-out behaviour for fibres used in this study, embedded at half of the fibre length. Based on this behaviour, the average maximum fibre pull-out force (F_{fPO_max}) is just more than 400 N, at a

displacement of 0.95 mm. At this maximum force, the fibre hook starts to straighten out as outlined in Section 4.1.1, thereby decreasing the load-carrying capacity of the fibre. However, it should be noted that even though the fibre's load-carrying capacity may decrease, it still has the potential to carry fatigue loading, as shown in Figure 4.14. The graph in Figure 6.11 is an average based on several single fibre pull-out tests. This may change with a change in fibre type, embedment length, fibre orientation, etc. and is used here as an indicator to the fibre hook deformation behaviour.

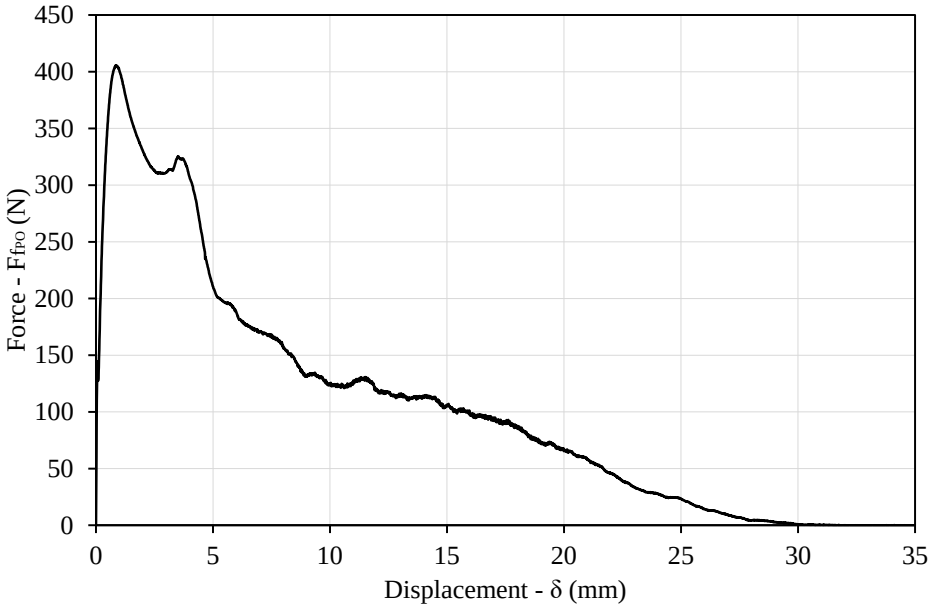

Figure 6.11: Average single fibre pull-out behaviour for this study

However, if the fibre hook is still intact, then fibre rupture it likely to occur after a substantial number of loading cycles have passed, since it is due to fatigue failure of the fibre itself. Based on the tensile stress of the fibre in Table 3.2, the tensile force that the fibre can withstand is approximately 738 N. From Table 4.1, fibre rupture was more predominant at the low pre-slips, and fibre pull-out at the larger pre-slips. This further corroborates the fact that the fibre hook is vital in determining whether the fibre will fail in pull-out or rupture.

6.3.3. Conditions for failure hypothesis

As the fatigue loading continues, the fibres continue to deform according to the crack width, its location from the notch, the load level applied, as well as the force experienced within each individual fibre (F_f). However, based on all the test results, the main concern is

whether the fibres will pull-out or rupture. As previously mentioned, if the fibres pull out, their load-carrying capacity diminishes up to a certain point. In contrast, when a fibre ruptures, it completely loses any load-carrying capacity, therefore, fibres which pull-out to a certain extent, have with a longer load-carrying ability than fibres which rupture. However, fibres which rupture may effectively carry larger forces in the individual fibres for a long time before failing.

The model framework presented in Figure 6.12 highlights the concepts outlined in Sections 6.3.1 and 6.3.2, and provide the conditions for various types of failure. The first event includes the fibre deformation and categorisation into various phases depending on the pre-crack. All the tensile loads get distributed into the fibres only, with each fibre carrying a different individual load depending on the factors mentioned in Section 6.3.1.

The second event deals with the fatigue loading and crack growth. Due to the fibre force distribution from the static loading, there are already fibres which are critical in carrying the load. This fibre/s is located closest to the notch and is assumed to carry the largest load in one or two individual fibres. As the crack width widens due to the pre-cracking process and/or fatigue loading, the critical fibre may either pull-out or rupture, thereby resulting in the redistribution of forces within the fibres and thus introducing new critical fibres. This phenomenon is outlined in Section 6.1.1.

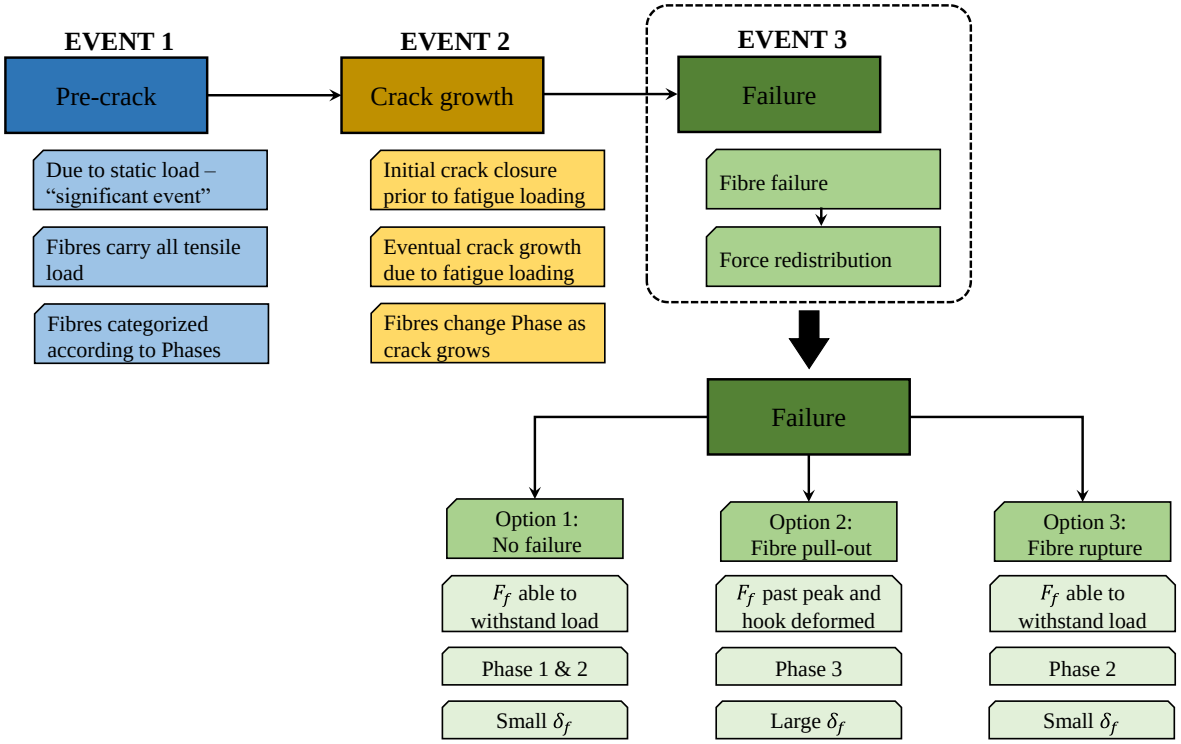

Figure 6.12: Hypothesised expected flexural fatigue behavioural model framework

Where:

F_f – force in an individual fibre,

F_{fPO_max} –maximum fibre pull-out force,

δ_f – displacement of the fibre,

w – crack width

Based on the force in the fibre, and the behaviour under fatigue loading, an estimation can be made whether the fibre will pull out or rupture. By referring to the single fibre pull-out graph in Figure 6.11 as a guideline, the following options may provide insight into the outcome of the fibre: (note that each single fibre pull-out graph will differ depending on the fibre and also the concrete)

Option 1: No failure

- If the force in the fibre is small and has not yet reached the maximum capacity, i.e. $F_f < F_{fPO\_max}$, with minimum fibre end pull-out (δ_f), then the fibre is categorised into Phases 1 or 2.

- At this point, the fibre still has sufficient load-carrying capacity since the hooks would not yet have been significantly deformed.
- The fibre requires more load applied by an increase in *w*, before any failure is considered.
- The fibre could either pull out or rupture.

Option 2: Fibre pull-out

- If the force in the fibre is smaller than the maximum pull-out force, i.e. $F_f < F_{fPO\_max}$, and the fibre end pull out is large, then the fibre is most likely to pull out.
- The fibre has already passed the maximum force. At this point, the fibre hooks have already started to deform, thereby resulting in the fibre end pull out.
- A further increase in *w* will result in the fibre to continue to pull out, thereby decreasing its load-carrying capacity.
- Since the maximum *w* in this study is 3.5 mm, the fibre is unlikely to completely straighten out. As a result, any fibre which "fails" in pull-out, has a reduced load-carrying capacity but still contributes to the overall load-carrying capacity.

Option 3: Fibre rupture

- If the force in the fibre is able to carry large loads, with little fibre end pull-out, then fibre rupture is likely to occur.
- At this point, the fibre still has the capacity to carry load, since the fibre hook has not yet deformed.
- The fibre is likely still within Phase 2 or possibly the beginning of Phase 3 and will remain there until failure.
- This failure is purely due to fatigue loading.

All the above-mentioned options may occur in all cracked FRC structures under fatigue loading. The framework provided is based on the results obtained from this study and provides a basis for further exploration. Although no failure of fibres would be ideal, it is not realistic especially for structures with large cracks. The ideal option would be to have

more fibres pulling out than rupturing due to the improved load-carrying capacity of pulled out fibres over ruptured fibres, as well as a gradual crack opening over time. Since it still maintains part of the fibre hooks, it is able to possibly extend the lifespan of the structure if more “pull-out failures” occur.

Although ruptured fibres may endure more fatigue load cycles before failure, they do not contribute to the load-carrying capacity after failing, thereby rendering them useless. The failure is also unexpected and brittle, which could cause multiple failures to surrounding fibres once the load gets redistributed after the rupture failure. This type of failure is not ideal since it is likely the cause of the accelerated crack growth which causes overall specimen failure. Fatigue failure of the fibres in rupture is an outcome which should be avoided.

6.4. Concluding summary

This chapter discussed the development of various approaches based on the experimental work in Chapters 4 and 5. The single fibre pull-out model which was developed in Chapter 4 serves as the basis for understanding the behaviours investigated in Chapters 5 and 6.

The fatigue behaviour led to the development of a behavioural fatigue model for pre-cracked flexural fatigue tests shown in Figure 6.13. The fatigue model consists of three stages, each affected by the pre-crack and/or load level. Based on the initial pre-crack and load level, there are three different outcomes: non-failure, gradual failure, and immediate failure. The non-failure outcome is valid for low pre-crack coupled with low load levels. The gradual failure outcome is valid for intermediate load level and pre-cracks, or combinations of high load level and small pre-crack or vice versa. Finally, the immediate failure outcome is valid for large pre-cracks coupled with high load levels.

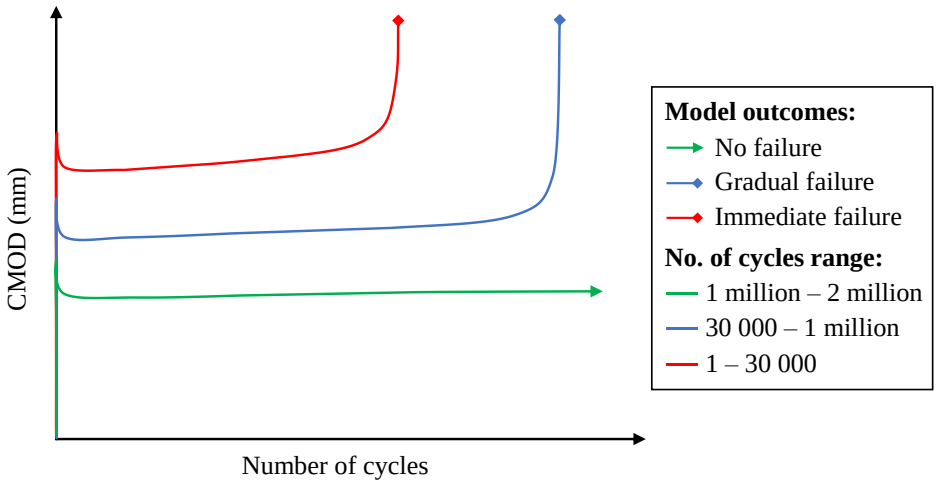

Figure 6.13: Fatigue model with three outcomes and the number of cycles each outcome may sustain

A fatigue life predictive approach was also developed based on the flexural fatigue results in Chapter 5. A modified S-N curve was developed to account for the pre-crack as well as the load levels. Test results from similar work performed by Hemmeter (2017) were used as a comparison for the modified S-N curve. The results show weaker fatigue life from Hemmeter (2017) due to deflection softening behaviour in the static tests. Therefore, this approach is limited to materials with similar mechanical performance. This approach also requires additional work before it can be implemented in practice, as this research is still in its infancy. It does, however, provide insight into the range of cycles that can be expected at a certain load level and pre-crack, based on the specific fibre and concrete type used in this study.

Finally, a hypothesis was put forward for the steps towards analytical modelling of pre-cracked flexural fatigue behaviour. Based on various “events” that are likely to occur under fatigue loading, as well as the pre-cracks and load levels, the single fibre pull-out model is used to estimate whether fibre pull-out or fibre rupture was likely to occur during the fatigue life of pre-cracked SFRC.

7. Conclusions and recommendations

In this research project, the fatigue behaviour of pre-cracked steel fibre reinforced concrete (SFRC) at a single fibre level and macroscopic level, using hooked-end 3D steel fibres, was investigated. Experiments were performed under static and fatigue loading at both levels and extensive X-ray Computed Tomography (CT) scans are conducted. Based on the behaviour under fatigue loading at the single fibre and macroscopic levels, as well as the failure mechanisms, various approaches were developed to aid in the prediction of the fatigue life of pre-cracked SFRC subjected to fatigue loading.

The conclusions drawn from the work performed in this study are presented in the following sections.

7.1. Single fibre level

- Based on the static pull-out behaviour, a single fibre pull-out model was developed to categorise the single fibre pull-out behaviour for 3D hooked-end steel fibres into five phases. Each phase represents a different degree of fibre hook deformation.
    - Phase 1 consists of the partial fibre debonding from the surrounding matrix.
    - Phase 2 is the complete debonding and activation of the first fibre hook.
    - Phase 3 occurs when the first fibre hook straightens out – the global peak occurs in this phase.
    - Phase 4 occurs when the second hook straightens out.
    - Phase 5 is the frictional pull-out of the straightened fibre.
- The fatigue behaviour depends mainly on the pre-slip, which places the fibres into different phases. As the phase changes due to a change in fibre pull-out, the fatigue limit also changes based on the applied load level.
- The fibre hook (mechanical anchorage) provides the predominant resistance to fatigue loading. Deformation of the fibre hook decreases the fatigue capacity. Once the hook is completely straight, there remains little to no fatigue resistance. Therefore, mechanical anchorage of fibres is essential to resist fatigue loading.
- The fatigue test results at different pull-outs and load levels show two failure mechanisms – fibre pull-out and fibre rupture. This differs from the static pull-out test results, which only shows fibre pull-out as the failure mechanism.

- Based on extent of fibre deformation prior to fatigue loading, the fatigue capacity as well as failure mechanism may be determined.
    - A small pre-slip coupled with a low load level may result in no failure of the fibre. The small pre-slip (≤ 1.2 mm) places the fibre in Phase 2 or beginning of Phase 3, and does not significantly deform the fibre hooks. The fibre still has sufficient anchorage to withstand the low fatigue load.
    - If the pre-slip remains small and a larger fatigue load level is applied, this could possibly result in fibre rupture, since the fibre hooks remain intact, and the load is not large enough to cause fibre pull-out. Instead, it results in pure fatigue failure of the steel fibre.
    - A larger pre-slip (> 1.2 mm) places the fibre well into Phase 3, where fibre hook deformation occurs, thereby reducing its anchorage. As a result, any fatigue load level applied could result in fibre pull-out.

7.2. Macroscopic level

- Based on the pre-crack, as well as the location of the fibre relative to the notch, the fibres can be classified according to the single fibre model proposed in Chapter 4. Based in the phase classification, the fatigue resistance may be estimated prior to fatigue loading.
    - The fibres of the 0.6 mm pre-crack at the notch are classified as Phase 2, and further away from the notch, they are in Phase 1. Fibres have little to no hook deformation and large loads are required to pull fibres out.
    - For the pre-cracks of 1.2 mm and 1.8 mm, the fibres at the notch show visible pull-out, but little to no fibre hook deformation, and are classified as Phase 3. Further away from the notch, the fibres can be classified into Phase 2. Since the fibre has started to pull-out, the fatigue capacity has diminished, and failure depends on the applied load level.
    - The 2.5 mm pre-crack shows visible fibre end pull-out for all the fibres bridging the crack, and are therefore, all classified as Phase 3. The fibre hooks have deformed and its load carrying capacity decreases significantly.
- The flexural fatigue results display a high degree of variability, with significant coefficient of variations obtained throughout the fatigue testing.

- An increase in pre-crack and load level decreases the fatigue capacity. This is more severe at the 2.5 mm pre-crack at 85% load level.
- The initial pre-cracks serve as an indicator as to when the specimen is likely to fail. Regardless of the load level, the specimens all failed once the CMOD reached the vicinity of the initial pre-crack. For the smaller pre-crack, failure occurs shortly after the CMOD passes the initial pre-crack. At the larger pre-cracks, failure occurred shortly before the CMOD reaches the initial pre-crack.
- X-ray CT scans performed on specimens tested under fatigue loading show that the dominating failure mechanism changes from fibre pull-out, which occurs in the static tests, to fibre rupture. This is significant since fibre pull-out failure occurs gradually as the cycles progress, which results in ductile failure. Since the failure CMOD is at 3.5 mm, the fibres that fail in pull-out may not completely straighten out and can still contribute to the load-carrying capacity. However, fibre rupture occurs instantly, and cannot contribute to the load-carrying capacity after failure.

7.3. Modelling framework

- CMOD over the duration of the fatigue tests shows distinct behaviour of a gradual increase in CMOD after the pre-crack, followed by accelerated crack growth at the region of the initial pre-crack. The gradual increase in CMOD is caused by the fibres pulling out during the fatigue loading, whereas the accelerated crack growth is due to fibre rupture failure.
    - Depending on the applied load level, the increase in CMOD may occur at a faster rate at higher load levels thereby resulting in quicker failure, and vice versa.
    - The accelerated crack growth usually occurs in the region of the initial pre-crack.
- A flexural fatigue behavioural model was developed from the flexural fatigue results to determine whether failure is likely to occur based on the load level and pre-crack. A non-failure outcome is likely to occur for low pre-cracks and load levels. Gradual failure can occur at intermediate load levels and pre-cracks, or a combination of low load level and large pre-crack, and vice versa. Immediate failure can occur at large pre-cracks and load levels.

- A flexural fatigue life prediction approach was developed in the form of a modified S-N curve to account for the load level as well as the pre-crack used based on the experimental results in Chapter 5. This approach provides a simplistic method of determining the average range of cycles to failure based on the pre-crack and applied load level. It was compared to test results obtained from another researcher and the results show that the approach overestimates the fatigue capacity. This is mainly due to the post-cracking behaviour, where a deflection hardening behaviour results in improved fatigue capacity over deflection softening behaviour.
- Finally, the framework for an analytical model is developed to predict the failure mechanisms under various load levels and pre-cracks. Depending on the degree of fibre deformation prior to fatigue loading, the likely fatigue failure outcome may be estimated. Fibres subjected to significant pull-out and fibre hook deformation prior to fatigue loading are likely to pull out under fatigue loading, whereas fibres with less deformation are more likely to rupture under fatigue loading.

7.4. Recommendations

Based on the experimental findings from this research study, the following recommendations are made for further investigations.

- Investigate the influence of orientation angles and embedment lengths for pre-slipped fatigue pull-out at a single fibre level.
- Develop a test setup which can accurately perform fatigue tests on several specimens at a time, at both single fibre level and macroscopic level.
- Investigate the influence of the matrix strength on the fatigue fibre rupture behaviour.
- Perform fatigue tests on a single fibre to determine its fatigue capacity at fibre rupture.
- Improve the empirical model to a more generalised behaviour which incorporates the effects of post-cracking behaviour.
- Develop a constitutive model under fatigue loading for pre-cracked SFRC, which incorporates the current analytical model in Chapter 6 as a basis for failure prediction behaviour.

References

Aas-Jakobsen, K. 1970. Fatigue of concrete beams and columns. Bulletin No. 70-1. *The Norwegian Institute of Technology, Trondheim*.

Abbas, S., Soliman, A.M. & Nehdi, M.L. 2015. Exploring mechanical and durability properties of ultra-high performance concrete incorporating various steel fiber lengths and dosages. *Construction and Building Materials*. 75:429–441.

Abdallah, S., Fan, M. & Zhou, X. 2017. Pull-out behaviour of hooked end steel fibres embedded in ultra-high performance mortar with various W/B ratios. *International Journal of Concrete Structures and Materials*. 11(2):301–313.

Abdallah, S., Fan, M. & Rees, D.W.A. 2018. Bonding Mechanisms and Strength of Steel Fiber–Reinforced Cementitious Composites: Overview. *Journal of Materials in Civil Engineering*. 30(3):04018001.

Abiola, O.S. 2017. Natural fibre cement composites. in *Advanced High Strength Natural Fibre Composites in Construction* Elsevier. 205–214.

Abu-Lebdeh, T., Hamoush, S., Heard, W. & Zornig, B. 2011. Effect of matrix strength on pullout behavior of steel fiber reinforced very-high strength concrete composites. *Construction and Building Materials*. 25(1):39–46.

Adepegba, D. & Regan, P.E. 1981. Performance of steel fibre reinforced concrete in axially loaded short columns. *International Journal of Cement Composites and Lightweight Concrete*. 3(4):255–259.

Akita, H., Koide, H., Tomon, M. & Sohn, D. 2003. A practical method for uniaxial tension test of concrete. *Materials and structures*. 36(6):365–371.

Anderson, T.L. 2017. *Fracture mechanics: fundamentals and applications*. CRC press.

Arunakanthi, E. & Kumar, J.D.C. 2016. Experimental studies on fiber reinforced concrete (FRC). *International Journal of Civil Engineering and Technology*. 7(5):329–336.

Aziz, M.A., Paramasivam, P. & Lee, S.L. 1981. Prospects for natural fibre reinforced concretes in construction. *International Journal of Cement Composites and Lightweight Concrete*. 3(2):123–132.

Babafemi, A.J. & Boshoff, W.P. 2017. Pull-out response of macro synthetic fibre from concrete matrix: Effect of loading rate and embedment length. *Construction and Building Materials*. 135(C):590–599.

Banjara, N.K. & Ramanjaneyulu, K. 2018. Experimental investigations and numerical simulations on the flexural fatigue behavior of plain and fiber-reinforced concrete. *Journal of Materials in Civil Engineering*. 30(8):4018151.

Banjara, N.K., Ramanjaneyulu, K., Sasmal, S. & Srinivas, V. 2016. Flexural fatigue performance of plain and fibre reinforced concrete. *Transactions of the Indian Institute of Metals*. 69(2):373–377.

Banthia, N. & Trottier, J.-F. 1991. Deformed steel fiber—cementitious matrix bond under impact. *Cement and Concrete Research*. 21(1):158–168.

Banthia, N., Trottier, J.F. & Pigeon, M. 1989. Fiber Pull Out Mechanisms: Effects of Fiber Geometry, Loading Rate and Sub-zero Temperatures. *Fibre Reinforced Cements and Concretes: Recent Developments*. 136–145.

Barr, B., Asghari, A. & Hughes, T.G. 1988. Tensile strength and toughness of FRC materials. *International Journal of Cement Composites and Lightweight Concrete*. 10(2):101–107.

Bathias, C. & Pineau, A. 2010. *Fatigue of materials and structures*. (ISTE). London : Hoboken: ISTE ; Wiley.

Batson, G., Ball, C., Bailey, L., Landers, E. & Hooks, J. 1972. Flexural Fatigue Strength of Steel Fiber Reinforced Concrete Beams. *Journal Proceedings*. 69(11):673–677.

Beaudoin, J.J. 1990. *Handbook of fiber-reinforced concrete: Principle properties, developments and applications*. Park Ridge, N.J. : Noyes Publications.

Beglarigale, A. & Yazici, H. 2015. Pull-out behavior of steel fiber embedded in flowable RPC and ordinary mortar. *Construction and building materials*. 75:255–265.

Bentur, A. & Mindess, S. 1990. *Fibre reinforced cementitious composites, 1990*. Vol. 449.

Bentur, A. & Mindess, S. 2006. *Fibre reinforced cementitious composites*. Crc Press.

Betterman, L.R., Ouyang, C. & Shah, S.P. 1995. Fiber-matrix interaction in microfiber-reinforced mortar. *Advanced Cement Based Materials*. 2(2):53–61.

Bhowmik, S. & Ray, S. 2018. An improved crack propagation model for plain concrete under fatigue loading. *Engineering Fracture Mechanics*. 191(January):365–382.

Boulekbache, B., Hamrat, M., Chemrouk, M. & Amziane, S. 2016. Flexural behaviour of steel fibre-reinforced concrete under cyclic loading. *Construction and Building Materials*. 126:253–262.

Brandt, A.M. 2008. Fibre reinforced cement-based (FRC) composites after over 40 years of development in building and civil engineering. *Composite Structures*. 86(1):3–9.

BS EN 14651. 2005. *Test method for metallic fibre concrete - Measuring the flexural tensile strength (limit of proportionality (LOP) residual)*.

BS EN 1992-1-1. 2004. *Eurocode 2: Design of concrete structures - Part 1-1: General rules and rules for buildings*. London: British Standard Institution.

Buratti, N., Mazzotti, C. & Savoia, M. 2011. Post-cracking behaviour of steel and macro-synthetic fibre-reinforced concretes. *Construction and Building Materials*. 25(5):2713–2722.

Buyukozturk, O. & Hearing, B. 1998. Crack propagation in concrete composites influenced by interface fracture parameters. *International Journal of Solids and Structures*. 35(31–32):4055–4066.

Cachim, P.B. 1999. Experimental and numerical analysis of the behaviour of structural concrete under fatigue loading with applications to concrete pavements. PhD thesis. University of Porto.

Cachim, P.B., Figueiras, J.A. & Pereira, P.A.A. 2002. Fatigue behavior of fiber-reinforced

concrete in compression. *Cement and Concrete Composites*. 24(2):211–217.

Cao, Y.Y.Y. & Yu, Q.L. 2018. Effect of inclination angle on hooked end steel fiber pullout behavior in ultra-high performance concrete. *Composite Structures*. 201:151–160.

Carlesso, D.M., de la Fuente, A. & Cavalaro, S.H.P. 2019. Fatigue of cracked high performance fiber reinforced concrete subjected to bending. *Construction and Building Materials*. 220:444–455.

Van Chanh, N. 2004. Steel fiber reinforced concrete. in *Faculty of Civil Engineering Ho chi minh City university of Technology. Seminar Material*. 108–116.

Chanvillard, G., Banthia, N. & Aïtcin, P.-C. 1990. Normalized load-deflection curves for fibre reinforced concrete under flexure. *Cement and Concrete Composites*. 12(1):41–45.

Chen, X., Bu, J., Fan, X., Lu, J. & Xu, L. 2017. Effect of loading frequency and stress level on low cycle fatigue behavior of plain concrete in direct tension. *Construction and Building Materials*. 133:367–375.

Cunha, V.M.C.F., Barros, J.A.O. & Sena-Cruz, J. 2007. Pullout behaviour of hooked-end steel fibres in self-compacting concrete. Universidade do Minho. Departamento de Engenharia Civil (DEC).

Daniel, J.I., Ahmad, S.H., Arockiasamy, M., Ball, H.P., Batson, G.B., Criswell, M.E., Dorfmueller, D.P., Fernandez, A. V, et al. 2002. State-of-the-art report on fiber reinforced concrete reported by ACI Committee 544. *ACI Journal Proceedings*. 96.

Deng, F., Ding, X., Chi, Y., Xu, L. & Wang, L. 2018. The pull-out behavior of straight and hooked-end steel fiber from hybrid fiber reinforced cementitious composite: Experimental study and analytical modelling. *Composite Structures*. 206:693–712.

Denneman, E., Kearsley, E.P. & Visser, A.T. 2011. Splitting tensile test for fibre reinforced concrete. *Materials and structures*. 44(8):1441–1449.

Diamond, S. & Huang, J. 2001. The ITZ in concrete--a different view based on image analysis and SEM observations. *Cement and concrete composites*. 23(2–3):179–188.

Do, M.-T., Chaallal, O. & Aïtcin, P.-C. 1993. Fatigue behavior of high-performance concrete. *Journal of Materials in civil Engineering*. 5(1):96–111.

Dobromil, P., Jan, C. & Radomir, P. 2010. Material model for finite element modelling of fatigue crack growth in concrete. *Procedia engineering*. 2(1):203–212.

Domone, P. & Illston, J. 2010. *Construction Materials Their Nature and Behaviour*. Oxon: Spon Press.

Dramix® steel fiber concrete reinforcement - Bekaert.com. 2018. [Online], Available: https://www.bekaert.com/en/products/construction/concrete-reinforcement/dramix-steel-fiber-concrete-reinforcement [2018, February 21].

Ellis, G. 2012. *Control system design guide: using your computer to understand and diagnose feedback controllers*. Butterworth-Heinemann.

Fantilli, A.P., Mihashi, H. & Vallini, P. 2009. Multiple cracking and strain hardening in

fiber-reinforced concrete under uniaxial tension. *Cement and Concrete Research*. 39(12):1217–1229.

Farzam, H., Hogan, M.B., Holub, E.P., Kaetzel, L.J. & Luther, M.D. 2000. ACI 116R-00 Cement and Concrete Terminology Reported by ACI Committee 116. 1–73.

Fu, H.C., Erki, M.A. & Seckin, M. 1991. Review of effects of loading rate on concrete in compression. *Journal of structural engineering*. 117(12):3645–3659.

Gao, L. & Hsu, C.T. 1999. Fatigue of Concrete under Uniaxial Compression Cyclic Loading. *ACI materials journal*. (95):575–582.

Germano, F., Tiberti, G. & Plizzari, G. 2016. Post-peak fatigue performance of steel fiber reinforced concrete under flexure. *Materials and Structures*. 49(10):4229–4245.

Gettu, R. & Stephen, S.J. 2020. Fatigue fracture of fibre reinforced concrete in flexure. *Materials and Structures*. 53:56.

Ghoddousi, P., Ahmadi, R. & Sharifi, M. 2010. Fiber pullout model for aligned hooked-end steel fiber. *Canadian Journal of Civil Engineering*. 37(9):1179–1188.

Goel, S., Singh, S.P. & Singh, P. 2012. Flexural fatigue strength and failure probability of self compacting fibre reinforced concrete beams. *Engineering Structures*. 40:131–140.

Gokoz, U.N. & Naaman, A.E. 1981. Effect of strain-rate on the pull-out behaviour of fibres in mortar. *International Journal of Cement Composites and Lightweight Concrete*. 3(3):187–202.

Gopalaratnam, V.S. & Shah, S.P. 1987. Tensile failure of steel fiber-reinforced mortar. *Journal of engineering mechanics*. 113(5):635–652.

Graf, O. & Brenner, E. 1934. Experiments for investigating the resistance of concrete under often repeated compression loads. *Bulletin 1*. 1:17–25.

Groth, P. 2000. Fibre reinforced concrete: fracture mechanics methods applied on self-compacting concrete and energetically modified binders. PhD thesis. Luleåtekniska universitet.

Hanson, J.M., Ballinger, C.A. & Linger, D. 1974. Considerations for design of concrete structures subjected to fatigue loading. *ACI Journal*. 71(3):97–120.

Hatzigeorgiou, G., Beskos, D., Theodorakopoulos, D. & Sfakianakis, M. 2001. A simple concrete damage model for dynamic FEM applications. *International Journal of Computational Engineering Science*. 2(02):267–286.

Hemmeter, R. 2017. The Flexural Fatigue Behaviour of Pre-cracked Steel Fibre Reinforced Concrete. University of Stuttgart.

Hoff, G.. 1984. *Fiber reinforced concrete : international symposium*. (Publication SP ; 73). Detroit, Mich.: American Concrete Institute.

Holmen, J.O. 1982. Fatigue of concrete by constant and variable amplitude loading. *Special Publication*. 75:71–110.

Hsu, T.T.C. 1981. Fatigue of plain concrete. in *Journal Proceedings* Vol. 78. 292–305.

Isla, F., Ruano, G. & Luccioni, B. 2015. Analysis of steel fibers pull-out. Experimental study. *Construction and Building Materials*. 100:183–193.

Johnston, C.D. & Zemp, R.W. 1991. Flexural fatigue performance of steel fiber reinforced concrete--influence of fiber content, aspect ratio, and type. *Materials Journal*. 88(4):374–383.

Jun, Z. & Stang, H. 1998. Fatigue Performance in Flexure of Fiber Reinforced Concrete. *Materials Journal*. 95(1):58–67.

Karadelis, J.N. & Lin, Y. 2015. Flexural strengths and fibre efficiency of steel-fibre-reinforced, roller-compacted, polymer modified concrete. *Construction and building materials*. 93:498–505.

Keerthana, K. & Chandra Kishen, J.M. 2018. An experimental and analytical study on fatigue damage in concrete under variable amplitude loading. *International Journal of Fatigue*. 111(November 2017):278–288.

Kolluru, S. V, O'Neil, E.F., Popovics, J.S. & Shah, S.P. 2000. Crack propagation in flexural fatigue of concrete. *Journal of engineering mechanics*. 126(9):891–898.

Lee, M.K. & Barr, B.I.G. 2004. An overview of the fatigue behaviour of plain and fibre reinforced concrete. *Cement and Concrete Composites*. 26(4):299–305.

Löfgren, I. 2005. Fibre-reinforced Concrete for Industrial Construction - a fracture mechanics approach to material testing and structural analysis. PhD thesis. Chalmers University of Technology.

De Luca, A., Matta, F. & Nanni, A. 2010. Behavior of full-scale glass fiber-reinforced polymer reinforced concrete columns under axial load. *ACI structural journal*. 107(5):589.

Mailhot, T., Bissonnette, B., Saucier, F. & Pigeon, M. 2001. Flexural fatigue behavior of steel fibre reinforced concrete before and after cracking. *Materials and Structures*. 34(6):351–359.

Marković, I. 2006. High-performance Hybrid-fibre Concrete : Development and Utilisation. PhD thesis. Delft University, the Netherlands.

Mayer, H. 2009. Fatigue damage of low amplitude cycles in low carbon steel. *Journal of materials science*. 44(18):4919–4929.

Medeiros, A., Zhang, X., Ruiz, G., Yu, R.C. & de Souza Lima Velasco, M. 2015. Effect of the loading frequency on the compressive fatigue behavior of plain and fiber reinforced concrete. *International Journal of Fatigue*. 70:342–350.

Van Mier, J.G.M. 1991. Mode I fracture of concrete: discontinuous crack growth and crack interface grain bridging. *Cement and concrete research*. 21(1):1–15.

Musuva, J.K. & Radon, J.C. 1979. The effect of stress ratio and frequency on fatigue crack growth. *Fatigue & Fracture of Engineering Materials & Structures*. 1(4):457–470.

Naaman, A.E. 1985. Fiber Reinforcement for Concrete. *Concrete International: Design and Construction*. 7(3):21–25.

Naaman, A.E. & Hammoud, H. 1998. Fatigue characteristics of high performance fiber-reinforced concrete. *Cement and Concrete Composites*. 20(5):353–363.

Naaman, A.E. & Najm, H. 1991. Bond-slip mechanisms of steel fibers in concrete. *ACI materials journal*. 88(2):135–145.

Naaman, A.E. & Reinhardt, H.-W. 2006. Proposed classification of HPFRC composites based on their tensile response. *Materials and structures*. 39(5):547–555.

Naaman, A.E., Namur, G.G., Alwan, J.M. & Najm, H.S. 1991. Fiber pullout and bond slip. II: Experimental validation. *Journal of Structural Engineering*. 117(9):2791–2800.

Namur, G.G., Alwan, J.M. & Najm, H.S. 1991. Fiber pullout and bond slip I: Analytical study. *Journal of Structural Engineering*. 117(9):2769–2790.

Nanni, A. 1991. Fatigue behaviour of steel fiber reinforced concrete. *Cement and Concrete Composites*. 13(4):239–245.

Nieuwoudt, P.D. 2016. Time-dependent Behaviour of Cracked Steel Fibre Reinforced Concrete. PhD thesis. Stellenbosch University.

Oh, B.H. 1986. Fatigue analysis of plain concrete in flexure. *Journal of Structural Engineering*. 112(2):273–288.

Otter, D.E. & Naaman, A.E. 1988. Properties of Steel Fiber Reinforced Concrete Under Cyclic Load. *Materials Journal*. 85(4):254–261.

Ou, Y.-C., Tsai, M.-S., Liu, K.-Y. & Chang, K.-C. 2012. Compressive behavior of steel-fiber-reinforced concrete with a high reinforcing index. *Journal of Materials in Civil Engineering*. 24(2):207–215.

Owens, G. 2013. *Fundamentals of Concrete*. 3rd ed. The Concrete Institute.

Park, Y.J. 1990. Fatigue of concrete under random loadings. *Journal of Structural engineering*. 116(11):3228–3235.

Parvez, A. & Foster, S.J. 2017. Fatigue of steel-fibre-reinforced concrete prestressed railway sleepers. *Engineering Structures*. 141:241–250.

du Plessis, A., le Roux, S.G. & Guelpa, A. 2016. The CT Scanner Facility at Stellenbosch University: An open access X-ray computed tomography laboratory. *Nuclear Instruments and Methods in Physics Research Section B: Beam Interactions with Materials and Atoms*. 384:42–49.

Plizzari, G.A., Cere, N. & Cangiano, S. 2000. Postpeak Behavior of Fiber-Reinforced Concrete under Cyclic Tensile Loads. *Materials Journal*. 97(2):182–192.

di Prisco, M., Plizzari, G. & Vandewalle, L. 2009. Fibre reinforced concrete: new design perspectives. *Materials and Structures*. 42(9):1261–1281.

Qi, J., Wu, Z., Ma, Z.J. & Wang, J. 2018. Pullout behavior of straight and hooked-end steel fibers in UHPC matrix with various embedded angles. *Construction and Building Materials*. 191:764–774.

Ramakrishnan, V., Tatnal, P. & Oberling, G. 1987. Flexural Fatigue Strength of Steel Fiber Reinforced Concrete. *Special Publication*. 105:225–246.

Robins, P., Austin, S. & Jones, P. 2002. Pull-out behaviour of hooked steel fibres. *Materials and structures*. 35(7):434–442.

Romualdi, J.P. & Batson, G.B. 1963. Mechanics of crack arrest in concrete. *Journal of the Engineering Mechanics Division*. 89(3):147–168.

Shah, S.P., Swartz, S.E. & Ouyang, C. 1995. *Fracture mechanics of concrete: applications of fracture mechanics to concrete, rock and other quasi-brittle materials*. John Wiley & Sons.

Simon, K.M. & Kishen, J.M.C. 2016. Influence of aggregate bridging on the fatigue behavior of concrete. *International Journal of Fatigue*. 90:200–209.

Singh, S.P. & Kaushik, S.K. 2000. Flexural fatigue life distributions and failure probability of steel fibrous concrete. *Materials Journal*. 97(6):658–667.

Singh, S.P. & Kaushik, S.K. 2003. Fatigue strength of steel fibre reinforced concrete in flexure. *Cement and Concrete Composites*. 25(7):779–786.

Singh, S., Shukla, A. & Brown, R. 2004. Pullout behavior of polypropylene fibers from cementitious matrix. *Cement and Concrete Research*. 34(10):1919–1925.

Soufeiani, L., Raman, S.N., Jumaat, M.Z. Bin, Alengaram, U.J., Ghadyani, G. & Mendis, P. 2016. Influences of the volume fraction and shape of steel fibers on fiber-reinforced concrete subjected to dynamic loading--A review. *Engineering Structures*. 124:405–417.

Stähli, P., Custer, R. & van Mier, J.G.M. 2008. On flow properties, fibre distribution, fibre orientation and flexural behaviour of FRC. *Materials and Structures*. 41(1):189–196.

Stephens, R.I., Fatemi, A., Stephens, R.R. & Fuchs, H.O. 2000. *Metal fatigue in engineering*. John Wiley & Sons.

Sujivorakul, C., Waas, A.M. & Naaman, A.E. 2000. Pullout response of a smooth fiber with an end anchorage. *Journal of Engineering Mechanics*. 126(9):986–993.

Tasdemir, M.A. & Karihaloo, B.L. 2001. Effect of type and volume fraction of aggregate on the fracture properties of concrete. *Mech. Concr. Struct*. 123–129.

Walraven, J.C. & others. 2010. *Model Code 2010-Final draft: Volume 1*. Vol. 55. fib Fédération internationale du béton.

Wang, Y., Shen, Y.N. & Ma, J. 2012. FEM Analysis on the Fatigue Properties of Reinforced Concrete Beams Strengthened with CFRP. *Applied Mechanics and Materials*. 166:1769–1772.

Wille, K. & Parra-Montesinos, G.J. 2012. Effect of beam size, casting method, and support conditions on flexural behavior of ultra high-performance fiber-reinforced concret. *ACI Materials Journal*. 109(3):379.

Wittmann, F.H. 1989. Structure and fracture mechanics of composite materials. *Fracture Toughness and Fracture Energy Test methods for concrete and rock*. 3–12.

Wu, K.-R., Chen, B., Yao, W. & Zhang, D. 2001. Effect of coarse aggregate type on mechanical properties of high-performance concrete. *Cement and Concrete Research*.

31(10):1421–1425.

Wu, Y., Tan, X., Liu, Q., Chen, W., Meng, X., Deng, X. & Li, W. 2016. Structural Foamed Concrete with Lightweight Aggregate and Polypropylene Fiber: Product Design Through Orthogonal Tests. *Polymers and Polymer Composites*. 24(2):173–178. [Online], Available: https://www.scopus.com/inward/record.uri?eid=2-s2.0-84959350114&partnerID=40&md5=33ecf61b89d992a58459363182715291.

Yakut, A. 2004. Reinforced concrete frame construction. *World Housing Encyclopedia—Summary Publication*.

Yin, W. & Hsu, T.T.C. 1995. Fatigue Behavior of Steel Fiber Reinforced Concrete in Uniaxial and Biaxial Compression. *Materials Journal*. 92(1):71–81.

Yoo, D.-Y., Yoon, Y.-S. & Banthia, N. 2015. Predicting the post-cracking behavior of normal-and high-strength steel-fiber-reinforced concrete beams. *Construction and Building Materials*. 93:477–485.

Yoo, D.-Y., Park, J.-J. & Kim, S.-W. 2017. Fiber pullout behavior of HPFRCC: Effects of matrix strength and fiber type. *Composite Structures*. 174:263–276.

Zaitsev, Y.B. & Wittmann, F.H. 1981. Simulation of crack propagation and failure of concrete. *Matériaux et Construction*. 14(5):357–365.

Zandi Hanjari, K. 2006. Evaluation of WST Method as a Fatigue Test for Plain and Fiber-reinforced Concrete-experimental and numerical investigation. Master's thesis. Chalmers University of Technology.

Zanuy, C., Albajar, L. & de la Fuente, P. 2011. The fatigue process of concrete and its structural influence. *Materiales de Construcción*. 61:385–399.

Zhang, B., Phillips, D. V & Wu, K. 1996. Effects of loading frequency and stress reversal on fatigue life of plain concrete. *Magazine of concrete research*. 48(177):361–375.

Zhang, J., Stang, H. & Li, V.C. 2000. Experimental study on crack bridging in FRC under uniaxial fatigue tension. *Journal of Materials in Civil Engineering*. 12(1):66–73.

Zīle, E. & Zīle, O. 2013. Effect of the fiber geometry on the pullout response of mechanically deformed steel fibers. *Cement and Concrete Research*. 44:18–24.

Appendix A

The raw data from the start of Step 2 – the unloading step – shows show the CMOD increases from 0.6 mm to 0.96 mm within the span of 1 second.

Total Time (s)	Elapsed Time (s)	Step	Load (kN)	CMOD (mm)
165.168	0	2	38.00309228	0.603898079
165.169	0.001	2	38.04285627	0.603756458
165.179	0.011	2	40.64647522	0.630498441
165.19	0.022	2	41.45663911	0.662917647
165.2	0.032	2	41.76900614	0.681021248
165.211	0.043	2	41.86930051	0.697404896
165.212	0.044	2	41.9658702	0.698566472
165.217	0.049	2	41.90858795	0.704026257
165.222	0.054	2	41.8501538	0.70962671
165.233	0.065	2	41.82191175	0.72041992
165.244	0.076	2	41.86339774	0.732627428
165.255	0.087	2	41.84411362	0.745695151
165.265	0.097	2	41.75006701	0.755909958
165.276	0.108	2	41.73904793	0.766933003
165.287	0.119	2	41.75984355	0.777871648
165.298	0.13	2	41.70909557	0.789758722
165.309	0.141	2	41.59681441	0.799538652
165.319	0.151	2	41.63766013	0.807640116
165.33	0.162	2	41.63563115	0.816383879
165.341	0.173	2	41.58934751	0.824987453
165.352	0.184	2	41.4677839	0.832383197
165.363	0.195	2	41.37312625	0.84259848
165.374	0.206	2	41.484849	0.851850552
165.384	0.216	2	41.41488122	0.859358831

165.395	0.227	2	41.31860681	0.866184278
165.406	0.238	2	41.35531271	0.872887178
165.417	0.249	2	41.42562255	0.880041643
165.428	0.26	2	41.35206166	0.886054083
165.438	0.27	2	41.25275839	0.890564009
165.449	0.281	2	41.31213102	0.89568238
165.46	0.292	2	41.31496692	0.901425884
165.471	0.303	2	41.22215699	0.905633495
165.482	0.314	2	41.17350523	0.90954499
165.493	0.325	2	41.1698975	0.913557575
165.503	0.335	2	41.16961099	0.91701083
165.514	0.346	2	41.08636125	0.920254753
165.525	0.357	2	41.03855442	0.923393773
165.536	0.368	2	41.03493207	0.926439808
165.547	0.379	2	41.00259112	0.929782914
165.557	0.389	2	40.94375643	0.931596326
165.568	0.4	2	40.90364161	0.934201764
165.579	0.411	2	40.91681831	0.936551618
165.59	0.422	2	40.8952567	0.938630628
165.601	0.433	2	40.8156644	0.940262842
165.612	0.444	2	40.82628295	0.942226457
165.622	0.454	2	40.8173601	0.944483327
165.633	0.465	2	40.77309667	0.946056413
165.644	0.476	2	40.70123147	0.947116899
165.655	0.487	2	40.71417428	0.949025202
165.666	0.498	2	40.69625841	0.950980711
165.676	0.508	2	40.64238217	0.951637316
165.687	0.519	2	40.58029059	0.952827978
165.698	0.53	2	40.58602963	0.954245615

165.709	0.541	2	40.54541779	0.955573607
165.72	0.552	2	40.45439711	0.956273127
165.731	0.563	2	40.44017083	0.956951189
165.741	0.573	2	40.44916677	0.958471346
165.752	0.584	2	40.40272526	0.95900445
165.763	0.595	2	40.35071136	0.959571886
165.774	0.606	2	40.3399554	0.960341978
165.784	0.616	2	40.32629339	0.961294222
165.785	0.617	2	40.36358108	0.961453486
165.795	0.627	2	40.29417463	0.961630392
165.806	0.638	2	40.24257003	0.962264109
165.817	0.649	2	40.24364299	0.963036585
165.828	0.66	2	40.25313887	0.963677931
165.839	0.671	2	40.19018775	0.964224864
165.85	0.682	2	40.1102183	0.964405585
165.86	0.692	2	40.15039744	0.964773226
165.871	0.703	2	40.13582326	0.965602446
165.882	0.714	2	40.04799223	0.965880442
165.893	0.725	2	39.98355884	0.966118861
165.904	0.736	2	40.01189152	0.966472674
165.914	0.746	2	39.99979656	0.966825534
165.925	0.757	2	39.91126387	0.966801215
165.936	0.768	2	39.89596463	0.967229892
165.947	0.779	2	39.90980206	0.967274714
165.958	0.79	2	39.88158925	0.967467833
165.969	0.801	2	39.83389935	0.967793036
165.979	0.811	2	39.80306406	0.96788745
165.99	0.822	2	39.80849905	0.968263198
166.001	0.833	2	39.77307369	0.968208361

166.012	0.844	2	39.7354264	0.968174983
166.023	0.855	2	39.71841685	0.968573619
166.033	0.865	2	39.72123228	0.968774844
166.044	0.876	2	39.67708873	0.968711425
166.055	0.887	2	39.63176696	0.968465377
166.066	0.898	2	39.61390079	0.96852212
166.077	0.909	2	39.59181001	0.969018031
166.087	0.919	2	39.56799138	0.968776274
166.098	0.93	2	39.51357134	0.969057132
166.109	0.941	2	39.51108627	0.968910743
166.12	0.952	2	39.47144215	0.969114829
166.131	0.963	2	39.42426389	0.968880702
166.142	0.974	2	39.42468489	0.969079543
166.152	0.984	2	39.42083158	0.969107199
166.163	0.995	2	39.38725686	0.968795348
166.174	1.006	2	39.3581465	0.968934584
166.185	1.017	2	39.35984219	0.969096709
166.196	1.028	2	39.35191045	0.96885686
166.206	1.038	2	39.30529644	0.968866874
166.217	1.049	2	39.27083295	0.968915034
166.221	1.053	2	39.23929892	0.969370414
166.228	1.06	2	39.27843726	0.969013739
166.239	1.071	2	39.25511271	0.968996573
166.25	1.082	2	39.20199076	0.968997527
166.261	1.093	2	39.15121646	0.968860675
166.271	1.103	2	39.1814261	0.969140101

Appendix B

All of the fatigue test results from this study are presented in the graph below. The average points are plotted and presented in Figure 6.6

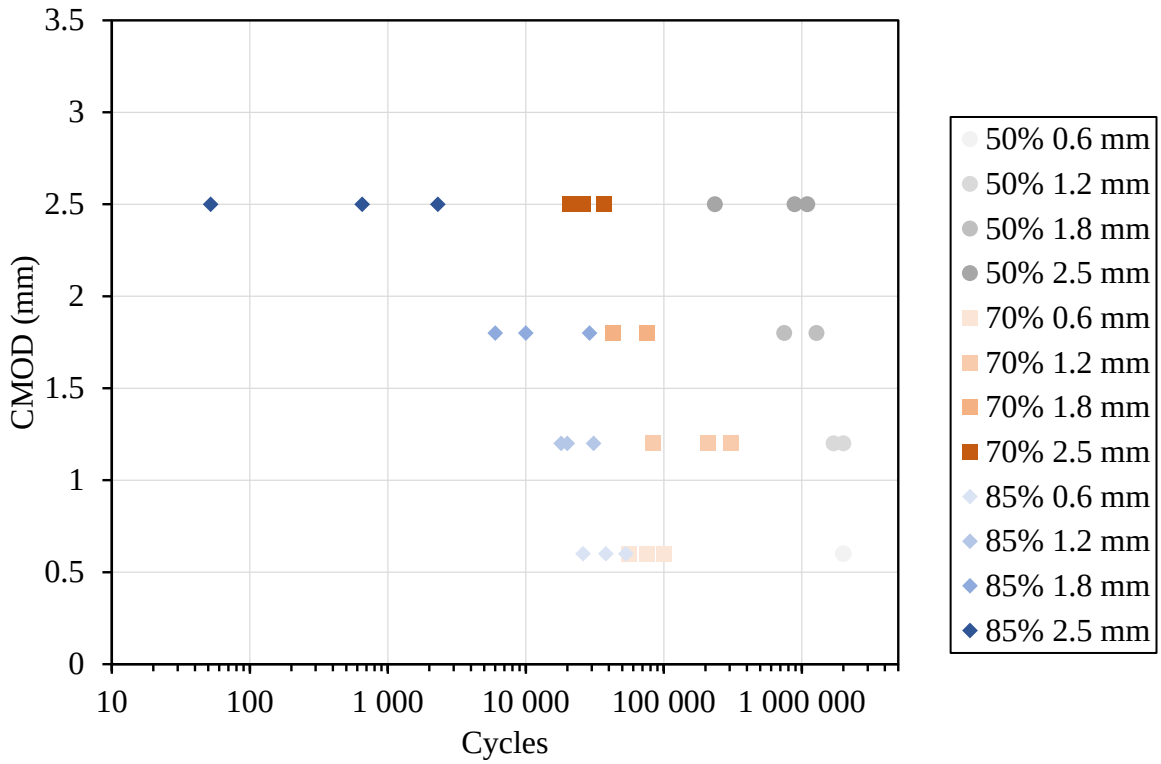

Appendix C

The modified S-N curve based on the results from this study is plotted in the graph below and is compared with all the experimental results performed by Hemmeter (2017).